# Synthesis and characterization of tin dioxide coated gold nanocomposites for applications in thermal heat conduction
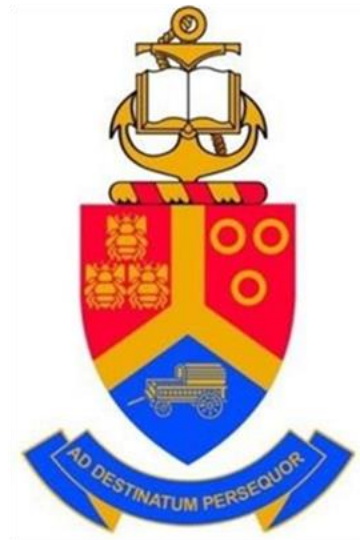
by

## Tshepho Trevor Makgale

## 14007739

A dissertation submitted in partial fulfillment of the requirements for the degree of

**MASTER OF SCIENCE IN PHYSICS**

Faculty of Natural and Agricultural Sciences

Department of Physics

University of Pretoria

**Supervisor:** Prof. Mmantsae M. Diale

**Co-supervisor:** Dr. Pannan I. Kyesmen

# DECLARATION

I, **Tshepho Trevor Makgale** declare that this dissertation, entitled *"Synthesis and characterization of tin dioxide coated gold nanocomposites for applications in thermal heat conduction"* which I hereby submit for the degree **Master of Science (MSc)** in the Department of Physics, University of Pretoria, South Africa has not previously been submitted by me for a degree at any other tertiary institution.

I understand what plagiarism is and am aware of the University's policy in this regard. I declare that this dissertation is my original work. Where other people's work has been used (either from a printed source, Internet, or any other source), this has been properly acknowledged and referenced following departmental requirements. I have not used work previously produced by another student or any other person to hand in as my own. I have not allowed and will not allow anyone to copy my work to pass it off as his or her own.

Student signature: …………………………… Date: 16/11/2023 ……………………

Supervisor signature: ………………… Date: …16/11/2023……………….…

# ACKNOWLEDGEMENTS

# Table of Contents

iii

# List of figures

# Abbreviations

Au – Gold

Au-NSs – Spherical gold nanoparticles

Au-NRs – Rod shaped gold nanoparticles

Au-NPRs – Prism shaped gold nanoparticles

$SnO_2$ – Tin dioxide

$Au@SnO_2$ – Tin dioxide coated Gold (Gold nanoparticles coated with Tin dioxide)

XRD – X-ray Diffraction spectroscopy

UV-Vis – Ultraviolet-Visible spectroscopy

TEM – Transmission Electron Microscopy

SEM – Scanning Electron Microscopy

EDS - Energy Dispersive X-Ray Spectroscopy

FCC – Face Centre Cubic lattice

LSPR – Localised Surface Plasmonic Resonance

NIR – Near Infrared

SERS – Surface Enhanced Raman Scattering

EG – Ethylene Glycol

# ABSTRACT

In this work, we synthesized three nanofluids based on tin dioxide-coated gold nanocomposites (Au@SnO$_2$) using a two-step method. First, we synthesized gold (Au) nanomaterials, then encapsulated them with tin dioxide (SnO$_2$) through spontaneous hydrothermal encapsulation. Finally, we dispersed them into an ethylene glycol base fluid. The materials were analysed using various physicochemical techniques, such as Powder X-Ray diffraction (XRD), Transmission and Scanning electron microscopy (TEM and SEM), and Ultraviolet-Visible spectroscopy (UV-Vis). The diffraction patterns of the materials showed that the composite structures consisted of an FCC Au core and a mesoporous SnO$_2$ shell.

TEM and SEM micrographs showed that the Au@SnO$_2$ nanocomposites had spherical, rod-like, and prism-like shapes. To assess the structural stability of these different types of Au@SnO$_2$ nanocomposites, their TEM micrographs were collected and analysed over a three-month period. The results showed that the Au@SnO$_2$ nanocomposites had better structural stability than their counterparts that were not coated with SnO$_2$ and were exposed to the same conditions.

During an additional evaluation of the materials' structural stability, their ultraviolet-visible absorption spectra were analysed over a three-month period. The results indicated that by encapsulating the Au nanostructures with SnO$_2$ with an appropriate coating thickness size in the range from 50 nm to 150 nm, both the structural stability and optical properties of the materials can be significantly improved. The study was based on the observation of localized surface plasmonic resonance absorption peaks at a wavelength of 550 nm, which showed an increase in intensity and a narrower bandwidth upon the encapsulation of the gold nanostructures with SnO$_2$. In contrast, the pure uncoated Au nanostructures showed low intensity and broad absorption peaks at the same wavelength. Furthermore, for the last two months of the study, a red shift to a higher wavelength of 600 nm was observed for the high intensity absorption peaks of the coated nanostructures, while the uncoated ones did not show any such shift.

Thermal conductivity of the Au-based nanofluids, both coated and uncoated with tin dioxide, was measured using the transient hot-wire method. The results showed that the thermal conductivity of the nanofluids made up of SnO$_2$-coated gold nanostructures increased by more than 10%. Additionally, the thermal conductivity of the SnO$_2$-coated Au

1

nanofluids was observed to rise with an increase in the thickness of the $SnO_2$ layer encapsulating the Au nanostructures. These findings suggest that the Au-based nanofluids coated with $SnO_2$ have potential applications in thermal energy management and electronic cooling systems.

# Chapter 1    Introduction

## 1.1    Background

Nanofluids are a type of fluid that contain metallic nanomaterials with controllable sizes, shapes, and compositions. These fluids have many potential applications in the collection and transportation of thermal energy in automotive heavy-duty engines, electronic devices, and heating appliances [1]. In traditional heat management systems, bulk materials are used as heat exchange media. However, to improve their efficiency the systems would require increasing the surface area available for the medium, which can lead to impractical increases in their size. Modern heat management systems that use nanofluids as the heat exchange medium can increase efficiency, lower weight, and reduce the complexity of the design demands. [2].

Nanometallic-based nanofluids are a type of fluid that contains noble metals such as gold (Au), silver (Ag), platinum (Pt), and gadolinium (Gd), dispersed in a base fluid like ethylene glycol (EG) or mineral oils. These metallic nanomaterials have different structural forms such as nanospheres, nanofibers, nanotubes, nanowires, nanorods, and nanosheets [1]. Among the noble metals, Au is considered the best material for nanofluids because of its unique chemical and physical properties. These properties include surface-enhanced Raman scattering, optical absorption, electrical and thermal conductivity, high thermal and chemical stability [3], biocompatibility [2], inertness, and ease of functionalization [3]. However, Au nanomaterials have a high surface area-to-volume ratio that increases with their decreasing size. This, unfortunately, increases their reactivity and favours the formation of aggregates. To decrease the formation of aggregates, surfactants are often used. However, surfactants are not suitable for most nanofluids used for improving heat transfer because of the harsh conditions involved. These conditions include high temperatures, pressure, and pH [4], which can nullify the functionality of the surfactants. A solution to this problem could be achieved through the study of the influence of tin dioxide ($SnO_2$) on limiting the formation of aggregates and improving the thermal efficiency.

$SnO_2$ is a metal oxide like silicon dioxide ($SiO_2$) and titanium dioxide ($TiO_2$) that has been studied as a possible alternative to the traditional surfactants [5]. The reason for this is that $SnO_2$ can remain thermally stable even when used in harsh nanofluid applications. The potential of $SnO_2$ towards improving the thermal efficiency of metallic nanomaterials while limiting particle agglomeration led to the definition of the following research problem, objectives, and statement elaborated in sections 1.2, 1.3 and 1.4 respectively.

## 1.2 Problem statement

Most applications that use Au-based nanofluids, such as thermal energy harvesting and transportation, face a significant challenge due to the poor structural stability of the constituent gold nanomaterials, as earlier stated [6]. This is because the high surface area-to-volume ratio and surface activity of the materials favour the formation of aggregates. Therefore, it is crucial to investigate ways to enhance the stability of the Au nanomaterials to ensure their effective use in various applications.

Studies have been carried out to enhance the structural stability of Au nanomaterials in colloidal suspensions. Until now, these studies have mainly focused on using metal oxides such as $SiO_2$, and $TiO_2$ as supportive hybrid components which are added as additional additives. However, there is a lack of research focusing on using $SnO_2$ as an alternative metal oxide to the traditional surfactants for stabilizing Au nanomaterials in colloidal suspensions [7].

## 1.3 Research objectives

The main objective of this study is to investigate the potential usage of $SnO_2$ as a structural stabilizer for Au nanomaterials. The research aims to achieve the following objectives:

- To prepare Au nanospheres (Au-NSs), Au nanorods (Au-NRs), and Au nanoprisms (Au-NPrs) using simple solution-based methods.
- To coat the synthesized Au nanostructures with $SnO_2$ of different coating thicknesses.
- To create nanofluids consisting of pure Au nanomaterials and $SnO_2$-coated Au (Au@$SnO_2$) materials dispersed in ethylene glycol.
- To evaluate the stabilization effects of $SnO_2$ on the Au nanomaterials and its impact on the thermal properties of the nanofluids.

## 1.4 Research statement

Considering the research problem and the objectives of the study stated above, it is suggested that the structural stability of Au nanomaterials could be significantly enhanced by coating them with $SnO_2$ nanocrystalline solids of a suitable thickness. The enhanced

4

stability could also improve the overall efficiency of Au-based nanofluids in thermal energy collection and transportation, and other applications.

Particle aggregation and formation of extended complex linked structures that occur in the suspensions of Au nanomaterials is partly due to the Van der Waals forces experienced by the particles [8]. This negatively affects the stability and is probably the source of much of the disagreement between theoretical predictions and experimental observations [9]. Thus, efforts to keep the Au nanomaterials separated through isolation using a distance holder material, such as $SnO_2$, can be useful in limiting particle aggregation and improving their structural and thermal stability.

## 1.5    Delineation and limitations of the study

This study is focused on investigating three Au nanostructures: nanospheres, nanorods, and nanoprisms, of a particular size, which will be defined in full detail in chapter 4 of this dissertation. An investigation of the effects of varying the sizes of the particles by increasing the diameters or aspect-ratio of the structures will not be conducted in this study, despite its significance. This is because, a significant number of studies already exist, which explored these relations [10], the same applies to the investigation of other metallic nanomaterials including Ag, Pt, Cu or Gd [10]. In addition, similar studies also exist on the use of other structures, including nanopyramids, nano-octahedrons, and nano-stars [4, 5].

The number of nanoparticles dispersed in fluids heavily affects the thermal conductivity of the resulting nanofluids [11]. In other words, when there is a higher volume fraction of nanoparticles dispersed, there is a greater increase in thermal conductivity. To accurately measure thermal conductivities, this study will prepare nanofluids using Au and Au@$SnO_2$ with the highest volume fraction of 10%.

## 1.6    Chapter Overview:

In Chapter 1, an introduction to the dissertation is presented by providing a brief background on the significance of the research work, the problem statement, the objectives, the research statement, the scope and limitations of the study, and an overview of the dissertation structure.

Chapter 2 gives an overview of Au, $SnO_2$, and $Au@SnO_2$ composite nanomaterials and nanofluids. A significant overview of the properties of nanofluids used in various thermal heat conduction applications is discussed. The chapter also summarises the current state of research on nanofluids and identifies the research gaps the study aims to fill.

Chapter 3 elaborates on the methodology of this study, providing a complete description of the research design and approach. It explains the synthesis process for the various Au nanostructures and the $SnO_2$-coated Au nanocomposites in detail. Characterization techniques for evaluating the physical and chemical properties of these nanostructures are also given in this chapter. The experimental setup and procedures for the transient hot-wire method for thermal conductivity measurements, and the data collection and analysis methods are also explained here.

Chapter 4 gives the presentation and interpretation of the experimental results, the analysis of the physical and chemical properties of $SnO_2$-coated Au nanocomposites, as well as the evaluation of the thermal conductivity of the nanofluids. The comparison of the findings with the existing literature and the discussion of the implications and significance of the results are elaborated.

Chapter 5 presents the conclusions made from this research, providing a summary of the main findings and their implications. The reiteration of research objectives and contributions to the field and the final remarks and recommendations for practical applications of $SnO_2$ coated Au nanocomposites in thermal heat conduction are also provided.

**Chapter 2    An overview of Au-based nanomaterials.**

**2.1  Introduction**

Novel nanomaterials differ significantly from classical ones in several ways. They are typically smaller in size, measuring less than 100 nanometers in at least one dimension, and have narrow size distributions with a standard deviation of less than 5-10% of the average particle diameter. They have a well-defined molecular composition, are highly isolable and dissolvable, and can be prepared reproducibly. And following recent technological advancements, many novel nanomaterials can be easily tailored to specific applications [12].

In this chapter, we will provide an overview of nanomaterials based on gold (Au). We will start by discussing the structure of Au nanomaterials in section 2.2. In sections 2.3, we will explore various unique properties of Au nanomaterials. Next, in section 2.4, we will describe the different methods used for synthesizing Au nanomaterials. We will then discuss the Au-based nanocomposite materials of the core-shell type in section 2.5. Section 2.6 will focus on the use of Au nanocomposite material-based nanofluids in thermal energy collection and transportation applications. Finally, in section 2.7, we will summarize the implications of this review with regards to the thesis of this study and the significance of the work.

**2.2 Structure of Au nanomaterials**

Au nanomaterials can display different crystal structures based on their size, shape, surface properties, and method of synthesis [13], [14]. At the nanoscale, Au can adopt crystal structures that are unlike its bulk, macroscopic form, as explained in section 2.2.1. The various crystal structures that Au nanomaterials can assume are described in this section. The subsequent sections, 2.2.2 and 2.2.3, elaborate on the surface characteristics and the diverse shapes of Au nanomaterials, respectively.

*2.2.1    Crystal structure of Au nanomaterials*

At the nanoscale, Au can have crystal structures that differ from its bulk, macroscopic form. The most common crystal structures of Au nanomaterials are the Face-Centred Cubic (FCC) structure and the Twinned structure. In the FCC structure, as depicted in figure 2-1, the Au atoms are arranged in a closely packed pattern with each atom surrounded by 12 neighbouring atoms. In their study using X-ray diffraction pattern analysis for Au

7

nanomaterials, Nguyen Thi Nhat Hang et al [13], observed diffraction peaks with 2θ angles at 38.20°, 44.40°, 64.60°, 77.54°, and 81.72°, corresponding to the fine crystal planes at (111), (200), (220), (311), and (222). This structure is stable and results in many of the well-known properties of Au, such as its metallic clusters and excellent electrical conductivity [15]. Twinned structures are often observed in Au nanorods and nanowires. They contain twin boundaries where the crystal lattice orientation abruptly changes, resulting in anisotropic properties that affect the nanomaterial's behaviour along different axes. According to Cheng Wang et al [16],these structures arise from a universal FCC to hcp phase transformation that occurs only when the Au nanomaterial sizes decrease well below a critical value.
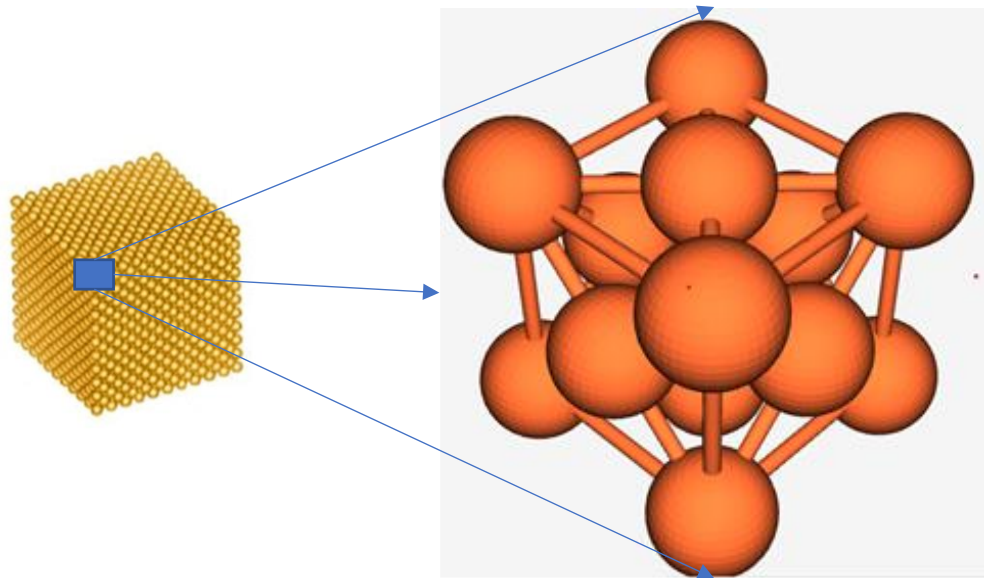


*Figure 2-1: The FCC crystal structure observed in bulk Au materials and most stable nanomaterials.*

Au nanomaterials can exhibit strained or deformed crystal structures as a result of their small size and unique shapes. This strain can cause variations in electronic and mechanical properties as compared to bulk Au material. Additionally, the crystal structures of Au nanomaterials may have defects like vacancies, dislocations, or stacking faults, which can significantly impact their reactivity and properties [17]. In section 2.2.2, we will discuss in detail how the surface characteristics of Au nanomaterials influence their crystal structures, leading to the formation of various Au nanomaterial shapes, which will be described in section 2.2.3.

8

### 2.2.2 Surface structure of Au nanomaterials

In general, nanomaterials have a surface which forms a sharp interface between the nanoparticle and its surroundings, as explained in [18]. This surface becomes more significant with a decrease in the nanomaterial's size, and its effects tend to extend to a depth of a few atoms below the interface. Therefore, nanomaterials are composed of two types of atoms: surface atoms that are closer to the interface and bulk atoms that are far away from it. The coordination numbers of these two atoms differ significantly, with surface atoms having lower coordination numbers and higher unsatisfied bonds than their counterparts, making them more chemically active. The surface atoms' chemical activity is due to the unbalanced forces they experience. Due to this high chemical activity, most nanomaterials tend to undergo surface reconstruction and surface relaxation to relieve and lower their chemical activities, as explained in [16], [19]. However, these processes usually result in the occurrence of defects in nanomaterials.

Furthermore, at the interface between nanomaterials and their surroundings, various processes occur, including particle nucleation, growth, dissolution, precipitation, chemical reactivity, and adsorption. For Au nanomaterials, different surface morphologies such as smooth, rough, faceted, porous, and functionalized are preferred depending on the synthesis methods and other conditions [20]. Smooth surfaces are suitable for controlled interactions with the surroundings while rough surfaces, with a larger area, are best for adsorption interactions. Faceted surfaces are characterized by specific crystal facets. Porous surfaces have high surface areas and increased accessibility for various molecules and ions, making them ideal for catalytic interactions. Functionalized surfaces, modified with various functional groups or biomolecules, allow specific interactions with target molecules or cells, essential in biomedical applications such as drug delivery, imaging, and biosensing.

### 2.2.3 Equilibrium shape of Au nanomaterials

When materials are in the nanoscale range and under equilibrium conditions, they tend to assume a shape that minimizes the free energy. In this range, the surface energy term contributes more to the total free energy and becomes dominant when the particle size is less than 10 nm. This means that when a nanomaterial consists mostly of surface atoms with high energies, these energies contribute more to the nanomaterial's free energy. To minimize high surface energies, most materials tend to reduce their overall surface area, resulting in a more spherical shape. However, for crystalline FCC solids like Au, each crystal plane has a different surface energy value. To predict the equilibrium shapes of a particle, Wulff's construction theorem [19, 20] can be used. According to this theorem, there is a point inside

9

an equilibrium form of a crystal where the perpendicular distance di from the ith face is proportional to the surface energy of that face. Thus, the shape of a crystal is influenced by its surface energy, as shown by the nanocluster structures in Figure 2-2.
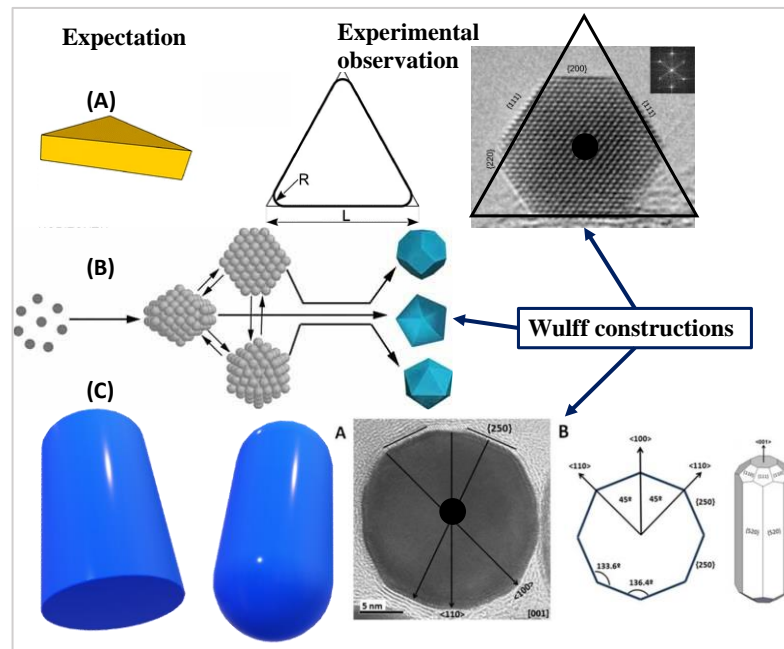


*Figure 2-2: Showing the modification of the crystal structures of Au a) nanoprisms, b) nanoclusters, decahedrals, and icosahedrals, and c) nanorods [21, 22].*

Au nanomaterials can take on different shapes based on how they are synthesized and the conditions under which they are formed. Figure 2.3 shows the various shapes that can be assumed by Au nanomaterials under equilibrium conditions, these include nanospheres, nanorods, nanowires, nanoprisms, nanocubes, nanostars, nanoshells, and nanocages [21]. Nanospheres are the simplest and most studied form of Au nanomaterials. They are spherical nanoparticles that can vary in size from a few to several tens of nanometers. Nanorods are elongated structures with an aspect ratio typically greater than 3. Their length-to-width ratio can be adjusted during synthesis, leading to specific optical properties and surface plasmon resonances [22].
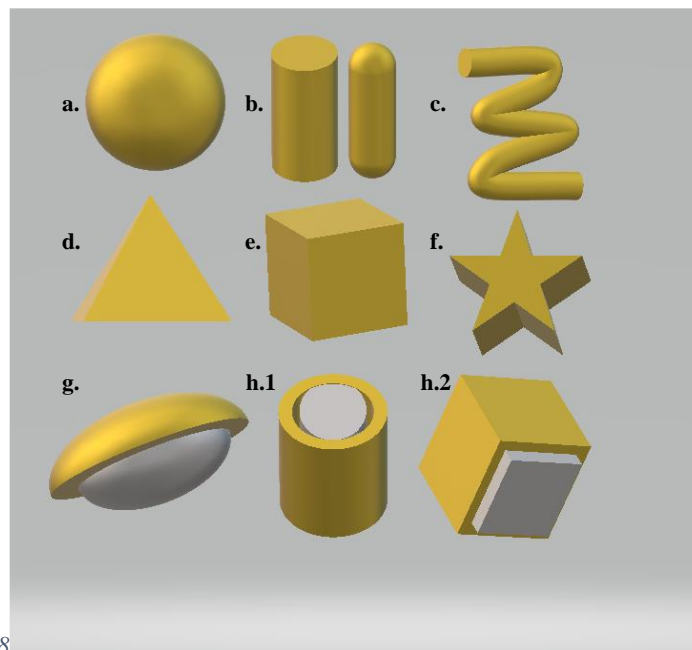
*Figure 2-3: Showing the various shapes Au nanomaterials can assume under equilibrium conditions. These include Au (a) nanospheres, (b) nanorods, (c) nanowires, (d) nanoprims, (e) nanocubes, (f) nanostars, (g) nanoshells and (h.1 - h.2) nanocages.*

Nanowires are one-dimensional structures with diameters in the nanoscale range and lengths that can extend up to micrometers. They have diverse applications in electronics, photonics, and sensing [23]. Nanoprisms and nanocubes are nanoparticles with specific geometries, exhibiting flat surfaces and sharp edges. They can be synthesized through various methods, including seed-mediated growth and template-assisted synthesis.

Nanostars have a branched structure that resembles a star. They possess enhanced electromagnetic field enhancements and are used in applications such as surface-enhanced Raman spectroscopy (SERS) and photothermal therapy. Nanoshells consist of a dielectric core surrounded by a thin gold shell. They have applications in biomedical imaging, photothermal therapy, and drug delivery [24]. Finally, nanocages are hollow structures with a cage-like morphology. They have high surface area and porous structure, which makes them useful in catalysis, drug delivery, and imaging.

## 2.3 Properties of Au nanomaterials

Au nanomaterials possess distinct properties at the nanoscale, which differ from those of bulk materials. These unique properties make them highly desirable for a wide range of

applications in fields such as catalysis, biomedicine, electronics, and materials science. In the following sections, we will describe some of the key properties of Au nanomaterials.

### 2.3.1   *Plasmonic and optical properties of Au nanomaterials*

Noble metals, such as Au, have unique optical properties. Specifically, they show localized surface plasmonic resonance (LSPR) phenomena, which is a direct result of their surface characteristics. When plasmonic nanomaterials interact with electromagnetic radiation of a specific wavelength i.e., plasmonic wavelength, their free surface electrons oscillate, causing the plasmonic resonance [25]. For Au nanomaterials, the plasmonic wavelengths are in the visible and infrared regions of the electromagnetic spectrum [26]. According to Wang Lu et al [26], achieving a tailor-made and adaptable application that utilizes the LSPR phenomena of plasmonic nanomaterials requires precise designing of physical features such as their size, morphology, and composition. This can be achieved by considering the critical role played by their fabrication or preparation method, as well as the permittivity of their surrounding media. To improve our understanding of the physics behind the LSPR phenomena of plasmonic nanomaterials, several studies have been conducted, adopting various calculation approaches such as Mie theory and Gans theory.

#### (1) Shape effects

In his Mie theory [18], Gustav Mie accurately calculated the optical cross sections of spherical nanomaterials based on Maxwell's equations for spherical particles. In these calculations, he considered the permittivity of the particles and their surroundings. Based on these calculations, it was observed that spherical particles exhibit predictable behaviour when interacting with light, including their core-shell geometries with different metals or dielectric components. This observation has been experimentally confirmed [27 – 29]. For spherical nanoparticles, only a single size-dependent resonance peak is observed, which corresponds to the transverse oscillation of the surface electrons. Moreover, the effective free path of the scattered electrons can be altered by the surface electron scattering features of the surrounding media. This accounts for the scattering on the surface between the core and the shell. Core-shell nanoparticles (composed of metal-metal, or metallic-dielectric in a core-shell arrangement), as confirmed by the Mie theory and experimentally by Lee Su [19], show significant resonance shifts in a size-dependent manner. The absorption spectrum in Figure 2-4 indicates that the resonance wavelength for Au nanospheres is approximately 520 nm.
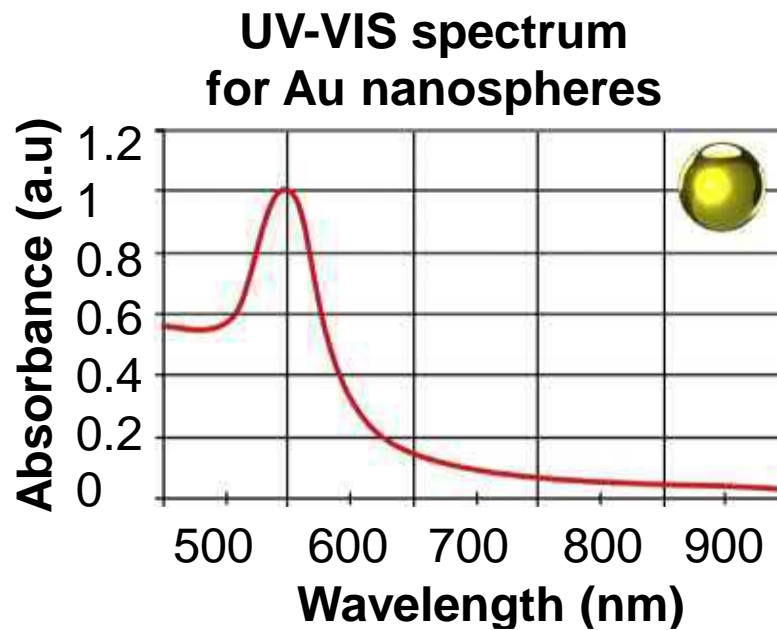
*Figure 2-4: Absorption spectra of Au nanoparticles with shape: spherical [27].*

For nanomaterials shaped like rods, two resonance peaks are expected and observed. These peaks correspond to the transverse and longitudinal oscillations of the resonating surface electrons. The transverse oscillation resonance peak is predicted to be weak and falls in the visible region. Meanwhile, the longitudinal oscillation resonance peak is strong and is in the red or NIR region [32, 33]. Moreover, it has been demonstrated that the longitudinal resonance peak of the rod-like nanomaterials of the material in question is sensitive to the aspect ratio. This is precisely as predicted and described by the Gans theory [28], which extends Mie theory to account for non-spherical particles. The absorption spectrum in Figure 2-5 shows that the resonance wavelengths for Au nanorods are approximately 520 nm for the transverse oscillation, and approximately 750 nm for the longitudinal oscillation.

**UV-VIS spectrum for Au nanorods**
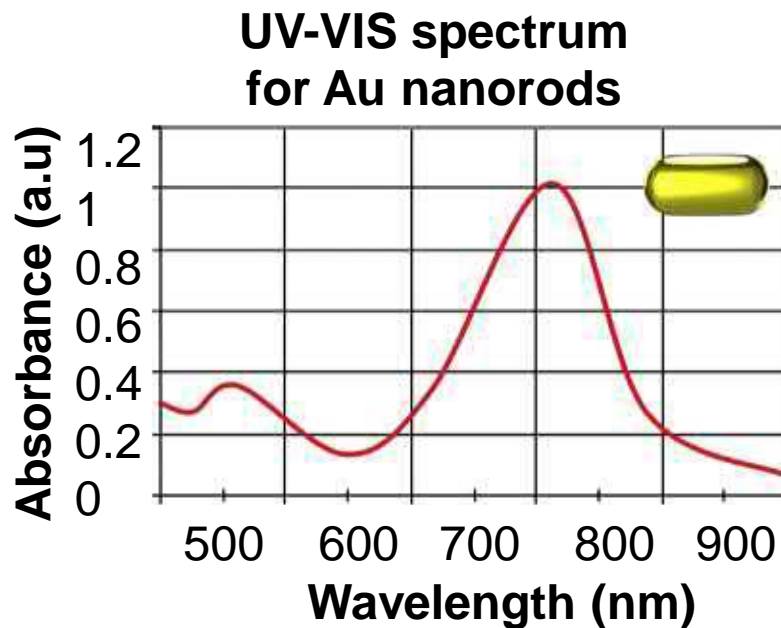


*Figure 2-5: Absorption spectra of Au nanoparticles with shape: rod-like [27]*

More complex nanostructures such as nano-cubes and nanoprisms exhibit a more intricate interaction behaviour with light that cannot be accurately predicted by Mie theory. However, advanced numerical methods such as finite difference time domain (FDTD) and finite element methods (FEM) are more suitable for predicting this behaviour) [26]. In all these approaches, the LSPR peaks for irregular nanostructures are expected to be wider, which corresponds to a broader range of plasmonic wavelengths [29].

(2) *Surrounding media effects*

The plasmonic resonance occurs when the permittivity of the nanomaterial, $e_r$, is close to twice the permittivity of the surrounding medium, $-2e_m$, which signifies the critical role played by the surrounding medium of the nanomaterials in the interaction with light [26]. In addition to determining the wavelength of the electromagnetic wave necessary for resonance and modifying the geometry of the electric field around nanomaterials, the surrounding medium also affects the polarization within individual particles [30].

Taking all these factors into account, and by remembering what has been suggested by Gonzalez [31] and Wang [26], one can synthesize nanomaterials of specific morphological and structural features which could result in any suitable combination of desired and selective properties including optical (LSPR in specific regions), electrical conductivity, chemical reactivity and catalysis. Subsections 2.3.2 – 2.3.5 below describe in full detail these properties of Au nanomaterials.

### 2.3.2 Electrical properties of Au nanomaterials

Au is widely recognized for its exceptional electrical conductivity. At the nanoscale, Au nanomaterials, including nanowires, continue to exhibit high electrical conductivity, which makes them valuable in a range of applications in the fields of electronics, sensing, and nanotechnology [23]. The electrical conductivity of Au nanomaterials can be influenced by their size. Small-sized nanomaterials may show different conductive properties from larger nanomaterials or bulk Au due to quantum confinement effects and changes in electron scattering mechanisms. Additionally, the shape and morphology of Au nanomaterials have been shown to impact their electrical conductivity. For example, nanowires can demonstrate enhanced conductivity along their length compared to other directions due to their anisotropic structure. Surface modifications, functional groups, and ligands on the surface can also affect electron transfer and conductivity. The presence of impurities or defects within the crystal structure of gold nanomaterials can also affect their electrical conductivity [32]. Defects such as vacancies or grain boundaries can impact electron mobility, thereby altering overall conductivity. Understanding and controlling the electrical properties of gold nanomaterials is crucial to optimizing their performance in diverse technological and scientific domains.

### 2.3.3 Thermal and chemical stability of Au nanomaterials

Au nanomaterials are known for their exceptional thermal and chemical stability. They possess a high melting point of approximately 1064.0°C, which is also exhibited by bulk Au materials. This thermal stability allows them to maintain their structural integrity and crystalline form even at elevated temperatures. Furthermore, they are resistant to sintering, which is the process of coalescence and agglomeration of nanoparticles at high temperatures [33], [34]. This property makes them suitable for applications requiring thermal stability, such as catalysis and high-temperature electronics. Additionally, Au nanomaterials demonstrate excellent thermal conductivity, which extends to the nanoscale. This property allows them to efficiently transfer heat, making them valuable in thermal management applications.

The remarkable chemical stability of Au materials is due in part to the exceptional inertness of the materials. This means that Au is highly resistant to chemical reactions with most acids and bases, making it highly stable in various environments, including biological

15

systems [35]. Au nanomaterials also exhibit this inertness, which makes them resistant to corrosion and degradation. This property, combined with their compatibility with biological systems, makes them safe to use in biomedical applications without eliciting significant immune responses. The chemical stability of Au nanomaterials is also a valuable property for drug delivery and imaging, as they remain stable in biological fluids and tissues. Additionally, Au nanomaterials are highly suitable for use in catalysis and chemical sensors, as they can withstand exposure to strong acids, bases, and other corrosive substances. The naturally occurring oxide layer on the surface of Au nanomaterials provides a protective barrier, further enhancing their chemical stability [35]. By functionalizing Au nanomaterials with ligands and molecules, their chemical reactivity and stability can be influenced and made more selective for applications.

The exceptional thermal and chemical stability of Au nanomaterials, coupled with their unique properties, makes them highly desirable in various applications, including catalysis, sensing, biomedicine, and nanoelectronics. This is why Au nanomaterials are widely used in both research and industry.

### 2.3.4    *Surface Enhanced Raman Scattering of Au nanomaterials.*

Surface-Enhanced Raman Scattering (SERS) is a spectroscopic technique that amplifies Raman signals of molecules adsorbed on or near the surface of certain materials like Au nanomaterials. Due to their unique surface plasmon resonance (SPR) characteristics and high chemical stability, Au nanomaterials exhibit excellent SERS properties. The SERS effect of Au nanomaterials arises from the electromagnetic field enhancement and chemical enhancement effects associated with the localized surface plasmon resonance of the Au nanomaterials [36]. This high sensitivity enables the detection and identification of trace amounts of target molecules, even down to single-molecule detection levels. As a result, SERS is used in diverse fields such as analytical chemistry, biochemistry, and biosensing. Au nanomaterials' SERS activity can be tailored by controlling their size, shape, and surface morphology. Nanospheres, nanorods, and nanoprisms exhibit distinct SERS properties, enabling the design of Au nanomaterials for specific sensing applications. These unique SERS properties of Au nanomaterials have led to their widespread use in various applications, including chemical and biological sensing, environmental monitoring, and medical diagnostics.

## 2.4 Synthesis of Au nanomaterials

The various methods employed in the preparation of modern nanomaterials are given in table 2-1 below, and these are categorized into two main types i.e., Top-down methods, and Bottom-up methods. These methods, referred to as the Divers methods, differ only in the starting material used in the preparation of nanomaterials [38, 39]. Nanomaterials with reduced particle sizes are produced from a bulk starting material after it has undergone the different physical, chemical, and mechanical processes in the top-down methodology. However, atoms or molecules are used as the starting materials in the bottom-up methodology [38, 40].

*Table 2-1: Top-down methods and bottom-up methods of nanoparticle preparation [33].*

| | Top-down methods | | Bottom-up methods | |
|---|---|---|---|---|
| | Methods | Examples | Methods | Examples |
| 1 | Mechanical milling | Ball milling Mechanochemical method | Solid state methods | Physical vapor deposition Chemical vapor deposition |
| 2 | Laser ablation | | **Liquid state synthesis methods** | Sol-gel methods **Chemical reduction Hydrothermal method** Solvothermal method |
| 3 | Sputtering | | Gas phase methods | Spray pyrolysis Laser ablation Flame pyrolysis |
| 4 | | | Biological methods | Bacteria Fungus Yeast Algae Plant extract |
| 5 | | | Other methods | Electrodeposition process Microwave technique Supercritical process Ultra-sound technique |

The synthesis of nanomaterials, using either of the above methods, is extremely sensitive to and is subject to a multitude of factors. Some, including the physical characteristics of the nanomaterials to be synthesized, were stated above, others are as simple as considering the type of glassware or other laboratory equipment used during the synthesis. All these factors may add foreign materials or result in unforeseen products. Acidic or basic conditions can change the average particle sizes and size distribution of the particles by increasing the dissolution rate to ionic form which can result in the re-deposition of the depositing atoms onto existing nanoparticles [34].

The synthesis of Au nanomaterials by the bottom-up liquid state synthesis methods such as chemical reduction, contain two major steps (Method of choice for this study):

17

- Reduction reaction step, utilising agents such as borohydrides, citric and oxalic acids, polyols, hydrogen peroxide, sulphites, and many others. These serve as the sources of electrons to reduce the gold ions, $Au^{3+}$ and $Au^+$ to the atomic $Au^0$. This reaction usually occurs in the presence of an Au salt solutions, here chloroauric acid or a derivative thereof.

- Stabilization step, utilising agents such as trisodium citrate dihydrate, sulphur ligands i.e., thiolates, phosphorus ligands, polymers, surfactants i.e., cetyltrimethylammonium bromide (CTAB), and many others [42, 43]. These protect the synthesized Au nanomaterials against agglomeration by imputing a strong repulsive force that limits the extended growth of the nanoparticles in terms of rate, final size, or geometrical shape, through one of the stabilization mechanisms discussed in section 2.5.1 (1) and (2) below.

The use of reducing agents in synthesis has several limitations associated with toxicity, high costs, poor reducing performance, and impurities [35]. In fact, Su Linjia et al, in their study, they successfully develop a fast and efficient process that replaced the classical CTAB stabilized synthesis method with a mercaptoundecanoic acid (MUA) one, on the grounds of toxicity concerns [36].

However, synthesizing nanomaterials through chemical reduction remains the simplest method [37]. In fact, considering the implications of their work, Su Linjia et al. [36] have demonstrated that the method can be modified with any suitable material that can be used as a stabilizing agent or distance holder – that must also prevent the tendency of the particles to form van der Waals bond clusters. The ability to overcome these limitations has been achieved through the addition of "secondary" phase which provides the first original motivation for the investigation of the use of metal oxides and/or semiconductor materials, such as $TiO_2$, $SiO_2$, and $SnO_2$ as stabilizing agents for the nanometallic particles. The following section 2.5 discusses characteristics of the various composite materials of Au.

## 2.5 Au nanocomposite materials

Nanocomposite materials made of Au are a combination of Au nanoparticles or nanostructures with other materials. This results in a hybrid material that incorporates the properties of both constituents. These nanocomposites often exhibit enhanced or novel properties when compared to the individual components. The most common Au nanocomposite materials include polymer-Au, metal oxide-Au, carbon-based-Au,

18

biopolymer-Au, and ceramic-Au nanocomposites. Subsection 2.5.1 provides more information on the characteristics of these nanocomposite materials. Following this, there is a detailed discussion on the metal oxide-Au type of nanocomposite materials.

### *2.5.1    Characteristics of Au-based nanocomposite materials.*

Figure 2-6 illustrates the three categories of nanocomposite materials, based on the dimensionality of their primary "active" phase. The categories are zero-dimensional, composed of isolated nanoparticles with sizes less than 100 nm in all dimensions, one-dimensional, consisting of isolated nanotubes or nanowires, and two-dimensional, composed of stacks, layers, or sheets/platelets of nanomaterials [38]. The secondary phases may consist of a variety of compatible materials, including polymer matrices, oils, gels, and fluids, as well as glass and other metals.
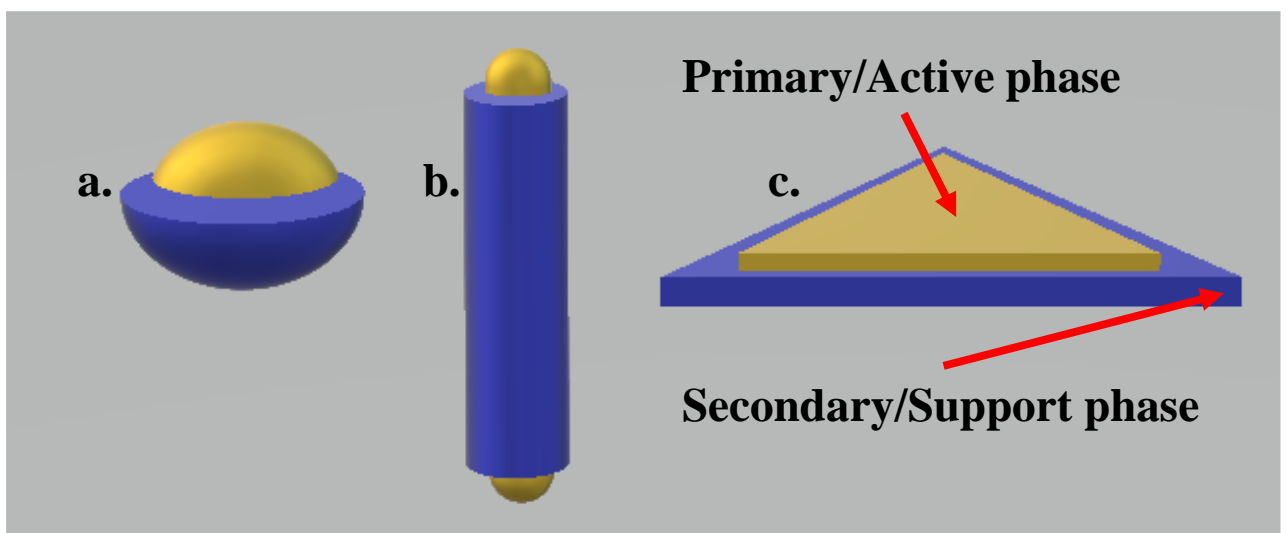


*Figure 2-6: Three categories of nanocomposite materials* [38]. *With (a) representing zeroth-dimensional (OD) nanocomposites, (b) representing one-dimensional nanocomposite (1D) and (c) representing the two-dimensional nanocomposites (2D).*

In addition, composite materials that self-assemble are often observed. Figure 2-7 [39]. provides a visual representation of these nanocomposites, which are often engineered through controlled synthesis methods. This allows for the precise arrangement of Au nanoparticles on a substrate or within a matrix. The self-assembly process is guided by intermolecular forces or templating agents, which lead to well-defined structures with tuneable sizes and shapes. These materials have found applications in various fields such as catalysis, sensing, imaging, and biomedical research. The controlled assembly of Au nanoparticles imparts enhanced properties, such as increased surface area, improved stability, and tailored reactivity. This makes these nanocomposites promising candidates for advancing technologies in nanoelectronics, optics, and other emerging fields.
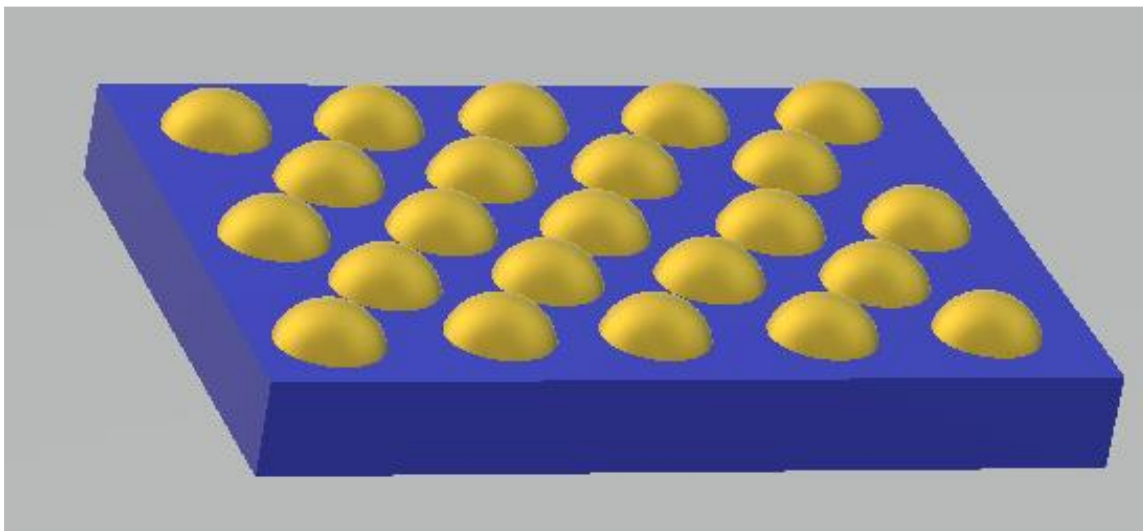
*Figure 2-7: Perfectly ordered zeroth-dimensional nanocomposite materials; made via a self-assembly process* [38].

In cases where the composite components are in different phases, such as in solid-liquid nanocomposites given in Figure 2-8, the secondary phase and the dispersed nanomaterials have mutual solubility. In such cases, a diffusion barrier is necessary to ensure the stability of the nanomaterials. Additionally, choosing an appropriate diffusion barrier and stabilization mode can significantly reduce the van der Waals forces between the nanomaterials, which in turn can prevent coagulation or aggregation of the particles. There are two types of stabilization modes, electrostatic and steric mechanisms.
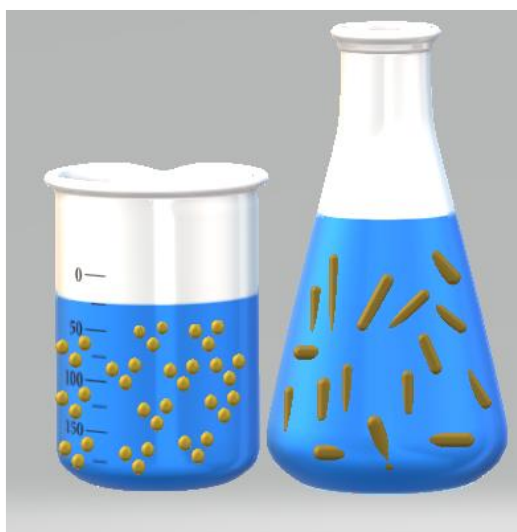


*Figure 2-8: Showing some of the solid-liquid type of nanocomposite materials also referred to as colloidal suspensions/nanofluids.*

In the electrostatic stabilization mechanism, stabilization is afforded to a suspension of particles due primarily to the charges on the particle surfaces, depicted in Figure 2-9.

20

Nanoparticles of oxides or halides such as silica ($SiO_2$) have charges on their surfaces when suspended in water. And this was demonstrated in the process of electrophoresis, when they respond to an external electric field applied to their colloid suspensions [39].
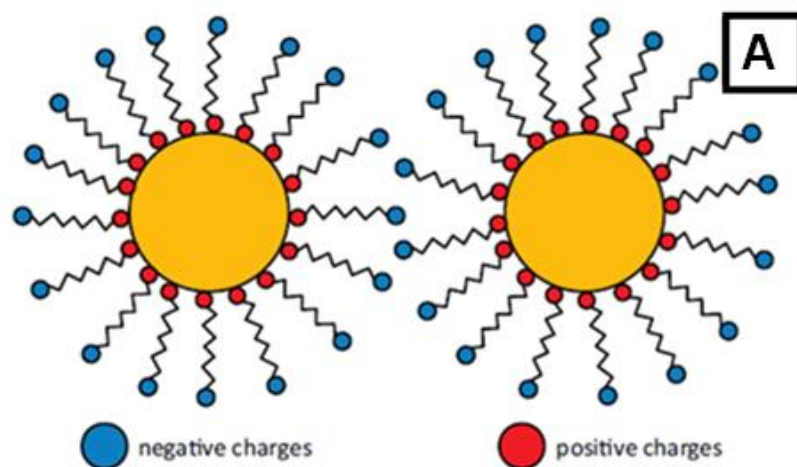


*Figure 2-9: The Electrostatic stabilization mechanism for colloidal suspension of nanomaterials.*

For Au nanomaterials, electrostatic stabilization can be achieved through the adsorption of ions to the electrophilic Au metal surfaces [40]. Since the suspension of these nanomaterials must remain electrically neutral, counterions with opposite charges must be present as well. To prevent neutralization between the charged nanomaterials and the counterions, the surfaces of the nanomaterials and the counterions in the suspension are further hydrated by layers of water molecules, which results in an electrical double/multi-layer. The thickness of this double layer is such that the attractive forces between the nanomaterials and the ions do not exceed their thermal kinetic energy, thus the nanomaterials remain separated from each other. In essence, stabilization is adequately afforded if sufficient electrical potential is present at the nanomaterial surface, and this may at times be pH sensitive.

Steric stabilization is achieved through the surrounding or coating of a nanomaterial core with a layer of material that is sterically bulky enough to afford the mutual repulsion of the nanomaterials, depicted in Figure 2-10. This is accomplished by using polymeric [13 – 15] or surfactant molecules (dispersants). Surfactants are usually long-chain organic compounds that are amphiphilic, containing both hydrophobic and hydrophilic groups. When the metals are dispersed in water, the polymers or the surfactants will diffuse in water and adsorb at the interfaces between water and the metal surfaces. These large adsorbates thus provide the steric barrier keeping the metallic nanoparticles separated. The necessary

21

thickness the of the polymers or surfactant around the metallic particles depends on the phenomenon to be investigated; it may be smaller in the case of enhancing the tunnelling of electrons between particles, but larger in the case of preventing dipole–dipole interaction.
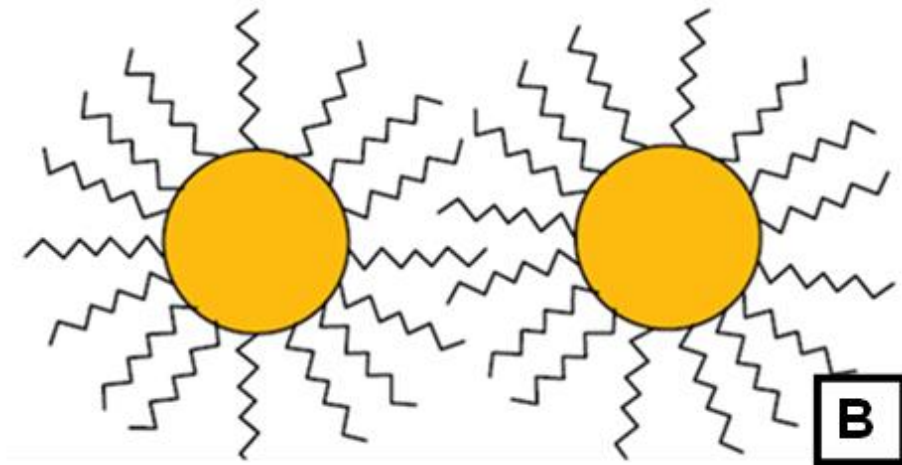


*Figure 2-10: The Steric stabilization mechanism for colloidal suspension of nanomaterials.*

As Vollath points out [9], by coating the metallic nanoparticles in suspensions with secondary or tertiary layers of suitable materials depending on the applications in mind, the following improvements can be afforded:

- The two phases will be homogeneously distributed on a nano-meter scale.
- The metallic nanoparticles "cores"- are separated from each other with a well-defined and easily controlled distance; therefore, the interaction of the particles is controlled.
- The metallic cores and one or more different coating materials may have different but complimentary properties, such as ferromagnetism and luminescence, which allows a combination of properties in one particle that would otherwise never exist together in nature (multi-functional materials [41])
- Additionally, hydrophilic, or hydrophobic behaviour of the composite material can be adjusted by selecting a suitable polymeric/surfactant material for the outermost layer.
- During densification (i.e., sintering) the growth of the metallic cores can be thwarted, provided that the core and coating show no mutual solubility.

Thus, from an application perspective, nanocomposite materials of the core-shell architectural type with suitable additional phases acting as stabilizing and enhancing phases are worth further exploration. Subsection 2.5.2. elaborates on the nanocomposite materials

22

of the core-shell type in which the shell material is the metal oxide tin dioxide ($SnO_2$), and the core material is Au.

### 2.5.2  *Nanocomposite materials of Au and $SnO_2$ in a core-shell arrangement.*

Tin dioxide ($SnO_2$) as a standalone material is a semiconductor with a 3.6 eV band gap [42], its nanocrystalline coatings are among the most intensely studied semiconductor metal oxide materials, owing to their emergence as future materials for a variety of technological applications such as protection against corrosion, ultrafiltration membranes, gas sensing, catalysis, anodes for lithium rechargeable batteries, and transparent electrodes for smart windows and solar panels. Like silicon dioxide ($SiO_2$), $SnO_2$ nanomaterials also possess excellent thermal stability.

When used as the stabilizing – coating material around Au nanomaterials, these nanocrystalline nanoparticles prevent the interactions between individual Au nanomaterials. This is crucial for avoiding the agglomeration process and the formation of nanoclusters or other complex linkages. With its properties, including refractive index of 2.2 [43], the properties of the Au nanomaterials, can be affected when coated with suitable amounts of $SnO_2$ in a core-shell architecture, by varying the ratio of the $SnO_2$ shell-to-Au core i.e., their mutual distribution, or by applying different materials, including organic and inorganic ones [49, 50]. This architectural type results in the formation of a new class of nanomaterials, called nanocomposite materials denoted as "metal-core@ metal oxide-shell" (pronounced metal oxide-coated metal nanocomposite materials).

However, the actual mechanisms of the nanocrystalline $SnO_2$ formation and growth, as well as the surface interaction of the various Au nanomaterials with $SnO_2$ nanoparticles and other molecules in the medium is complicated by many factors, including chemical and physical adsorption phenomena and dissolution of surface atoms.

Any application of any nanomaterial is limited by the stability of that nanomaterial, whether it is thermal stability, chemical stability, or structural stability. Stability is vital. Lee Ho et al [44] investigated the stabilizing effects of $SnO_2$ and $SiO_2$ on Au nanospheres, which was demonstrated to be pH dependant. The study also demonstrated that the stability can be re-established upon controlling the pH of the suspensions. Furthermore, the study investigated the effects of varying the $SnO_2$ and $SiO_2$ - coating thicknesses on the stability and properties of the Au nanospheres. A similar study by Zhong Na et al [43], utilised Au

23

nanorods instead. However, studies on Au nanoprisms, as well as the application of these Au@SnO$_2$ nanocomposite materials in nanofluids for improved thermal transfer is still lacking. Section 2.6 discusses the application of the Au based nanocomposite materials of the core-shell type in nanofluids used for thermal energy collection and transportation.

## 2.6 Au@SnO$_2$-based nanofluids

Nanofluids are defined as composite materials of the solid-liquid type, as opposed to the solid-solid type. Herein we make this definition more technical, nanofluids are therefore defined as the stable suspensions of solid nanomaterials in a liquid base. Modern nanofluids consist of up to 10% volume fraction of nanomaterials and typically more than 10% volume fraction of surfactant. Oils, gels, or fluids such as water, are usually used as the carrier "base" liquids and the suspensions are developed in a manner that Brownian molecular movement inhibits the sedimentation of the carried particles [9].

The justification for the use of nanotechnology or nanomaterials in fluids such as ethylene glycol (EG) was first introduced and explored by the Argonne national laboratory in Illinois, U.S. A [45]. They were among the first to recognise potential uses of these nanofluids in thermal engineering. Today, these nanofluids are utilised as heating or cooling fluids. These applications make use of the thermal stability and conductivity properties of the fluids, which play a crucial role in the development of energy-efficient heat transfer equipment [46]. Subsection 2.6.1 describes the nanofluids that are used for improved heat transfer.

### 2.6.1    Nanofluids: Improved heat transfer

The heat transfer capabilities of most conventional fluids are relatively poor as opposed to most solids [8, 52]. Table 2-2 shows the thermal conductivities of a variety of materials including solids and liquids at room temperature. Observations from the table indicate that most solid materials have 1-3 orders of magnitude higher thermal conductivities than conventional fluids such as ethylene glycol, water, or oils. Thus, the high heat capacity and conductivity of the nanoparticles of these solids, coupled with the ability of these particles to produce stable suspensions with the fluids, provide the second motivation for the investigation of the thermal transport properties of nanofluids [47]. Additionally, such suspensions may potentially demonstrate unprecedented combinations of two or more of the properties or features that may otherwise never exist, which are highly required in thermal systems.

24

*Table 2-2: The thermal conductivities for various materials at room temperature [47].*

| Material | | Thermal conductivity (W/m*K) |
|---|---|---|
| Metallic solids | Silver<br>Copper<br>Gold | 429<br>401<br>318 |
| Non-metallic solids | Diamond<br>Silicon<br>Tin(IV) oxide<br>Alumina ($Al_2O_3$) | 3300<br>148<br>40<br>40 |
| Metallic liquids | Sodium at 644K | 72,3 |
| Non-metallic liquids | Water<br>Ethylene glycol<br>Oils (Engine) | 0,613<br>0,253<br>0,145 |

The common techniques utilised in the preparation of nanofluids are discussed in the following subsection 2.6.2, followed by a description of the physico-chemical properties of these nanofluids in subsections 2.4.3.

### 2.6.2 Common nanofluid preparation techniques

The preparation of nanofluids can be accomplished using a two-step method in which nanoparticles are first separately synthesised as dry powders and then dispersed into a carrier fluid in a second process step. Alternatively, the one-step method is utilised which involves the synthesis of nanoparticles directly into the carrier fluid. Each fabrication method has its own merits and drawback, and these are further discussed in detail in sections (1) and (2).

#### (1) One-step method for the fabrication of nanofluids containing metallic nanoparticles and metal oxides.

Due to recent advances in modern technology, several methods exist for the fabrication of nanofluids via a single step process. These include the recent works by McGlynn et al [48] which involves the use of Plasma-Induced Non-equilibrium Electrochemistry (PINE) to synthesise surfactant-free nanoparticles directly into the carrier fluid, here also used as a solvent. In this method, both metallic nanoparticles and metal oxide nanocrystalline materials can be synthesized by a careful selection of precursor salts. Other methods include thermal decomposition of organometallic precursor in the presence of a stabilizing agent, chemical reduction, and polyol synthesis (the organic solvents are usually used as both stabilising and reducing agents). Apart from being highly efficient, the high energies needed required for operation make the method impractical.

25

Polyol synthesis method is one of the most popular fabrication pathways to noble metal nanoparticles. In this process, a transition metal salt serving as a precursor is dissolved in an organic polyol solvent (usually EG), the reaction conditions of the mixture are then further adjusted to allow the reduction of the metallic ions in solution by the polyol itself. This is finally followed by the particle nucleation and metal particle growth. The method is simple, however the requirement to adjust and maintain these conditions offer a potential source of difficult.

In both methods, the nanomaterials that are synthesized are surfactant-free, and there are limited ways of improving the prolonged structural stability of the nanomaterials in the suspensions.

(2) *Two-step method for the fabrication of nanofluids containing metallic nanoparticles and metal oxides.*

The fabrication of nanofluids via a two-step method begins with the separate preparation of the metallic and metal oxide nanomaterials that are to be dispersed in the carrier fluid followed by the mixing of these materials with the carrier fluid. The first step is the crucial step since the stability of the suspension in the carrier fluid relies on the stability of the nanoparticles going in.

The various synthetic methods employed in the preparation of nanomaterials were described above. Sang-Ho et al [49] described a process in which the synthesized nanomaterials can be coated with a suitable material as an intermediate step. This intermediate step occurs between nanomaterial fabrication and dispersion in a carrier suitable fluid. The intermediate step uses the hydrothermal method in the preparation of $SnO_2/SiO_2$-coated Au nanomaterials.

Hydrothermal method is based on the reaction of aqueous vapours with solid materials at high temperatures, which results in the deposition of small particles of metal oxides on surfaces of the metallic nanomaterials. That is, it results in the coating of the metallic nanomaterials with metal oxides [33]. The nanomaterials synthesised using this method have controlled sizes and shapes, and due to the stability afforded from the coating, the resulting powder thereof is thus composed of well-crystallized nanomaterials with high crystallinity.

The potential pitfalls encountered in the two-step method relating to particle agglomeration, are those that stem from the drying, storage, and redispersal of the nanomaterials in the fluid. However, by incorporating the above "hydrothermal" process one

26

can ensure that structural stability of the nanomaterials can be re-established by other means i.e., temperature or pH control [44].

### 2.6.3 *Physico-chemical properties of nanofluids*

James Clerk Maxwell [50] had the original idea of dispersing solid submicron particles into liquids. In recent years, this interest has been lacking due to the instability and rheological issues associated with the notion of the use of nanomaterials in nanofluids. However, the improved heat transfer capabilities of the nanofluids compared to the conventional fluids is undeniable and highly sought after.

The heat transfer capabilities of nanofluids involve three parameters i.e., Viscosity, Thermal conductivity, and Heat capacity [58, 59]. These are elaborated on in the sub-subsections below.

### (1) Viscosity

In most nanofluid applications, the nanofluids are subjected to otherwise harsh flow conditions, either through force or natural convection. As such, the rheological flow properties of the nanofluids are of considerable importance.

Viscosity is one of the most important transport rheological properties of a fluid. Viscosity is the fluid's resistance to flow motion which is due to the frictional forces acting between the fluid's molecules [51]. By evaluating the viscosity of the fluid, one can determine the flow behaviour of the fluid, which can be either Newtonian flow or non-Newtonian flow [52].

*Newtonian flow behaviour*- As Isaac Newton observed, the shear forces acting on a fluid can be proportional to the flow velocity. Hence, a fluid can be classified as Newtonian if the viscosity remains constant with a variation in shear rate. A small degree of deviation or complexity is expected for fluids supplemented with particles. The flow behaviour is as described using Newton's law equation (A):

$$\tau = \gamma \star \eta \ldots\ldots\ldots\ldots\ldots\ldots\ldots\ldots. \text{(A)}$$

where $\tau$ is the shear stress, $\gamma$ is the shear rate, and $\eta$ is the viscosity.

*Non-Newtonian flow behaviour*- This flow behaviour is observed in fluids with viscosities that vary with a variation in shear rate. The fluids in this classification can be

27

further classified as having shear-thinning and shear-thickening flow behaviour. The Power law (Ostwald/de Waele) describes the flow behaviour using the equation (B):

$$\tau = c \star \gamma^p \ldots\ldots\ldots\ldots\ldots\ldots\ldots \text{(B)}$$

where c is the flow coefficient (power law index), and the following conditions apply for the exponent p:

*For shear-thinning flow p < 1*

*For shear-thickening flow p >1*

*For p = 1, the Power law refers to the Newtonian law.*

The non-Newtonian as described by the Power-law has the following pitfalls, that is, it cannot be fitted well to curves with very low or very high shear rates, which are typical for most polymer suspensions.

### (2) Thermal conductivity

Xuan et al denoted that "thermal conductivity of nanofluids can be influenced by the heat transfer properties of the base fluid and the suspended particles, their volume fraction, their size, and their shape, as well as the distribution of these suspended particles [53].

*The transient Hot-wire technique-* The transient hot-wire method is the most widely used technique for the determination/measuring of thermal conductivity of nanofluids. In essence, the technique involves the measuring of the temperature/time response of a platinum wire, immersed into the fluid, to an abrupt electrical pulse [54].

### (3) Heat capacity

Heat capacity is a property of a material that expresses the ability of the material's internal energy to change with changes in temperature. It is measured by monitoring the resulting temperature changes that accompany the heating of a sample of a known amount (mass) [55]. It is determined by the ratio of the supplied energy as heat, q, to the temperature change, ΔT.

## 2.7 Summary

The literature review as provided above, outlines several important positions that current studies and research have taken in terms of the use of noble metallic nanomaterials, such as gold (Au), as potential additives in nanofluids. Firstly, it is known that noble metallic nanomaterials possess several important properties, including surface-enhanced Raman

scattering, optical behaviour, electrical and thermal conductivity, and high thermal and chemical stability, and catalytic activity- which make them attractive candidates for uses in many applications. However, because of their limited prolonged structural stability, their applicability in these applications is also limited.

Secondly, it was demonstrated that for spherical nanoparticles, the structural stability can be improved by using different surfactants, stabilizing agents, or distance-holders; $TiO_2$, $SiO_2$, $SnO_2$, and a few others have been investigated as potential distance-holding agents. However, the studies on the effects of these stabilizing agents on other structures remains lacking. Thirdly, the motivation for stabilizing Au nanoparticles by coating them with a suitable metal oxide, was provided. That is, in addition to improving the structural stability of Au nanoparticles, metal oxides can also offer additional benefits that could prove useful in further applications. However, understanding the reaction mechanisms initiated at the metallic nanoparticle interface for the coating process is complicated by many factors including spatial non-uniformities and variable timescales. Therein lies one of the purposes of this study- provide a study of the metallic nanoparticle-metal oxide coating systems i.e., $Au@SnO_2$ systems which might have some general relevance in broadening our understanding the interactions between the particle-particle, particle-coating material, and particle-coating material-surrounding medium.

Lastly, the nanofluids supplemented with metal oxide stabilized Au nanomaterials are predicted to have potential for use in improved heat transfer applications. However, the mechanism of heat transfer remains a challenge, especially with the lack of background theory from Nanotechnology.

# Chapter 3    Experimental method

## 3.1 Introduction

Chapter 3 provides detailed information on the experimental methods utilised for the sample preparations and elaborates on the techniques used for characterization of the material properties and thermal conductivity measurements. Section 3.2 is the research design section, which names the techniques and discusses the overall approaches that are used in testing the thesis statement of the study: including the strengths and weaknesses of each method used. The detailed explanation and implementation-steps of the techniques used, and the methodology used for sample preparation are provided in section 3.3 - this will include the instrumentations i.e., equipment and chemicals, data, and the analysis.

Figure 3-1 shows the schematic illustration of the research design for the project including the various techniques employed. Liquid state synthesis approaches, which include chemical reduction and hydrothermal methods were employed for the synthesis of the various Au and $SnO_2$ nanomaterials. The confirmation for the successful synthesis of these structures was accomplished through the morphological and structural characterization of the as-synthesized materials using Ultraviolet-Visible spectroscopy, TEM and SEM-EDS microscopy, and X-ray diffraction spectroscopy technique.
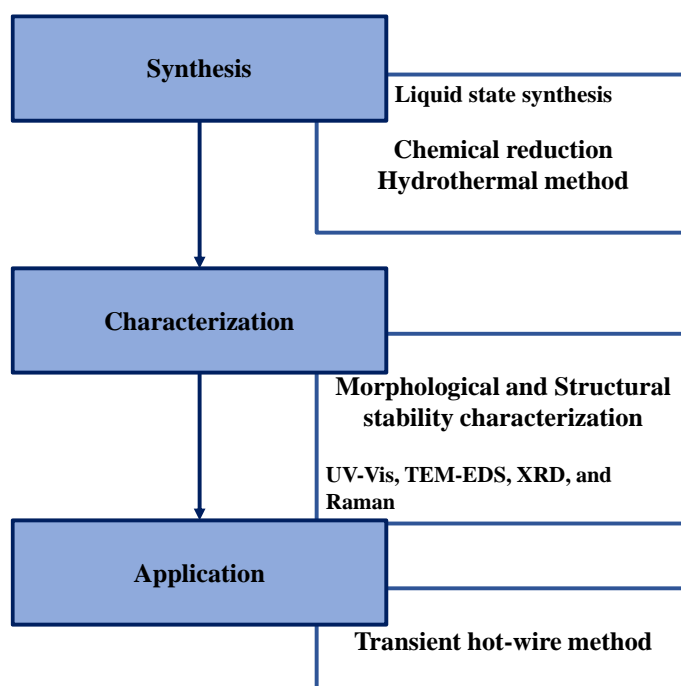


*Figure 3-1: Research design techniques and their relation in terms of workflow.*

Upon the successful synthesis of the Au@SnO$_2$ nanocomposite material, nanofluids supplemented with the Au@SnO$_2$ structures were prepared. Afterward, the transient hot-wire technique was used to evaluate the thermal conductivity of the nanofluids.

## 3.2 Experimental

### 3.2.1 Preparation of Au nanocomposite materials (Au@SnO$_2$)

The syntheses of the various Au nanostructures, including gold nanospheres (Au-NSs), gold nanorods (Au-NRs), and gold nanoprisms (Au-NPrs), are based on published seed-mediated growth procedures by Na Zhou et al [43] and Youju Huang et al [56], with some modifications. Figure 3-2 shows the experimental setup and the implementation steps taken in the synthesis of the Au nanostructures.
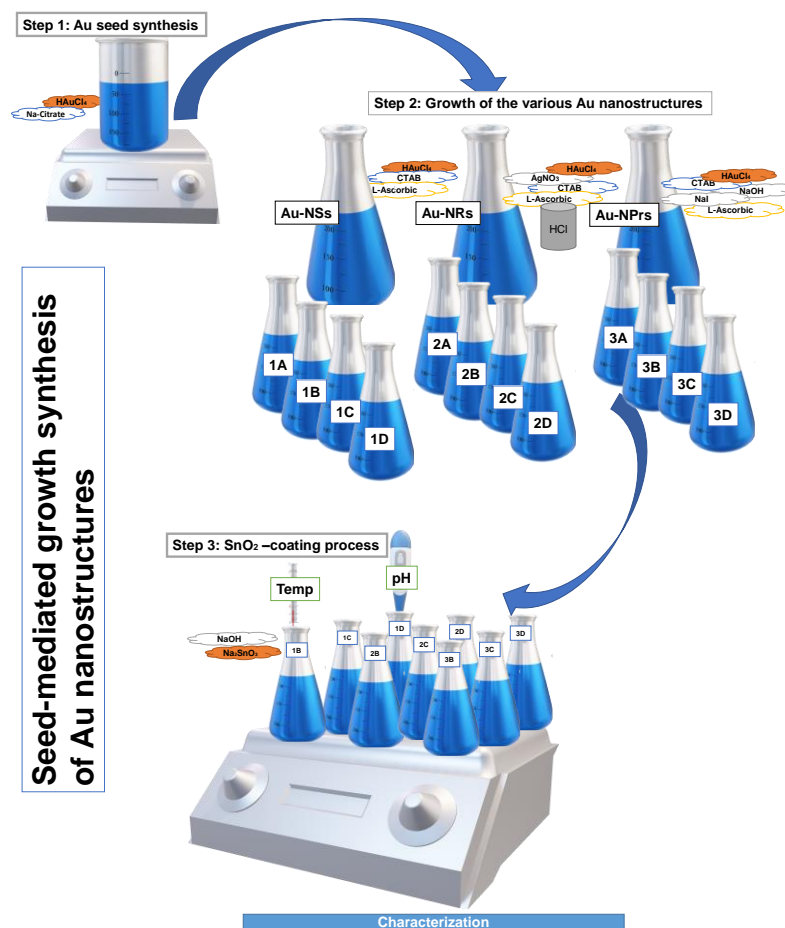


*Figure 3-2: Experimental setup and implementation for the syntheses of the various Au nanostructures.*

The chemicals, instruments and the general considerations of the process are provided ahead of the preparation steps involved in the process. And these are as follows, commercial samples of chloroauric acid trihydrate ($HAuCl_4 \cdot 3H_2O$), cetyltrimethylammonium bromide (CTAB), silver nitrate ($AgNO_3$), sodium citrate, sodium hydroxide (NaOH), sodium iodide (NaI), sodium stannate trihydrate ($Na_2SnO_3 \cdot 3H_2O$), hydrochloric acid (HCl), and L-ascorbic acid, were purchased from Sigma-Aldrich and used as received. All manipulations including weighing and material transfers were performed in air. All glassware was cleaned and rinsed well with deionized water prior to use. Ultra-pure water and deionized water obtained from the Modulab Water system, was used in the synthetic preparations and stability measurements.

(1) *Step 1: Au-nano seed synthesis*

**Preparation of Au nanoseeds (Au-Seeds):** The initial step in the preparation of various Au nanostructures is the synthesis of Au nanoseeds. The ruby-red seed solution was first prepared through a hydrothermal process by heating 20 ml of the pale-yellow $2.5 \times 10^{-4}$ M $HAuCl_4$ solution for 30 min. Followed by rapid addition of 2 ml of 1% sodium citrate solution into the boiling Au precursor solution. After 20 min of consistent heating, the colour of the boiling mixture solution changed from pale-yellow to the ruby-red colour, indicating the formation of the citrate-capped Au nanoparticles in the solution. The Au-seed solution was cooled to room temperature and used without modification for the following preparations.

(2) *Step 2: Seed-mediated growth*

**Seed-mediated growth of the various Au nanostructures:** The second step involves the use of the prepared Au-seeds for the synthesis of Au-NSs, Au-NRs, and Au-NPrs. To achieve effective control over the desired shapes and the sizes, different concentrations of the surface passivation reagents i.e., $AgNO_3$, NaI, L-ascorbic acid, are used to induce the desired selective directional growth of the Au-seeds.

**Preparation of the Au nanospheres (Au-NSs):** Four portions of the growth solution consisting of 225 μl of 0.01 M $HAuCl_4$, 9 ml of 0.01 M CTAB, and 50 μl of 0.1 M of freshly prepared L-ascorbic acid were prepared by gentle stirring for 2 min, and placed in four separate flasks, labelled 1A,1B,1C, and 1D. The growth solutions were initially yellow orange in appearance, which then turned clear upon the addition of the L-ascorbic acid. Finally, 500 μl of the Au-seed solution was added into each flask mixture and kept at room

32

temperature overnight. The CTAB-capped Au-NSs were obtained as deep wine-red solutions.

**Preparation of the Au nanorods (Au-NRs):** A 45 ml growth solution was prepared by carefully and sequentially adding a mixture of 2 ml of 0.01 M $HAuCl_4$ and 280 μl of 0.01 M $AgNO_3$ to 40 ml of 0.1 M CTAB solution and mixed well by gentle shaking. To this solution mixture, 320 μl of 0.1 M freshly prepared L-ascorbic acid was added, followed by a subsequent addition of 800 μl of 1.0 M HCl. The growth solution was initially pale-yellow due to the dissolution of the gold salt, however upon the addition of $AgNO_3$ the solution became milky orange. Further colour changes occurred following the addition of L-ascorbic acid, from milky orange to milky white, and from milky white to clear after the addition of HCl. 96 μl of the prepared Au-seed solution was added into the clear coloured growth mixture. The growing reaction mixture was left overnight undisturbed to allow longitudinal growth of the Au-seeds. Finally, 40 ml of CTAB-capped Au-NRs was divided into 4 portions 10 ml each and placed into four separate flasks, labelled 2A, 2B, 2C, and 2D.

**Preparation of Au nanoprisms (Au-NPrs):** The growth solution was prepared by sequentially mixing the following solutions in the order provided, 108 ml solution of 0.025 M CTAB, 1.5 ml solution of 0.02 M $HAuCl_4$, and 600 μl solution of 0.1 M NaOH, 54 μl solution of 0.1 M NaI, and 600 μl solution of L-ascorbic acid. The colour changes of the solution mixture went from pale orange to milky white, after the addition of L-ascorbic acid. To allow for the anisotropic growth of the triangular Au-NPrs, it was imperative to use glass beakers for the addition of the Au-seeds, which was handled in a multistep manner as follows. First, 100 μl of the Au-seed solution was added into 900 μl of the growth mixture with gentle shaking, this was immediately followed by a slight colour change from milky white to pale purple, indicating formation of Au-nanoparticles. Secondly, the pale-purple mixture was immediately added to 9 ml of the growth mixture with gentle shaking. Finally, the 10 ml pale-purple mixture was further added to the remaining 92 ml of the growth solution. An hour into the growth process, the mixture turned deep purple, it was further left undisturbed overnight to allow for the attachment of the triangular nanoparticles to the walls of the glass beakers. Lastly, 40 ml of CTAB-capped Au-NPrs was divided into 4 portions 10 ml each and placed into four separate flasks, labelled 3A, 3B, 3C, and 3D.

(3) *Step 3: SnO₂-coating around the Au nanostructures*

**Preparation of the SnO₂ -coated Au nanostructures (Au@SnO₂):** The procedure for the formation of the SnO₂-coated nanocomposite materials of Au-NSs and Au-NRs was as outlined by Na Zhou et al [43], which we extended to the preparation of Au-Prs@SnO₂. Table 3-2 shows the reaction conditions used for the SnO₂ coating of the Au nanostructures. Briefly, 5 ml from each of the CTAB-capped Au-NSs, Au-NRs, and Au-NPrs samples (labelled 1B, 1C, 1D, 2B, 2C, 2D, 3B, 3C, and 3D) were diluted to 20 ml with deionized water and placed in separate round-bottom flasks, labelled similarly. The pH of each solution was adjusted to 10.5 by adding NaOH. The solutions were heated to a temperature of 75⁰C under vigorous stirring for 15 min, followed by rapid additions of 3 ml of the freshly prepared $Na_2SnO_3 \cdot 3H_2O$ in the amounts indicated in table 3-2. After 2 h of stirring, the obtained Au@SnO₂ samples were centrifuged at 7000 rpm, washed twice, and redispersed in 5 ml of deionized water.

*Table 3-1: Reaction conditions for the SnO₂-coating of the Au nanostructures. Each of the samples contain the same amounts of their respective Au nanostructures i.e., Au-NSs, Au-NRs, and Au-NPrs, however the concentration of the distance-holder is varied.*

| | Au-NSs (5 ml) Samples | Au-NRs (5 ml) Samples | Au-NPrs (5 ml) Samples |
|---|---|---|---|
| $Na_2SnO_3 \cdot 3H_2O$ (3 ml) | 1A - | 2A - | 3A - |
| | 1B 4 mM | 2B 4 mM | 3B 4 mM |
| | 1C 2 mM | 2C 2 mM | 3C 2 mM |
| | 1D 1 mM | 2D 1 mM | 3D 1 mM |

### 3.2.2 *Characterization of the Au@SnO₂ nanocomposite materials*

Figure 3-3 shows the characterization techniques that are employed to evaluate the morphologies, crystallinity, and the optical properties of the prepared nanomaterials Au nanospheres, nanorods, nanoprisms, and their nanocomposites.
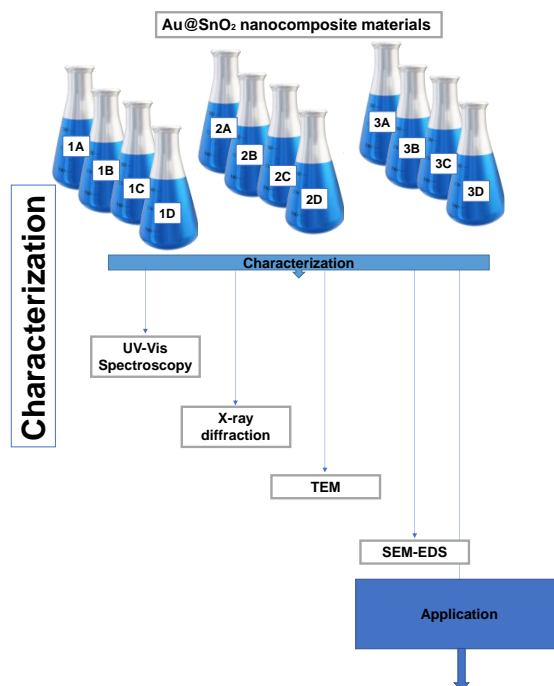
34

*Figure 3-3:The characterization techniques employed for the characterization of the synthesized Au@SnO₂ nanocomposite materials.*

UV-Vis spectroscopic analyses were performed using a Varian Cary 500 UV spectrometer within the wavelength range from 200 nm - 1100 nm to study the optical properties and colloidal stabilities of the pristine Au nanospheres, nanorods, nanoprisms and their Au@SnO$_2$ nanocomposite material. The as-synthesized samples were dissolved in deionized water and placed in a clean quartz cuvette and diluted to the mark with deionized water. The measurements were performed thrice on each sample at intervals of 1 month for a comparative analysis of their colloidal stab.

XRD measurements were performed using CuKα-radiation with wavelength λ equal to 1.5418 Å, and the diffractometer was operated in the 2θ mode (30 - 90º range) with step-scan of 0.05º on the prepared samples. The prepared solutions of the nanoparticles were deposited on glass substrates using a pipette and used for the XRD measurements.

The size and morphology of the SnO$_2$-coated and uncoated Au nanostructures were determined using a JEOL FEGTEM-2100 FX transmission electron microscope (TEM) operating at a bias voltage of 200 kV. Several TEM micrographs were obtained for the samples at similar magnifications and analysed using ImageJ software.

Zeiss 540 Ultra and Zeiss 540 X-beam (FEGSEM) scanning electron microscopes were used together with the energy dispersive spectrometer to provide further information and determine the morphologies of the as-synthesized Au@SnO$_2$ samples. The elemental

35

compositions of the as-prepared materials were studied using EDS coupled to the SEM instrument.

### 3.2.3 *Transient hot-wire apparatus measurements.*

**Synthesis of the Au@SnO$_2$ nanofluids:** To prepare the nanofluids, 10 ml of each Au@SnO$_2$ sample solution was transferred into an empty 50 ml test tube. 40 ml of ethylene glycol was added into each test tube containing the samples, with gentle shaking. The suspensions were thus, consisting of a mixture of ethylene glycol, deionized water, and the Au@SnO$_2$ nanocomposite materials. Figure 3-4 shows the arrangement of these Au@SnO$_2$-Ethylene glycol (EG) nanofluids.
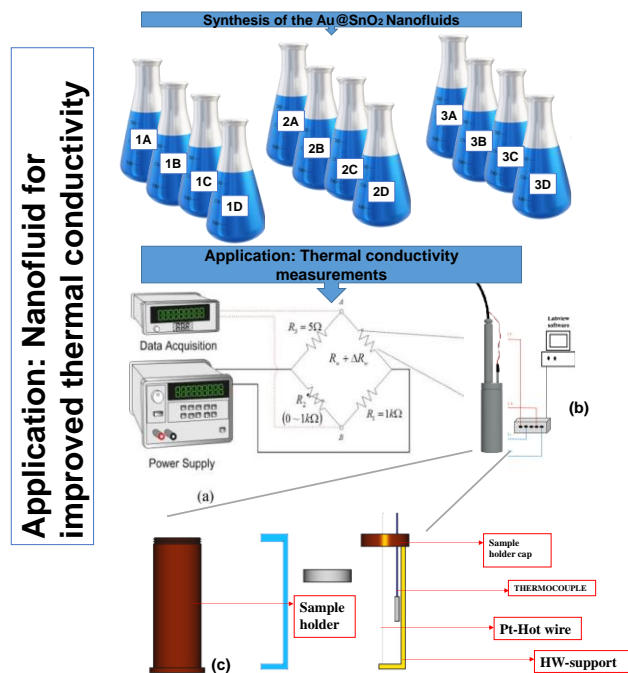


*Figure 3-4: Setup of the apparatus for the transient hot-wire method for thermal conductivity measurements of the Au@SnO$_2$ nanofluids.*

**Apparatus (Transient hot-wire device):** The hot-wire device setup is as shown in Figure 3-4 (a – b). The apparatus setup included a 10 cm long 0.404 mm diameter platinum wire heat source. Other apparatus included a power supply, digital data-logger, a Wheatstone bridge consisting of 3 resistors (with the hot-wire serving as the fourth resistance), and a nanovoltmeter. Figure 3-5 shows the actual 45 ml capacity cell device for thermal conductivity measurements. All the components are connected to a computer equipped with LabView software program to allow for automatic control of the instruments, the data acquisition, and storage of the data. The parameters controlled with the software were the voltage and the power supplied by the source.

36

*Figure 3-5: The actual experimental thermal conductivity cell device.*

**Determination of the thermal conductivity of the nanofluids (Au@SnO₂-EG):** The mathematical model governing the hot-wire technique considers a thin and infinitely long linear source of heat with a uniform temperature distribution, that is immersed into a homogeneous and infinite test material. The model assumes that, due to the conductive heat transfer to the material, the temperature of the source will vary as a function of time. The working equation developed for the phenomenon is derived from the non-stationary heat diffusion Fourier equation with proper boundary conditions, and with a well-known solution [57]. For extended periods of measurement so that $t \gg r^2/\alpha = \tau$ , where r is the source radius and $\alpha$ is the material thermal diffusivity, and by neglecting heat losses through convection and radiation, leads to

$$\Delta T(t) = \frac{q}{4\pi k} \ln \frac{4t\alpha}{r^2 C}$$

$$= \frac{q}{4\pi k} \ln \frac{4t}{\tau C} \qquad (3-1)$$

From the several methods proposed for the measurement of thermal conductivity, the hot-wire technique is the most employed and well established. The following procedures and implementation are as followed by most published works, such as that by Alvarado et al [58].

37

Equation 3-3 (A), rewritten below,

$$V(t) = I * R_0 \left\{ 1 + \sigma \left[ \frac{q}{4\pi \mathbf{k}} \ln \frac{4t}{\tau C} \right] \right\} \dots\dots\dots\dots\dots\dots\dots\dots\text{(A)}$$

can be linearized as follows:

$$V(t) - I * R_0 = I * R_0 * \sigma \left[ \frac{q}{4\pi \mathbf{k}} \ln \frac{4t}{\tau C} \right]$$

$$\Delta V(t) = m * \ln t + B \dots\dots\dots\dots\dots\dots\dots\dots\dots\dots\dots\dots\text{(B)}$$

Here $\Delta V(t) = V(t) - I*R_0$, where $V(t)$ is the voltage at any instant $t$, $m = I*R_0*\sigma*q/4\pi k$, and $B = m*\ln(4/\tau C)$. Differentiating the linear equation with respect to $\ln(t)$, we obtain

$$\frac{d\Delta V(t)}{d(\ln t)} = m$$

$$= \frac{I^3 R_0{}^2 \sigma}{4\pi L k} \qquad\qquad (3-4)$$

Thus, the slope m of the curve of $\Delta V(t)$ as a function of $\ln(t)$ is obtainable by taking the least-square fit in linear region of the curve. If the initial resistance of the wire $R_0$, its temperature coefficient $\sigma$, and the current $I$ are known and controllable variables, then the thermal conductivity $\mathbf{k}$ can be calculated from the value of the slope m.

The first experiment consisted of a heating process (heating for a duration of 5 min) in which the potential difference $V(t)$ across the terminals of wire was measured (measurements were performed every second). A plot of the data of the potential difference $V(t)$ as a function of $\ln(t)$ was obtained, from which the slope m of the linear region of the graph and the current value were noted.

To confirm that the selected linear region is correct, equation 3-4 also shows that there is a relationship existing between the slope m and the applied current $I$.

$$m = b * I^3 \qquad\qquad (3-5)$$

Where $b = \frac{R_0{}^2 \sigma}{4\pi L k}$. Thus, by taking the natural logarithm on both sides of equation 3-4, we can get

$$\ln(m) = 3 * \ln(I) + \ln(b) \qquad\qquad (3-6)$$

By performing the above experiment for different values of the current (50, 75, 100, 125, 150, 175, 200 mA), one can then calculate the slopes at each current iteration. This was the second experiment, from which a plot of each slope as a function its current in a double

logarithmic scale graph, was obtained. Thus, if as given in equation 3-6, the gradient of the resulting linear graph is 3, then one can be certain that the selection is correct.

Finally, to determine the conductivity of the nanofluids the following observation was made. Equation 3-5 shows that there is a linear relationship between the slopes m and the values of cubic currents $I^3$. By plotting a curve of the slopes m as a function of the cubic currents $I^3$, one will obtain the gradient is equal to b, from which the thermal conductivity was calculated using equation 3-5.

**Chapter 4      Nanofluids composed of the various Au nanomaterials.**

As mentioned in chapters 2 and 3, noble metallic nanomaterials such as gold (Au) together with its various sub-structures; gold nanospheres (Au-NSs), gold nanorods (Au-NRs), and gold nanoprisms (Au-NPRs), have impeccable properties making them exceptional candidates in nanofluid synthesis. These properties are strongly depended on their morphological and structural features, such as size, shape, dimensionality, crystallinity, and surface characteristics (or parameters).

In thermal engineering, nanofluids are often synthesized by supplementing conventional fluids with nanocrystalline solids. However, despite being the best candidates having 1-3 orders of magnitude higher thermal conductivities compared to the conventional fluids, most nanocrystalline solids like noble metallic nanomaterials lack the structural stability crucial for most practical applications.

Herein, we aimed to overcome this issue through the preparation of monodisperse metallic nano-colloids protected by an agent (a surfactant or a distance-holder), whose primary purpose is to prevent particle agglomeration, and the results obtained for the gold based nanofluids are reported in the following sections. Distance-holder coatings on particles are said to reduce susceptibility to particle aggregation, enhance the underlying properties of the particle and protect particle surfaces from oxidation [90]. Furthermore, we report on the thermal properties of the nanofluids.

Section 4.1 reports the results of the synthesis of the nanofluids composed of gold nanospheres, which include the morphological and structural properties of the particles, as well as the thermal properties of the nanofluids. The same reporting approach is followed for the nanofluids composed of gold nanorods, in section 4.2; and finally, for the nanofluids composed of gold nanoprisms in section 4.3. Section 4.4 summarises the discussions of the results.

**4.1 Synthesis, structure, and thermal properties of Au spherical nanofluids.**

The preparation of CTAB-stabilized and $SnO_2$-coated Au nanospheres, in contrast to the synthesis of their nanofluids, is well documented in literature [49]. These studies have resulted in particles with sizes ranging from 20 nm to 50 nm, with optical surface plasmonic resonance (SPR) absorption in the range 520 nm to 550 nm, and structural properties typical of FCC crystallinity. For this study, the structures were synthesized using procedures adapted from the indicated literature.

The morphological properties -with respect to particle formation and size distribution were investigated and are reported in sections 4.1.1 and 4.1.2. The optical properties -with respect to UV-VIS wavelength absorbency, of the colloids and their structural properties are reported in sections 4.1.3 and 4.1.4. The thermal properties -the thermal conductivity of various ethylene glycol-based nanofluids are reported in section 4.1.5.

### 4.1.1 Morphological properties: TEM

Transmission electron microscopy (TEM) was used to study the size and morphology of the gold nanospheres (Au-NSs). Figure 4-1 (A-C) shows the TEM micrographs with corresponding particle size distributions. For a comparative analysis, the CTAB-stabilized Au-NSs were monitored for a prior of three months. Figure 4-1 (A) shows a TEM micrograph revealing well-dispersed and crystalline Au nano-spherical particles with an average size less than 12 nm. A particle size distribution of $\sim 12 \pm 24$ nm was obtained in the first month after the optimized synthesis conditions, this led to pure spherical products with negligible amounts of by-products. The size distribution is relatively broad. Figure 4-1 (B) shows a TEM micrograph revealing partially well-dispersed and crystalline Au nano-spherical particles with an average size less than 31 nm. A particle size distribution of $\sim 31 \pm 32$ nm was obtained in the second month after the synthesis. At this stage agglomerate products with sizes between 20-30 nm were observed. Figure 4-1 (C) shows a TEM micrograph revealing mostly agglomerate products with sizes more than 31 nm. A particle size distribution of $\sim 27 \pm 14$ nm was obtained in the third month after the synthesis.
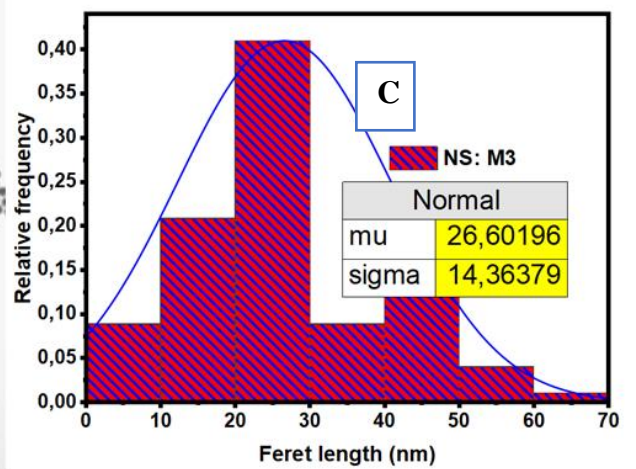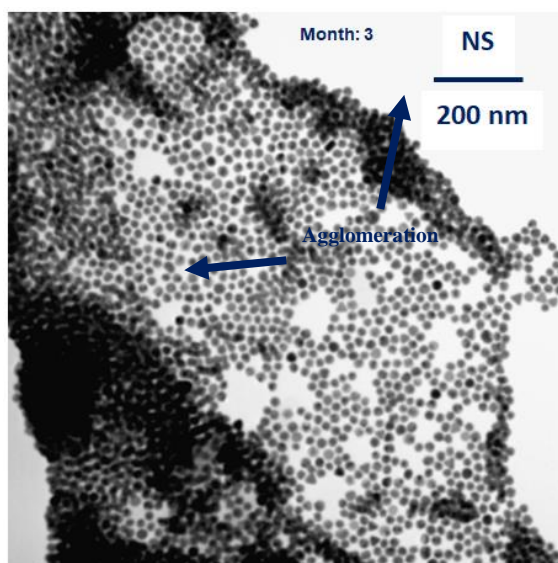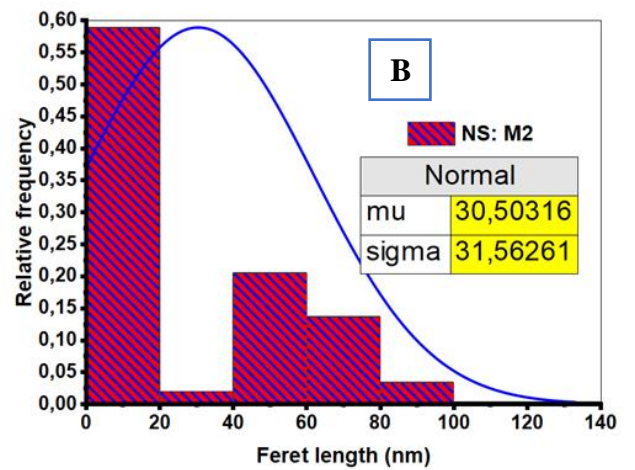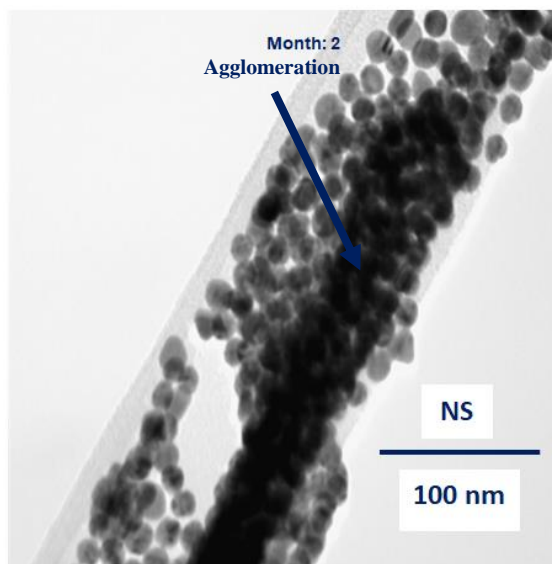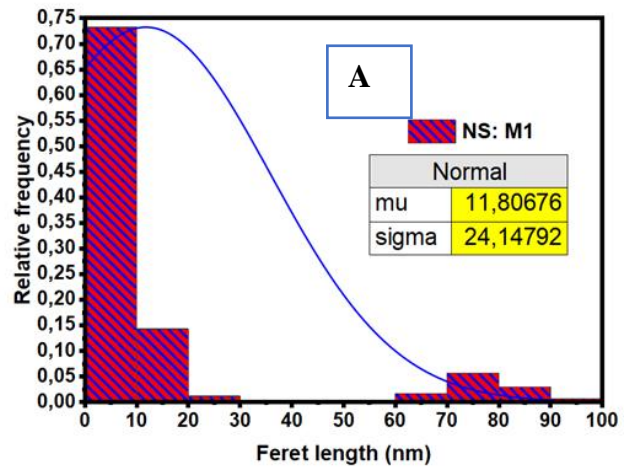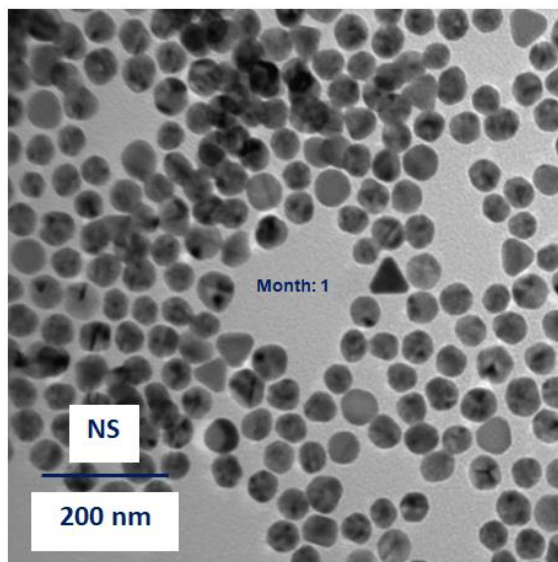
*Figure 4-1: TEM micrographs of the CTAB stabilized- Au nanospheres (Au-NSs) and their corresponding particle size distributions. A- for the Au-NSs a month after synthesis, B- for the Au-NSs two months after synthesis, and C- for the Au-NSs three months after.*

42

Transmission electron microscopy (TEM) was also used to study the size and morphology of the $SnO_2$-coated gold nanospheres (Au-NSs@$SnO_2$). Figure 4-2 (A-E) shows the TEM micrographs with corresponding particle size distributions. All the particles in these micrographs are assumed to have the same particle diameter sizes as those in first month, that is (~12 ± 24 nm). Thus, the particle size distributions in Figure 4-2 indicate the coating thickness of $SnO_2$ around these 12 nm diameter Au-NS particles. Figure 4-2 (A) shows a TEM micrograph revealing well-dispersed and crystalline Au nanospheres coated with a $SnO_2$ with an average coating thickness size less than 13 nm, giving rise to average composite particle diameters of ~25 nm. Figures 4-2 (B-C) show TEM micrographs revealing still well-dispersed and crystalline Au nanospheres coated with a $SnO_2$ with average coating thickness sizes less than 22.5 and 52 nm, respectively, giving rise to average composite particle diameters of ~34 and ~64 nm, respectively. The largest $SnO_2$ coating thicknesses are observed in Figures 4-2 (D-E), which show TEM micrographs revealing still well-dispersed and crystalline Au nanospheres coated with a $SnO_2$ with average coating thickness sizes of 91.3 and 155 nm, respectively, giving rise to average composite particle diameters of ~103.3 and ~167 nm, respectively. These micrographs also reveal a significant presence of gold-free $SnO_2$ nanocrystalline materials, representing less than ~10% of the particle distributions.

44
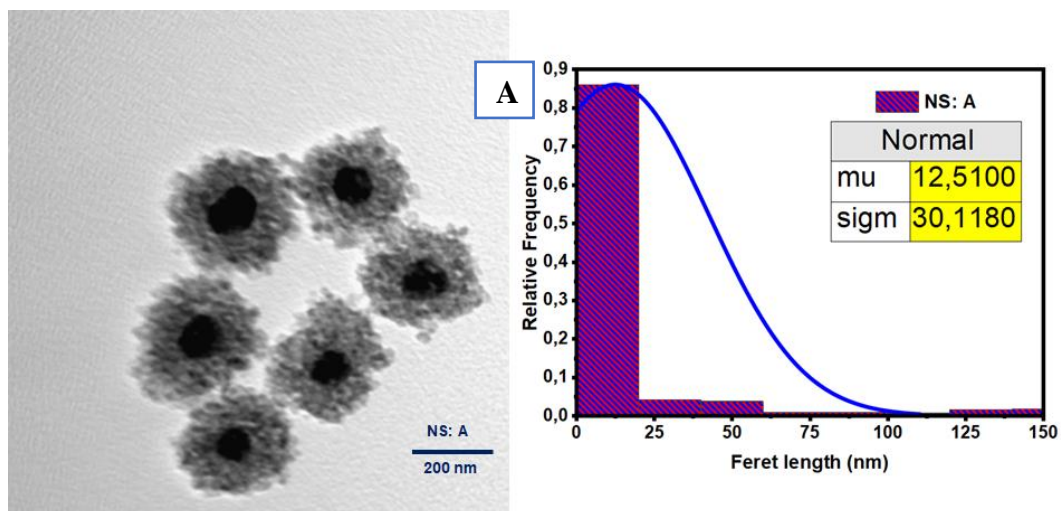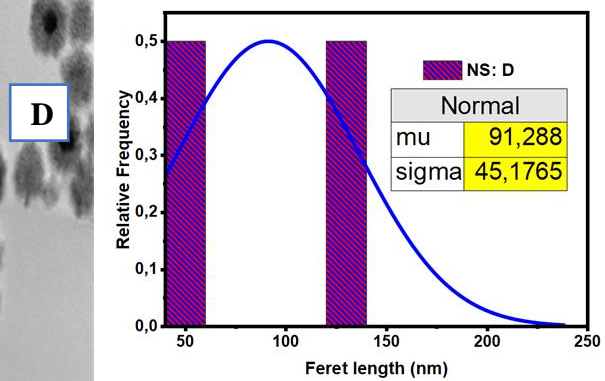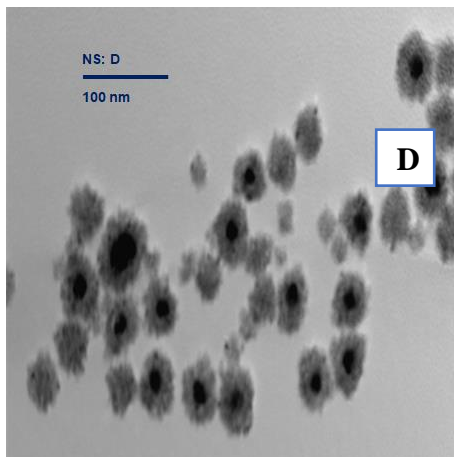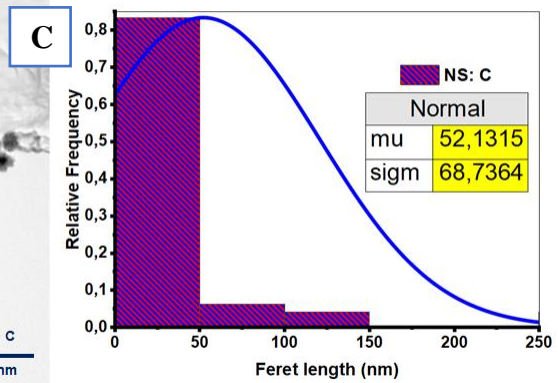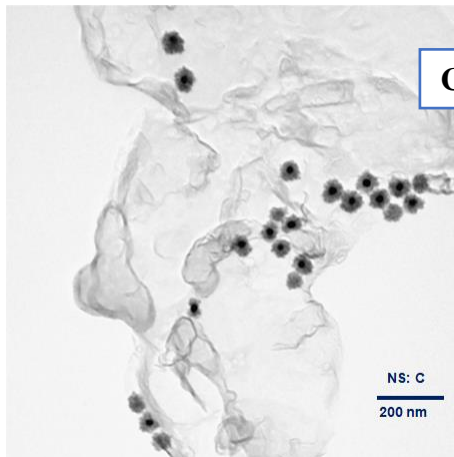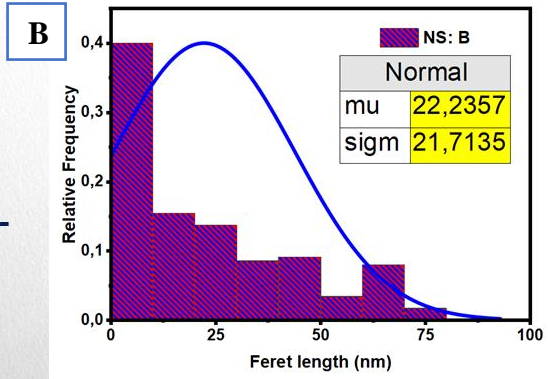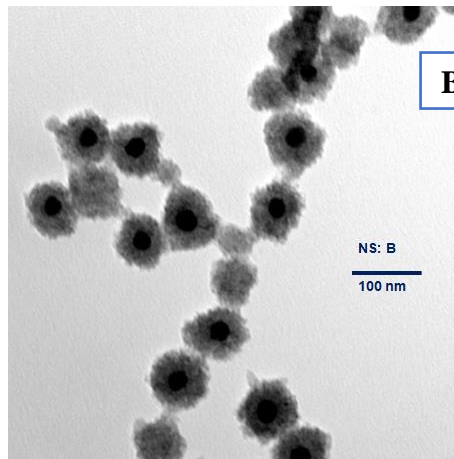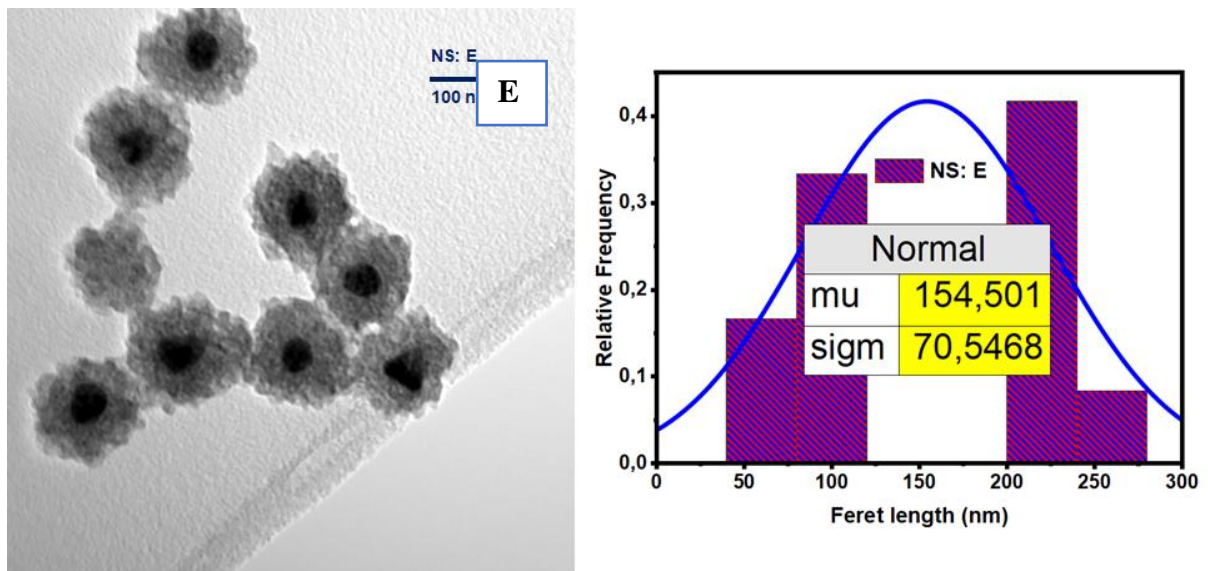
*Figure 4-2: TEM micrographs of the SnO₂ stabilized- Au nanospheres (Au-NSs) and their corresponding particle size distributions. A- for 1 mM SnO₂ concentration, B- for 2 mM SnO₂ concentration, C- for 3 mM SnO₂ concentration, D- for 4 mM SnO₂ concentration and E- for 5 mM SnO₂ concentration.*

### 4.1.2 *Morphological properties: SEM-EDS*

The extended morphological features of the Au-NSs samples and the relationship between the structures and composite elemental distributions were characterized using the Scanning electron microscope (SEM) coupled with Electron Energy Dispersive Spectroscopy (EDS).



*Figure 4-3: SEM micrographs of the CTAB stabilized- Au nanospheres (Au-NSs), photographed a month and three months after synthesis.*

The scanning electron microscopy (SEM) micrographs in Figure 4-3 show the particle formations and the size distributions of the CTAB-stabilized Au-NSs, in the first and third month after the initial synthesis. In the first month, SEM micrographs reveal that the nano-

45

spherical particles had little to limited agglomeration present, as demonstrated by the small sized aggregate formations. The micrograph also shows a significant number of smaller sized (< 100 nm) mono-dispersed Au-NSs. However, in the third month, a significant fraction of the image is composed entirely of large sized aggregates (>200 nm).



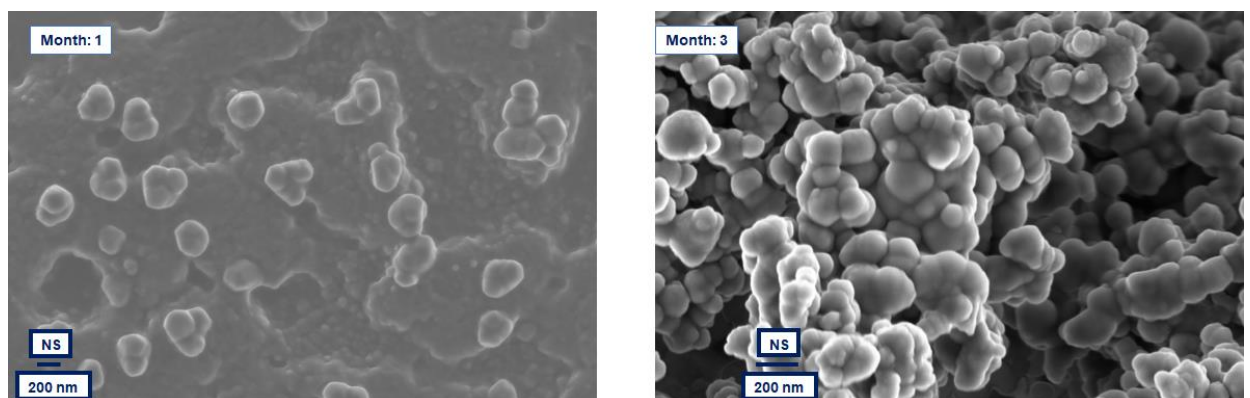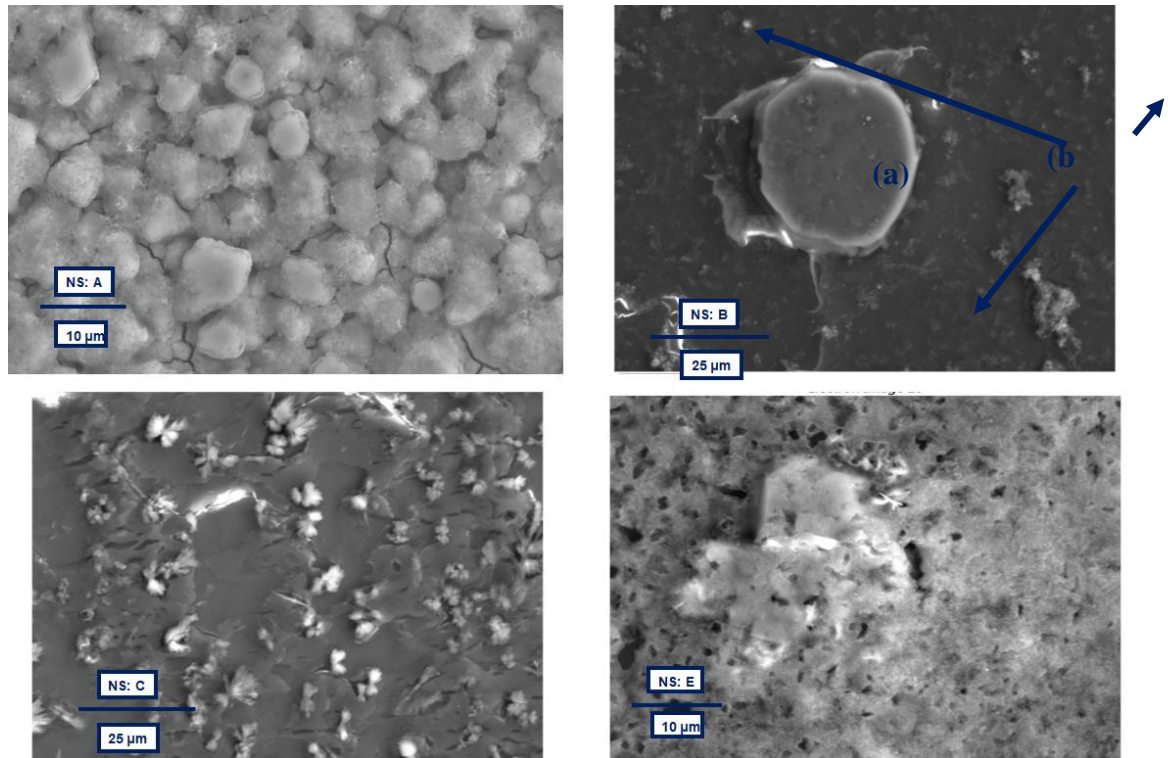*Figure 4-4: SEM micrographs of the SnO₂ stabilized- Au nanospheres (Au-NSs). NS: A-for 1 mM SnO₂ concentration, NS: B- for 2 mM SnO₂ concentration, NS: C- for 3 mM SnO₂ concentration, for NS: E- for 5 mM SnO₂ concentration.*

Figure 4-4 (A-E) show SEM micrographs revealing SnO$_2$-coated gold (Au@SnO$_2$) nanocrystalline materials with varying sizes. Image (NS: B) reveals a planar spherical large composite material (a) and other small size composites (b). This image was further investigated with EDS instrument to reveal the elemental composition of the structures.

Figure 4-5 consists of the elemental EDS micrographs revealing which elements are presents in the SEM micrograph (NS: B). From the Figure, we observe the elements of Au, Sn and Na. These appear to be in significant amounts in region (a) and only in trace amounts in region (b). O is present in large amounts of in region (b) but only in small traces in region (a).

Figure 4-6 shows an in-depth elemental analysis of the image (NS: B), this reveal that elements are present as averaged in the accompanying table. The table shows that the amounts of the elements of Sn and O are slightly higher than that for Au, consistent to the expectations of Au being coated with SnO$_2$.

46
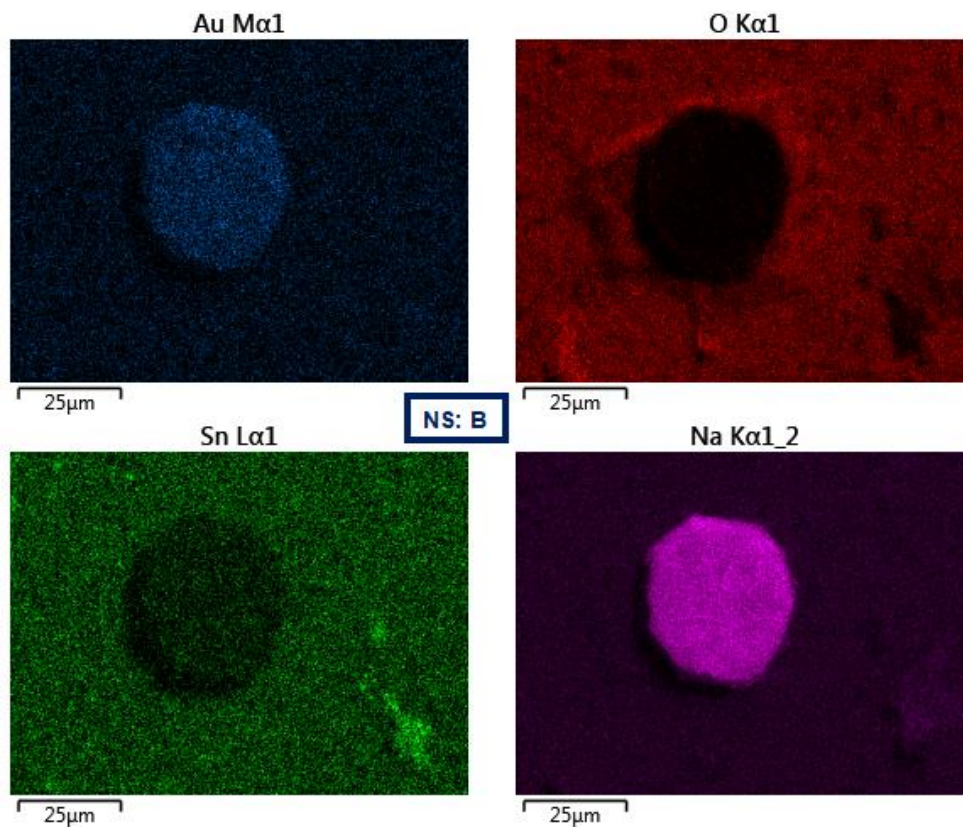
*Figure 4-5: EDS micrograph of sample NS: B for the 2 mM SnO₂ stabilized- Au nanospheres (Au-NSs).*
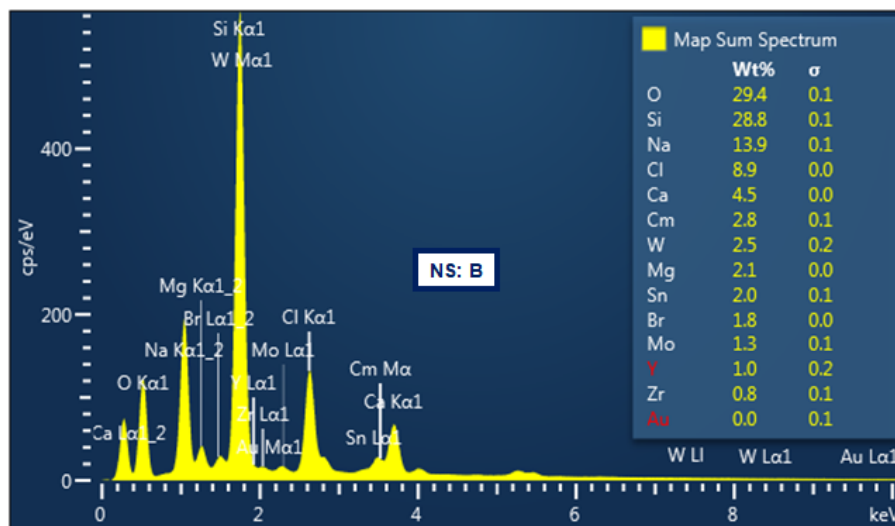


*Figure 4-6: EDS absorption spectrum of sample NS: B for the 2 mM SnO₂ stabilized- Au nanospheres (Au-NSs). Elemental analysis table showing the percentage amounts of the elements Au, Sn, and O.*

47

### 4.1.3   *Optical properties: UV-Vis*

As Murphy et al. [59] illustrated in their report, Isotropic Au-NSs exhibit single localised surface plasmonic resonance (LSPR) corresponding to the length of the particles, known as the transverse surface plasmon resonances (SPRT). Similar remarks were reported by Lee et.al [43]. Therein, the SPRT mode was observed as a strong peak with the peak position that can be tuned artificially in a UV-VIS spectral region by altering either the sizes of the Au-NSs or the surrounding conditions and arrangement [11, 12].

Figure 4-7 shows the optical absorption properties of the CTAB-stabilized and the $SnO_2$-coated Au nanospheres (Au-NSs). To analyse the structural stability of the Au-NSs, their optical properties were measured and monitored for a period of three months. In the first month, the SPRT band is observed at ~520 nm for the CTAB-stabilised Au-NSs and at ~530 nm for the Au@SnO2 solutions, respectively, consistent with previously reported values [17,28]. The largest redshift is observed for the highly concentrated sample (NS: E). The red shifts of the SPRT bands for the coated particles are attributable to the high refractive index of $SnO_2$ coatings of (2.2) [30]. Notably, these SPRT positions and redshifts are consistently observed for the second and third months.  SPRT band broadening is observed for the CTAB-stabilized Au-NSs in the second and third months, this is attributable to the increasing size distributions of the concerned particles – owing to the agglomeration of the particles.

The SPRT band for the CTAB-stabilised Au-NSs is relatively broad, consistent with the particle size distribution shown in Figure 4-1. The optical absorption spectra of the $SnO_2$-coated Au-NSs also reveal the dependence of the absorption on the $SnO_2$ concentration, this indicates an increase in absorption with an increase in $SnO_2$ concentration.
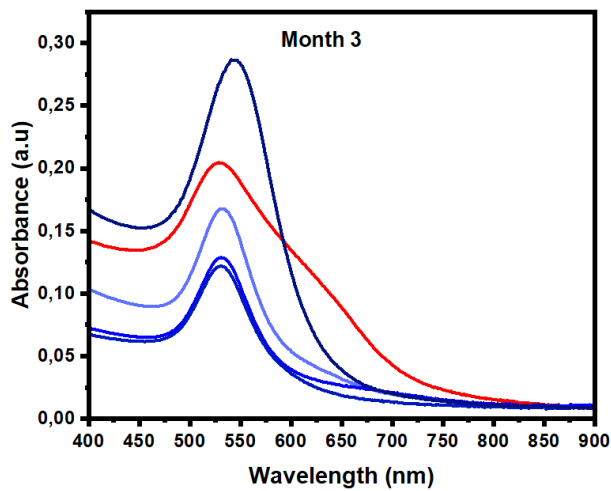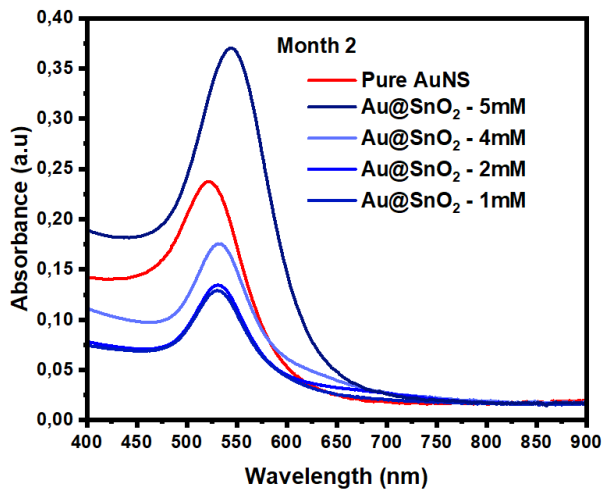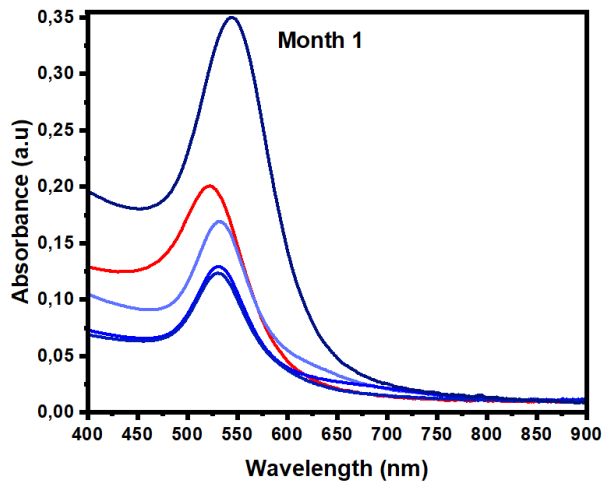
*Figure 4-7: UV-VIS spectra obtained for the CTAB-stabilized and the SnO$_2$-stabilized Au-NSs. The spectra are obtained for Month 1, Month 2, and Month 3 after synthesis. These show absorption in the region where gold nanoparticles are known to absorb (~520 nm).*

49

![University of Pretoria logo]

### 4.1.4 *Structural properties: XRD*

The crystalline structure of the gold nanospheres were reported from previous studies by Song et al. [60]. From their reported XRD profile, it was demonstrated that with increasing shell thickness, the intensity of the $SnO_2$ peaks increase due to an increase in crystallinity.

The XRD profile reported in Figure 4-8 confirms that the gold nanospheres were crystalline. The diffraction peaks can be indexed to those of pure face-centred cubic (FCC) crystal lattice, corresponding to the (111), (200), (220), and (311) planes respectively, in good agreement with literature [102]. Similar observations were made for the profile for the $SnO_2$-coated Au-NSs, that is, the FCC planes are also observed together with the planes for the $SnO_2$ crystallinity, corresponding to planes (110), (101), (200), (210), (211), (220) and (002), typical for a rutile tetragonal lattice structure. The proposed crystal lattice structure for $SnO_2$ is provided in Figure 4-9.

Figure 4-8 also reveals that the intensity of the XRD peaks of the Au-NSs is reduced after $SnO_2$, this behaviour could be attributed to the masking of the faces (planes) of the structures. This implies that the surface is thus less active compared to the pure uncoated Au-NSs.
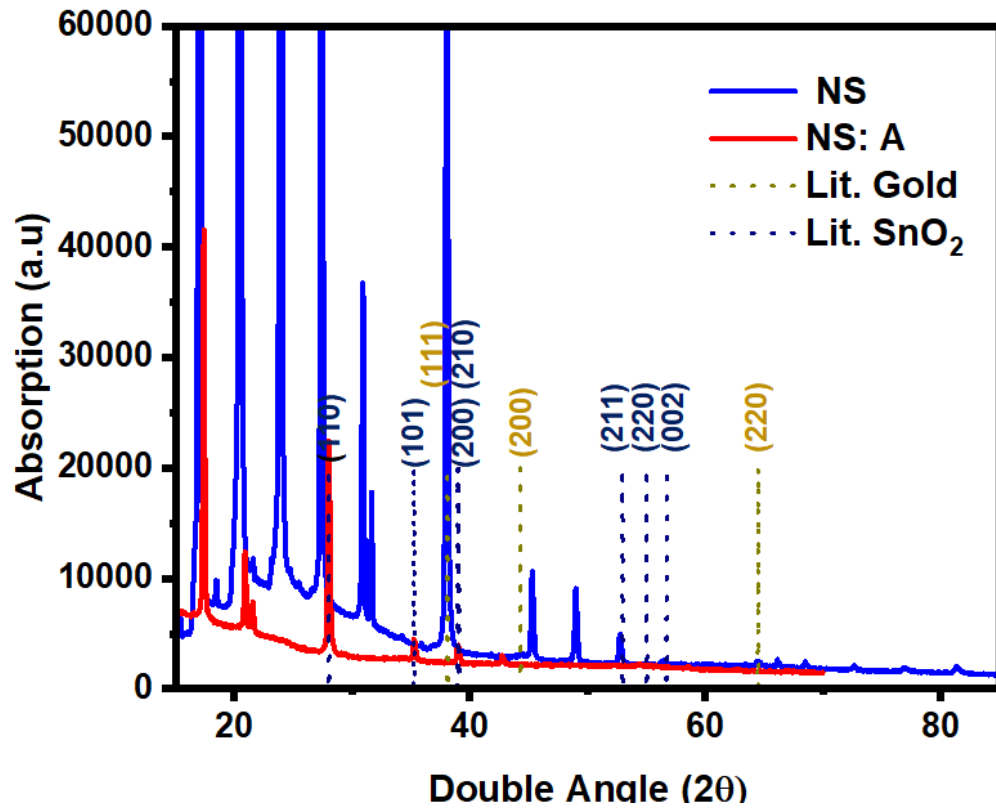
*Figure 4-8: XRD patterns of the pure and SnO$_2$-protected gold nanospheres.*
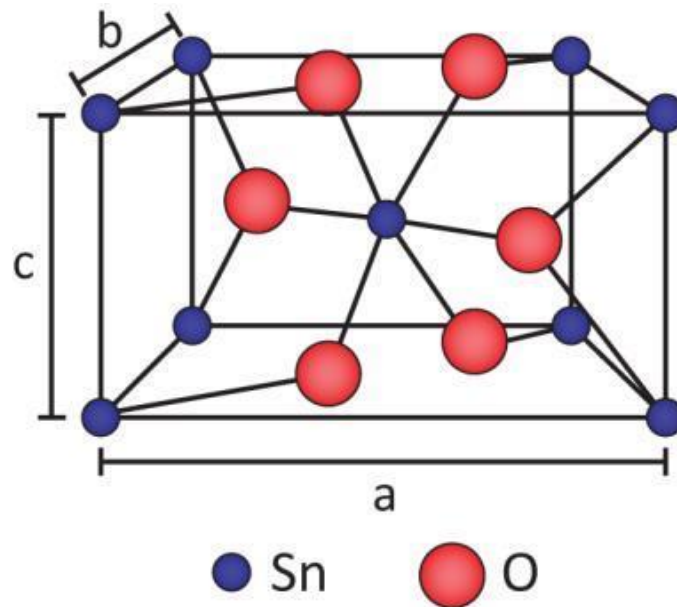


*Figure 4-9: The reported proposed crystalline structure of SnO$_2$.*

### 4.1.5   Nanofluid application: Thermal conductivity

Ethylene glycol is a dihydroxy alcohol derivative of aliphatic hydrocarbons. It is mostly found in various antifreeze solutions and liquid coolants. It is often used as a liquid coolant for heat transportation in automotive heavy-duty engine radiators. Other similar substances include methanol, mineral oils, transformer oils and water.

As mentioned in chapter 3, nanofluids can be prepared using either a one-step method or a two-step method. For this study, a two-step method was followed. This method involved combining a conventional heat transfer fluid, ethylene glycol, with metallic nanomaterials that have a much higher thermal conductivity than the fluid. The properties of the metallic nanospheres were reported in the sections above. The thermal properties of the nanofluids composed of these particles are reported as follows.
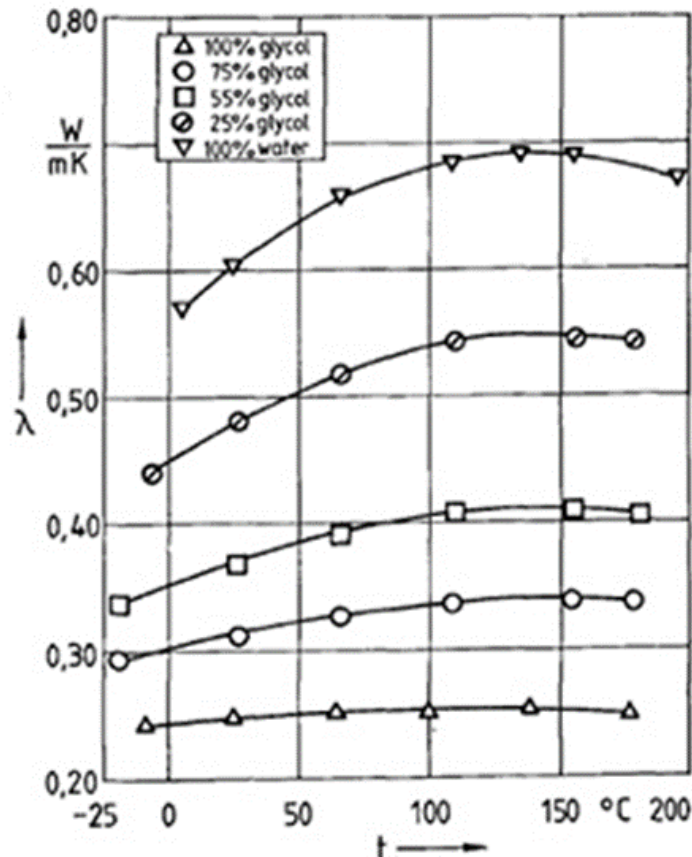


*Figure 4-10: The literature thermal conductivities of Ethylene glycol-water mixtures [61].*

For this study, the nanospheres were initially carried in appropriate amounts of distilled water, as indicated in chapter 3. As such, to avoid disturbing of the structural stability of the colloidal solutions -by drying the products, we prepared nanofluids from a

52

mixture of Ethylene glycol and the water in the colloids. Figure 4-10 shows the literature reported thermal conductivities of various ethylene glycol-water mixtures, to be used as a reference guide for analysis.

Figure 4-11 shows typical results obtained for our Ethylene glycol (EG)-water mixture of 60% EG. As was illustrated by Alvarado et al [58], the theoretical model of the transient hot-wire technique relies only on the heat transfer by conduction. This mode of heat dissipation causes appreciable deviations in the behaviour of the curve of the change in voltage ΔV as a function of time t when the heating current exceeds a certain value. This can be appreciated in Figure 4-11 (A) for the measurements carried out with currents from 200 to 250 mA, where significant deviations are observed in the path of the curve revealing the presence of convection. For this reason, these measurements were not used to determine the thermal conductivity. From the remaining ΔV versus ln(t) plots, the solid lines represent the best least-squares linear fits following equation (3-4) from which the slopes m were obtained. The linear regions in the graphs of Figure 4-11 (A) have been selected by trial and error according to the discussion in chapter 3. Figure 4-11 (B) shows that the slope of the least-squares linear fit of the graph ln(m) versus ln(I) is equal to 2.9023, which is close to 3, the value required by equation. From the graph of m versus $I^3$, the value of coefficient b is obtained from a least-squares linear fit using equation (3-5) and it is equal to $0,0607558 \pm 0,000171114$. Then using the equation for the thermal conductivity, we obtained the thermal conductivity for our 60%EG mixture of $k = (0.502 \pm 0.384)$ W∘m$^{-1}$∘K$^{-1}$, from Figure 4-10 this implies that our mixture had more water content than expected. Applying the same procedure for the other investigated nanofluids the observed results are shown in the last subsections in each section 4.1, 4.2 and 4.3.
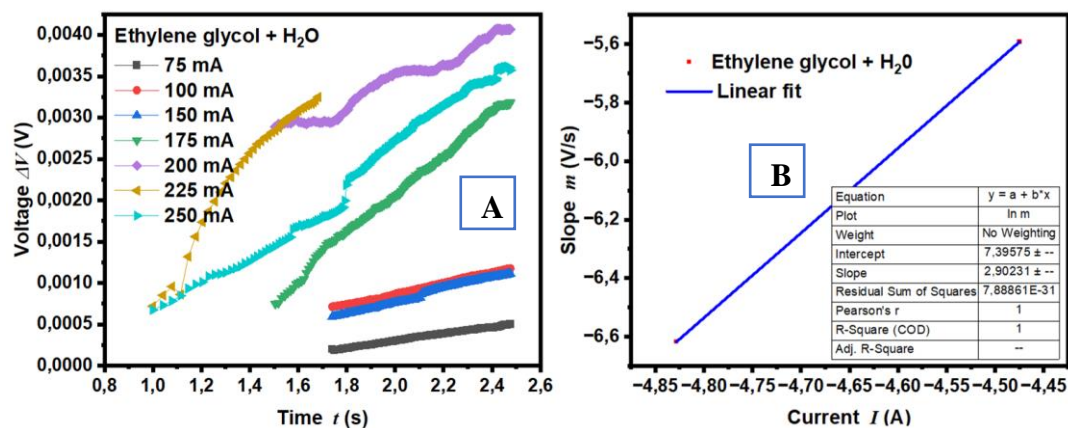


*Figure 4-11: A- Semi-logarithmic plot of the voltage increases as a function of time for different current values showing the best least-squares linear fit over the linear regions of the curves. B- Plot of the slopes ln(m) versus ln(I). The solid line represents the results of the best least-squares linear fit. These are obtained from the Ethylene glycol (EG) – water mixture base fluid.*

53

*Table 4-1: Showing the measured thermal conductivity of our Ethylene glycol-water mixture (80% EG) and the literature values of the pure substances (Water and EG).*

| | k (W m−1 K−1) | Std. |
|---|---|---|
| Ethylene glycol + Distilled Water | 0,502 | 0,384 |
| Ethylene glycol (J T Baker 99.90%) Reported | 0,256 | |
| Distilled Water (Q P) Reported | 0,609 | |

The nanofluids composed of the CTAB-stabilised and $SnO_2$-coated gold nanospheres Au-NSs, are shown in Figure 4-12. The Figure includes images of the samples before and after pure ethylene glycol was added to make the ~60% EG mixture solutions.
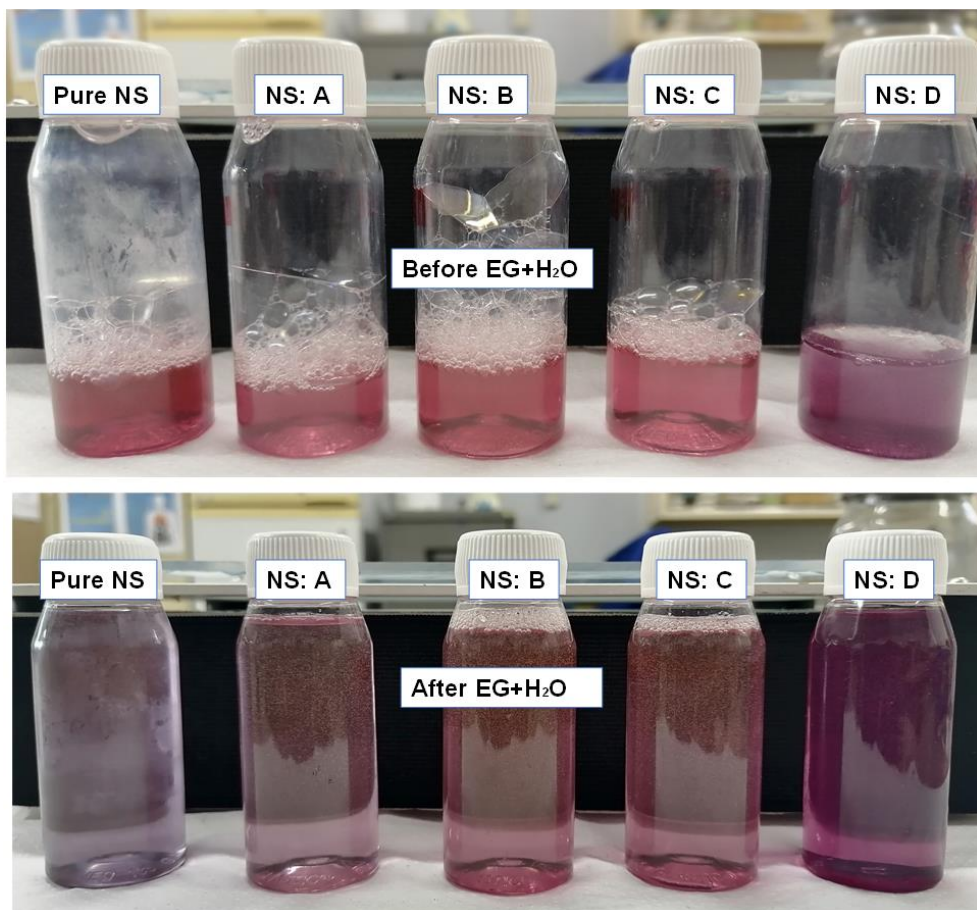


*Figure 4-12: The pure Au-NSs and Au@SnO$_2$ based nanofluids.*

Figure 4-13 (A1, A2 and A3) shows the $\Delta V$ versus ln(t) plots for the rejected (Noisy) and the accepted (Linear) currents. From these plots, the graphs of m versus $I^3$ were obtained as shown in Figure 4-13 (B1, B2 and B3), whose least-square linear fits are also displayed. The CTAB-stabilised Au-NSs (A1 and B1) sample resulted in a fitted plot with slope

54

$3.39269 \pm 0.86409$, which is close to 3 as required. The SnO$_2$-coated Au-NSs (A2 and B2, and A3 and B3) samples resulted in fitted plots with slopes $2.57738 \pm 0.7541$ and $2.23377 \pm 0.19735$, respectively, which are also close to the required value of 3. The deviation is attributed to a less-than good choice of the required linear regions.



| Equation | y = a + b*x |
|---|---|
| Plot | ln m |
| Weight | No Weighting |
| Intercept | 17,70628 ± 6,6394 |
| Slope | 3,39269 ± 0,86409 |
| Residual Sum of Square | 17,80727 |
| Pearson's r | 0,86896 |
| R-Square (COD) | 0,75509 |
| Adj. R-Square | 0,70611 |



| Equation | y = a + b*x |
|---|---|
| Plot | ln m |
| Weight | No Weighting |
| Intercept | -15,58069 ± 3,536 |
| Slope | -2,57738 ± 0,7541 |
| Residual Sum of Squa | 0,72417 |
| Pearson's r | -0,92402 |
| R-Square (COD) | 0,85381 |
| Adj. R-Square | 0,78071 |



| Equation | y = a + b*x |
|---|---|
| Plot | ln m |
| Weight | No Weighting |
| Intercept | 6,99714 ± 0,99142 |
| Slope | 2,23377 ± 0,19735 |
| Residual Sum of Squares | 0,03042 |
| Pearson's r | 0,99612 |
| R-Square (COD) | 0,99225 |
| Adj. R-Square | 0,98451 |

*Figure 4-13: A- Semi-logarithmic plot of the voltage increases as a function of time for different current values showing the best least-squares linear fit over the linear regions of the curves. B- Plot of the slopes ln(m) versus ln(I). The solid line represents the results of the best least-squares linear fit. These are obtained from the nanofluids of (1)- pure Au-NSs, (2)- 1 mM Au@SnO$_2$, and (3)- 2 mM Au@SnO$_2$, carried in 80% Ethylene glycol (EG) – water mixture base fluid.*

55

Then by using the corresponding equations and the graphs of m versus $I^3$ to obtain the value of the coefficient b, we were able to obtain the thermal conductivities shown in Figure 4- 14.

Figure 4-14 reveals that the CTAB-stabilised Au-NSs resulted in thermal properties in the order like that of the base fluid (60% EG mixture) with thermal conductivity of 0.501 ± 0.216 W∘m$^{-1}$∘K$^{-1}$, while the SnO$_2$-coated Au-NSs (NS: A) resulted in the expected improvement in the thermal properties with thermal conductivity of 1.242 ± 0.955 W∘m$^{-1}$∘K$^{-1}$. The unexpected low thermal conductivity (0.105 ± 0.072 W∘m$^{-1}$∘K$^{-1}$) of the higher concentrated SnO$_2$-coated Au-NSs for the NS: B sample is observed. This unexpected result may be caused by excessive precipitation of Au@SnO$_2$ particles created by over coating, that later occurred.
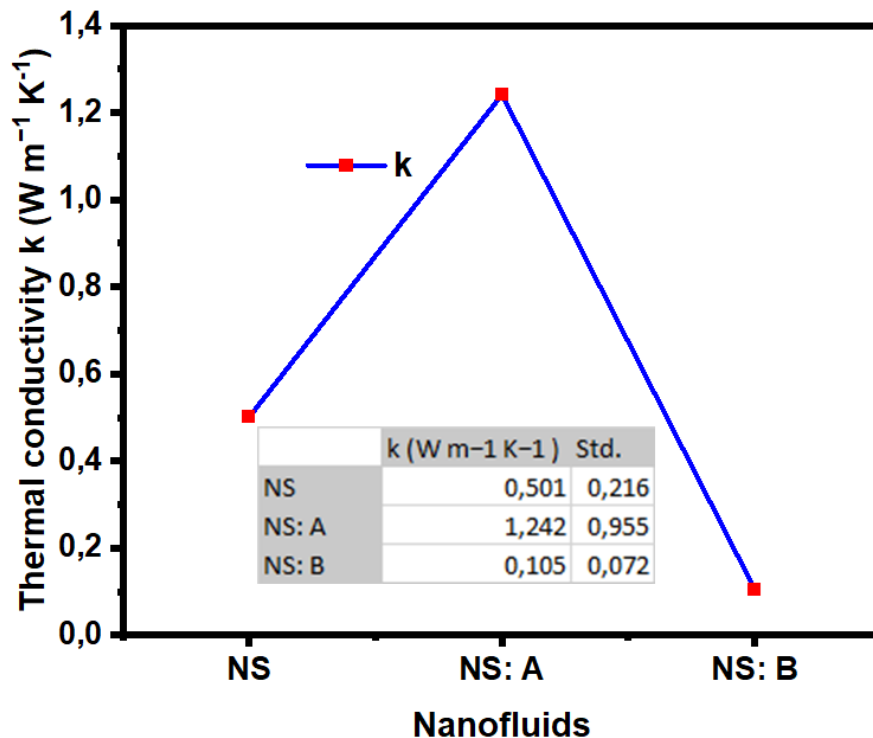


*Figure 4-14: Thermal conductivity variation as a function of SnO$_2$ coating thickness concentration for the Au-NSs.*

## 4.2 Synthesis, structure, and thermal properties Au rod nanofluids.

The preparation of CTAB-stabilized and SnO$_2$-coated gold nanorods was as described in the method chapter of this report, based on published materials [48, 4]. The published studies have reported particles with a length averaging 45 ± 2 nm and a diameter averaging of 12 ± 1.5

nm. These are very high aspect-ratio nanorod structures with optical localised surface plasmonic resonance (LSPR) absorptions in the range 520 nm to 700 nm, and structural properties typical of FCC crystallinity. For our study, the structures were synthesized using modified procedures adapted from the indicated literatures.

The morphological properties -with respect to particle formation and size distribution were investigated and are reported in sections 4.2.1 and 4.2.2. The optical properties -with respect to UV-VIS wavelength absorbency, of the colloids and their structural properties are reported in sections 4.2.3 and 4.2.4. The thermal properties -the thermal conductivity of various ethylene glycol-based nanofluids are reported in section 4.2.5.

### *4.2.1 Morphological properties: TEM*

Transmission electron microscopy (TEM) was used to study the size and morphology of the gold nanorods (Au-NRs). Figure 4-15 shows the TEM micrograph with the corresponding particle length distribution. The TEM micrograph reveals well-dispersed and crystalline Au nanorod particles with average diameter size like those of their constituent Au-seeds of less than 12 nm, the micrograph reports their lengths of ~110 nm. A particle size distribution of ~110 ± 48 nm was obtained in the first month after the optimized synthesis conditions, this led to pure rod products with negligible amounts of by-products.



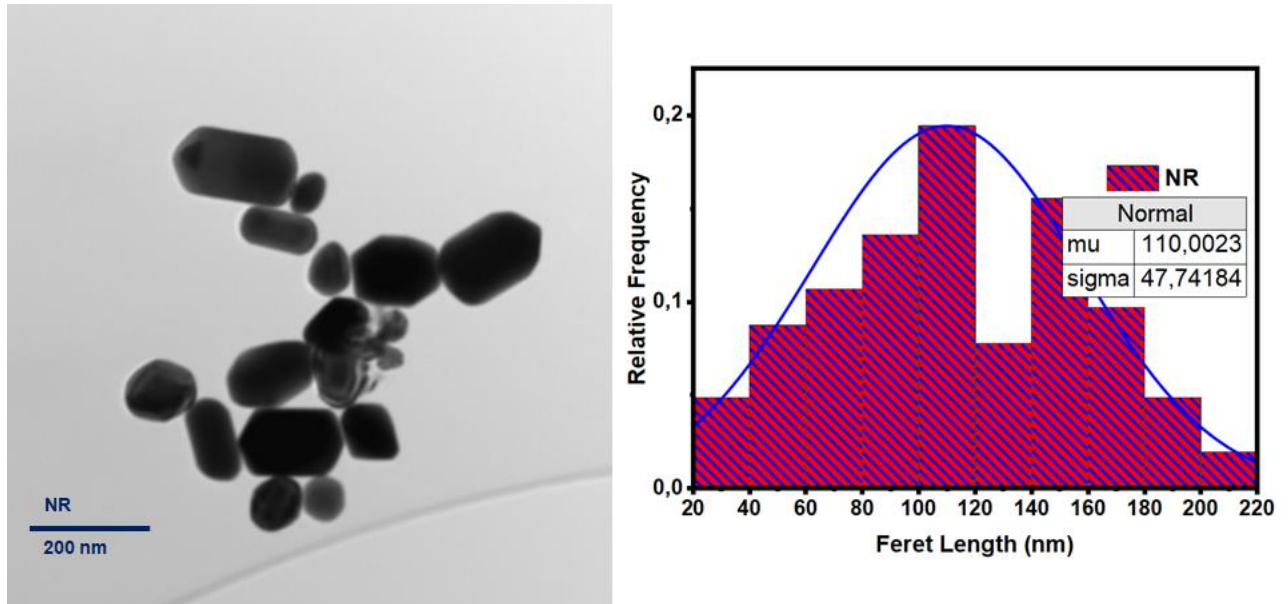*Figure 4-15: TEM micrograph of the CTAB stabilized- Au nanorods (Au-NRs) and their corresponding particle size distributions.*

Transmission electron microscopy (TEM) was also used to study the size and morphology of the $SnO_2$-coated gold nanorods (Au-NRs@$SnO_2$). Figure 4-16 (A-D) reports the TEM micrographs with corresponding coating thickness -length- distributions. All the particles in

57

these micrographs are assumed to have the same particle diameter sizes and lengths as those of their constituent Au-seeds solution of ~12 ± 24 nm and ~110 ± 48 nm, respectively. Thus, the distributions in Figure 4-16, report on the $SnO_2$-coating thickness.

Figure 4-16 (A) shows a TEM micrograph revealing well-dispersed and crystalline Au nanorod structures coated with a $SnO_2$ with an average coating thickness size less than 25 nm, giving rise to composite particles with average dimensions of ~37 and 122 nm for the diameter (d) and length (l:), respectively. Figures 4-16 (B-C) show TEM micrographs revealing still well-dispersed and crystalline Au nanorod-like structures coated with a $SnO_2$ with average coating thickness sizes of ~110 and 127 nm, respectively, giving rise to composite particles with average dimensions of [~ 122 and 220 nm for the diameter (d: ) and length (l: ) for NR: B] and [~ 139 and 237 nm for the diameter (d: ) and length (l: ) for NR: B], respectively. For (NR: B), a significant presence of gold-free $SnO_2$ nanocrystalline materials, representing more than ~10% of the particle distribution. The largest $SnO_2$ coating thicknesses are observed in Figures 4-16 (D), which show TEM micrographs revealing still well-dispersed and crystalline Au nanorod-like structures coated with a $SnO_2$ with average coating thickness sizes of 186 nm, giving rise to composite particles with average dimensions of ~198 and 296 nm for the diameter (d) and length (l), respectively. These micrographs also reveal a significant presence of gold-free $SnO_2$ nanocrystalline materials, representing more than ~30% of the particle distributions.
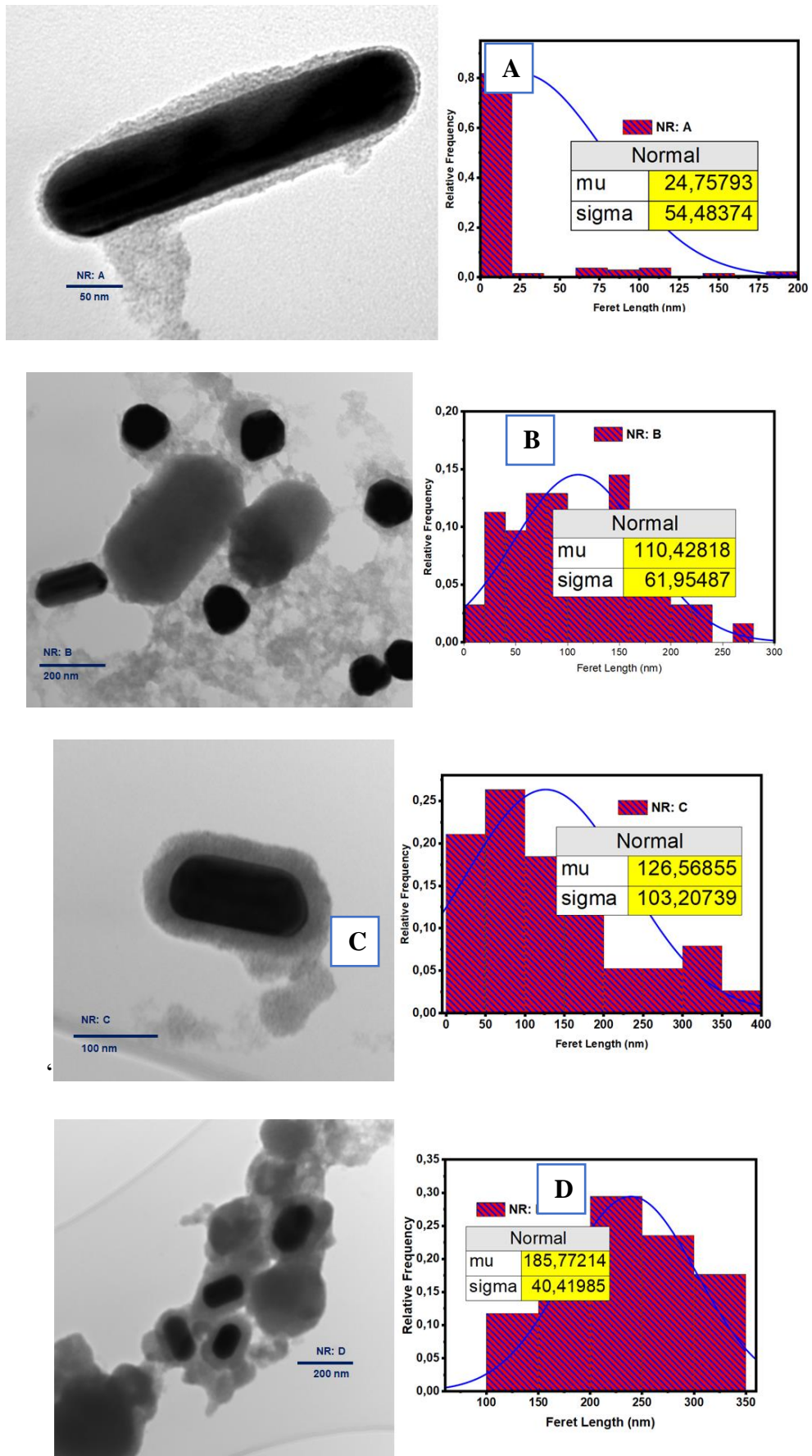
*Figure 4-16: TEM micrographs of the SnO₂ stabilized- Au nanorods (Au-NRs) and their corresponding particle size distributions. A- for 1 mM SnO₂ concentration, B- for 2 mM SnO₂ concentration, C- for 3 mM SnO₂ concentration, and D- for 4 mM SnO₂ concentration.*

59

### 4.2.2 Morphological properties: SEM-EDS

Additional morphological features of the Au-NRs samples and the relationship between the structures and composite elemental distributions were characterized using the Scanning electron microscope (SEM) coupled with Electron Energy Dispersive Spectroscopy (EDS).
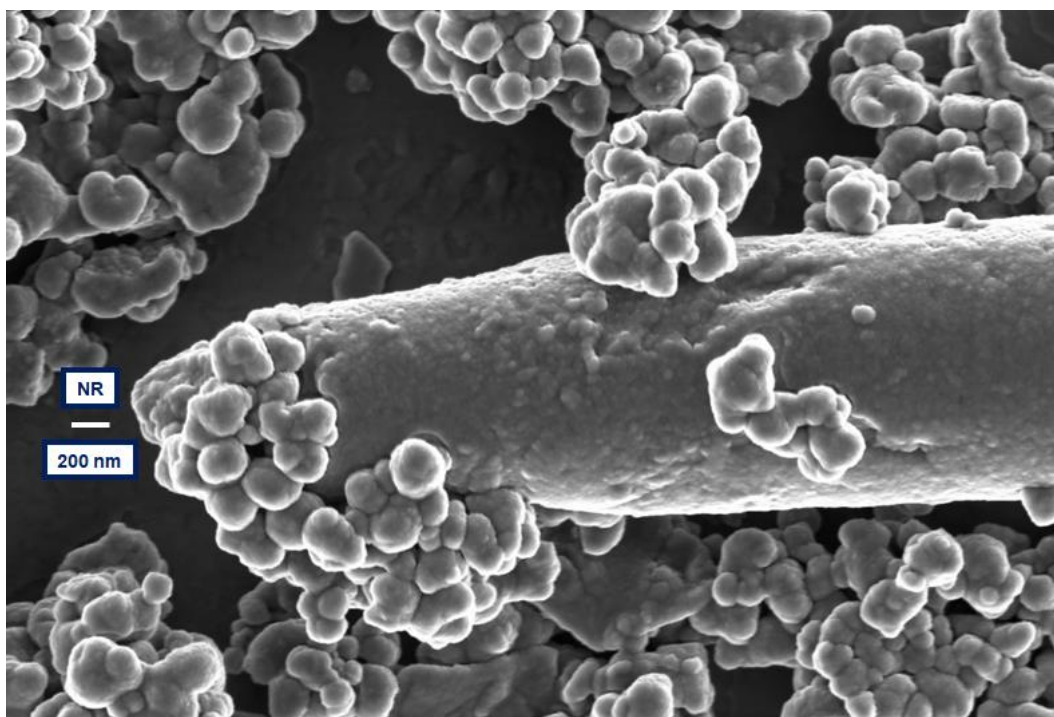


*Figure 4-17: SEM micrograph of the CTAB stabilized- Au nanorods (Au-NRs).*

The scanning electron microscopy (SEM) micrograph in Figure 4-17 shows the particle formation and the size distributions of the CTAB-stabilized Au-NRs. The SEM micrographs reveal the nanorod particle with other non-rod particle having little to limited agglomeration, as demonstrated by the small sized aggregate formations.

Figure 4-18 (A-C) show SEM micrographs revealing $SnO_2$-coated gold (Au@$SnO_2$) nanocrystalline materials with varying sizes. The images reveal planar structures composed of the composite material Au-NRs. These images were further investigated with the EDS instrument to reveal the elemental composition of the structures.

60
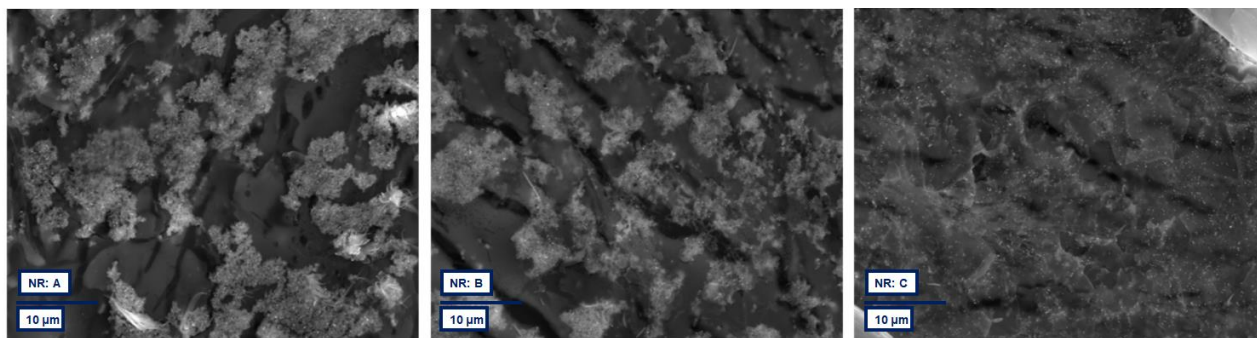
*Figure 4-18: SEM micrographs of the SnO₂ stabilized- Au nanorods (Au-NRs). NR: A- for 1 mM SnO₂ concentration, NR: B- for 2 mM SnO₂ concentration, and NR: C- for 3 mM SnO₂ concentration.*

Figure 4-19 consists of the elemental EDS micrographs revealing which elements are presents in the SEM micrographs (NR: A, NR: B and NR: C). From the Figures, we observe the elements of Au, Sn and O. The elements of Sn and O appear to be in larger concentration amounts compared to Au, which is consistent to the expectation of the Au-NRs being covered by $SnO_2$.
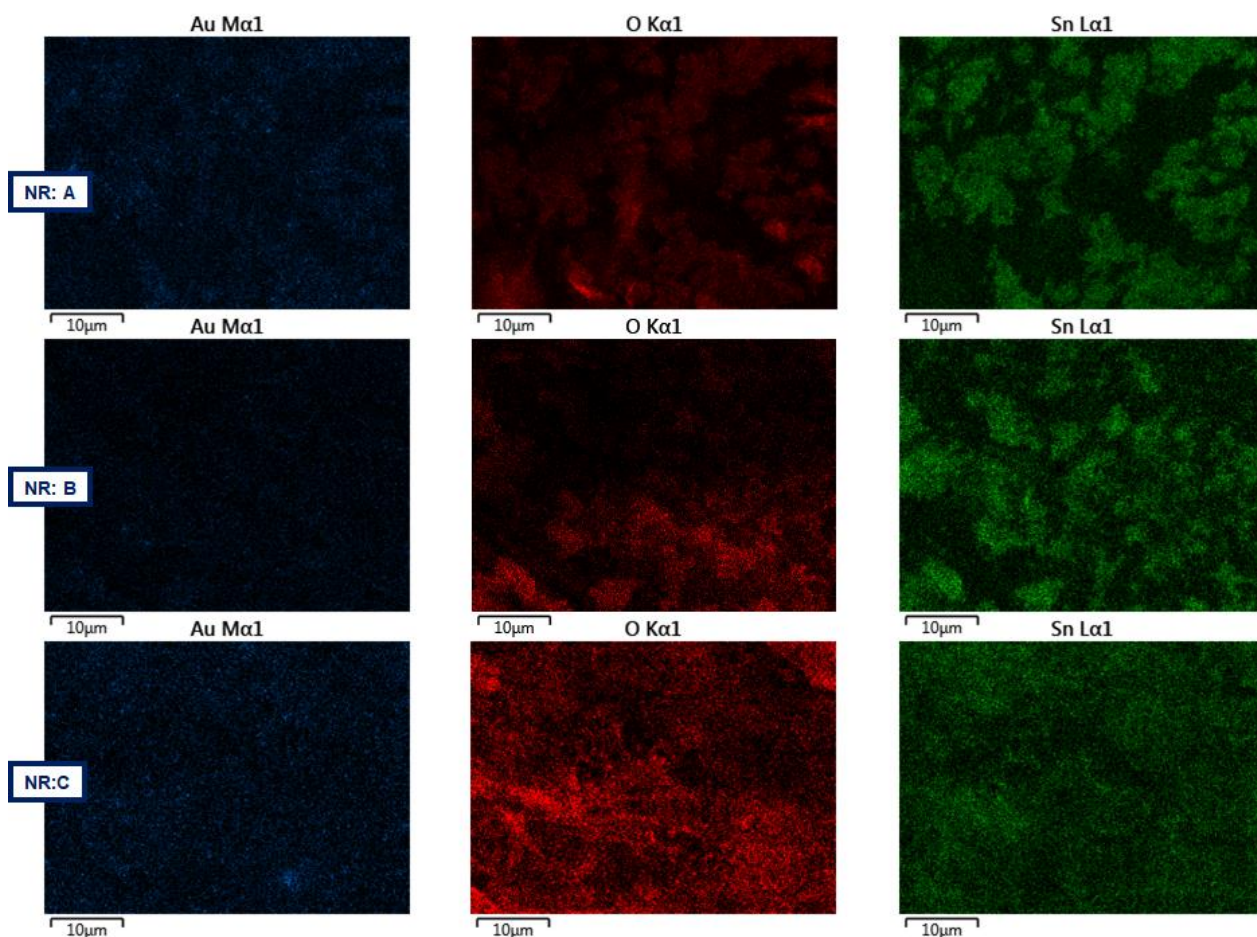


*Figure 4-19:  EDS micrographs of samples NR: A- for 1 mM SnO₂ concentration, NR: B- for 2 mM SnO₂ concentration, and NR: C- for 3 mM SnO₂ concentration.*

61

Figure 4-20 shows the in-depth elemental analysis of the samples NR: A-C, from this analysis we were able to present the average amounts of each element, as presented in the accompanying tables. For each sample, the elements of Sn and O are in excess amounts compared to that of Au, as expected for coated materials.
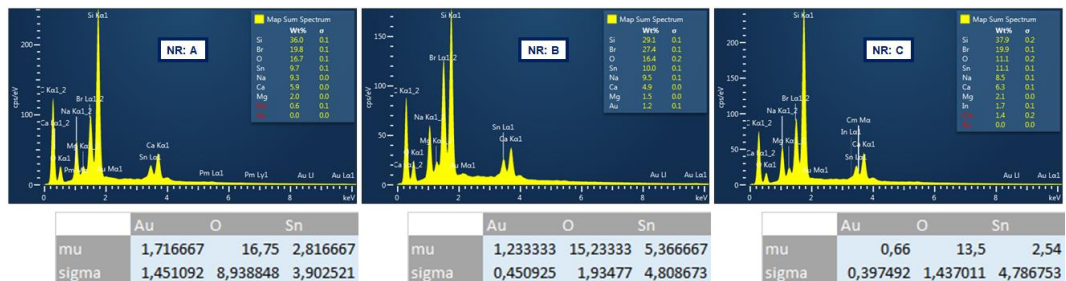


| | Au | O | Sn |
|---|---|---|---|
| mu | 1,716667 | 16,75 | 2,816667 |
| sigma | 1,451092 | 8,938848 | 3,902521 |

| | Au | O | Sn |
|---|---|---|---|
| mu | 1,233333 | 15,23333 | 5,366667 |
| sigma | 0,450925 | 1,93477 | 4,808673 |

| | Au | O | Sn |
|---|---|---|---|
| mu | 0,66 | 13,5 | 2,54 |
| sigma | 0,397492 | 1,437011 | 4,786753 |

*Figure 4-20: EDS absorption spectra for the samples NR: A, B, C for the $SnO_2$ stabilized- Au nanorods (Au-NRs). Elemental analysis tables showing the percentage amounts of the elements Au, Sn, and O.*

### 4.2.3    Optical properties: UV-Vis

Anisotropic nanomaterials such as those for Au-NRs have been reported [59] exhibiting two localised surface plasmonic resonances (LSPR) corresponding to the width and length of the particles, respectively known as the transverse surface plasmon resonances (SPRT) and longitudinal surface plasmon resonances (SPRL). In these literature reports, the SPRT is weak usually without any observable red-shifting, while the SPRL mode is strong with the peak position that can be tuned artificially in a large Visible to Near Infrared (VIS–NIR) spectral region by altering either the aspect ratio (the width or length) of the Au nanorods or the surrounding conditions and arrangement [11, 12].

Figure 4-21 shows the optical absorption property of the CTAB-stabilised and $SnO_2$-coated Au nanorods. The absorption spectra show SPRT band modes that are stronger than SPRTL band modes, which is an interesting contradiction to literature reports. The strong SPRT band modes are observed at ~540 nm for the CTAB-stabilised Au-NRs and at ~550 nm for $SnO_2$. The weak SPRL band modes are observed at ~675 nm for the CTAB-stabilised Au-NRs and at ~700 nm for the $SnO_2$-coated materials. The redshift is attributable to the refractive index of $SnO_2$, was observed for the Au-NSs. While the interesting variation in the strengths of the SPR band mode is suspected to be attributable to the low aspect-ratio of the Au-NRs structures.

62
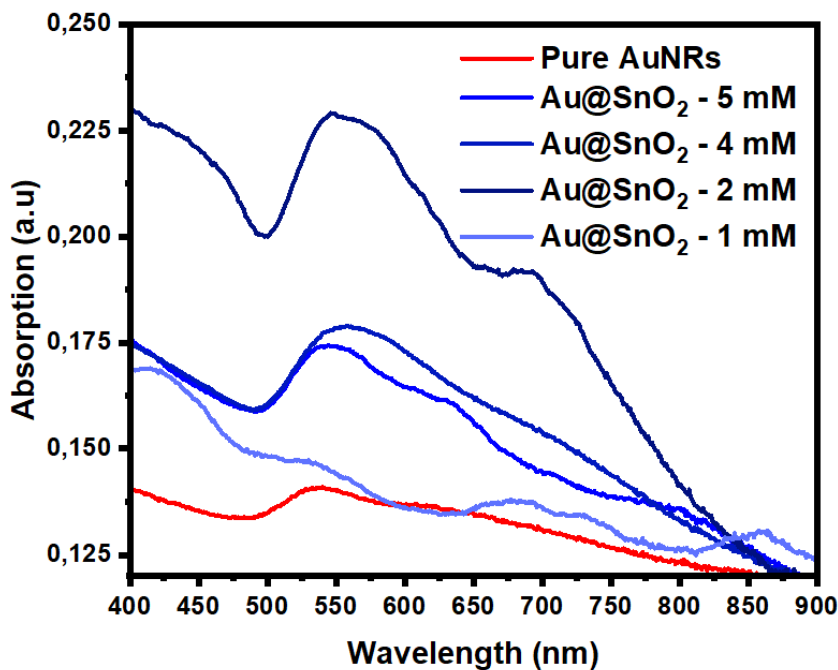
*Figure 4-21: UV-VIS spectra obtained for the CTAB-stabilized and the SnO₂-stabilized Au-NRs. These show absorption peaks in the regions where gold nanorods are known to absorb (~520 nm and ~740 nm).*

### 4.2.4    Structural properties: XRD

The XRD profile reported in Figure 4-22 confirms that the gold nanorods were crystalline. The diffraction peaks can be indexed to those of pure face-centred cubic (FCC) crystal lattice, corresponding to the (111), (200), (220), and (311) planes respectively, in good agreement with literature [102] and as observed for the Au-NSs. Similar observations were made for the profile for the $SnO_2$-coated Au-NRs, that is, the FCC planes are also observed together with the planes for the $SnO_2$ crystallinity, corresponding to planes (110), (101), (200), (210), (211), (220) and (002). The proposed crystal lattice structure for $SnO_2$ is provided in Figure 4-9.

Also, as was observed for the Au-NSs case, Figure 4-22 also reveals that the intensity of the XRD peaks of the Au-NRs is also reduced after $SnO_2$. For the composite materials Au-NRs@$SnO_2$ the intensity of the XRD peaks is also observed to be dependent on the $SnO_2$ coating thickness, with particles in NR: A having greater intensity and less coating than the particles in NR: B.
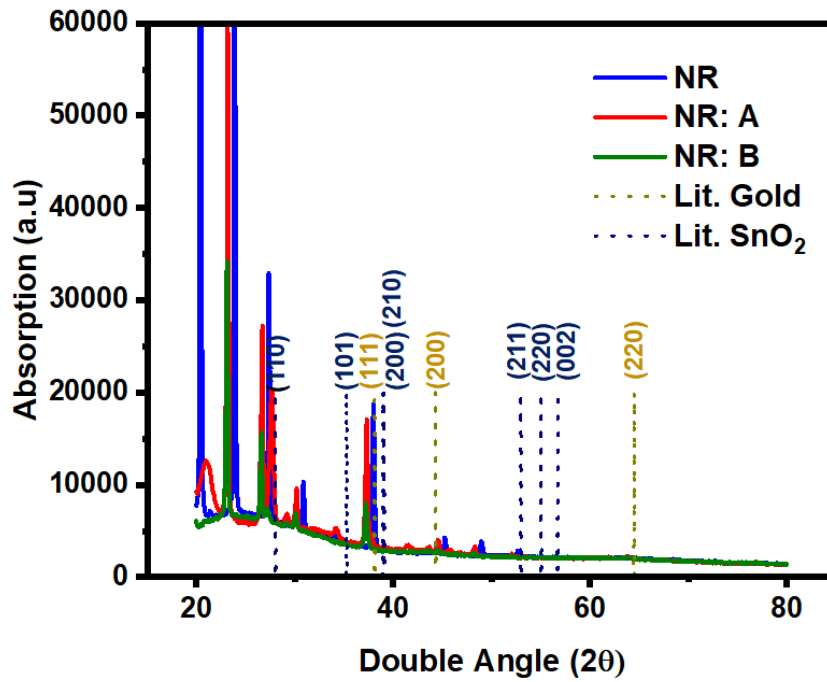
*Figure 4-22: XRD patterns of the pure and SnO₂-protected gold nanorods.*

### 4.2.5 Nanofluid application: Thermal conductivity

The nanofluids composed of the CTAB-stabilised and $SnO_2$-coated gold nanorods Au-NRs, are shown in Figure 4-23. The Figure includes images of the samples before and after pure ethylene glycol was added to make the ~60% EG mixture solutions.

64
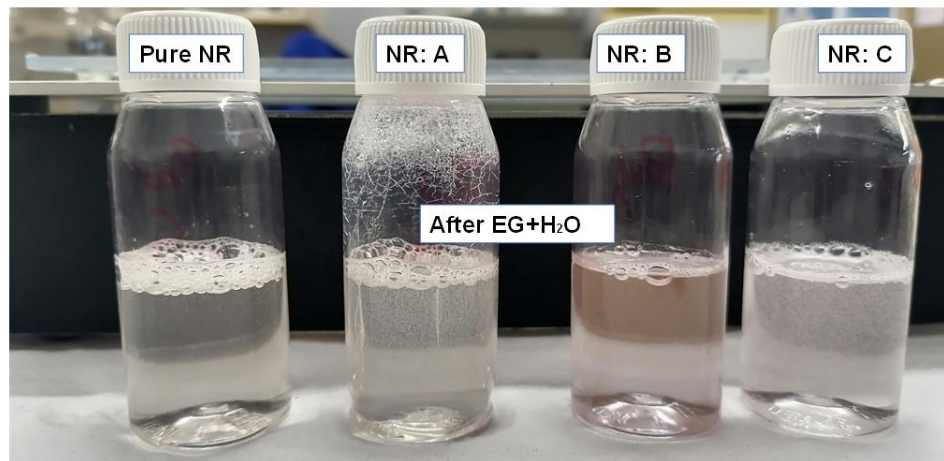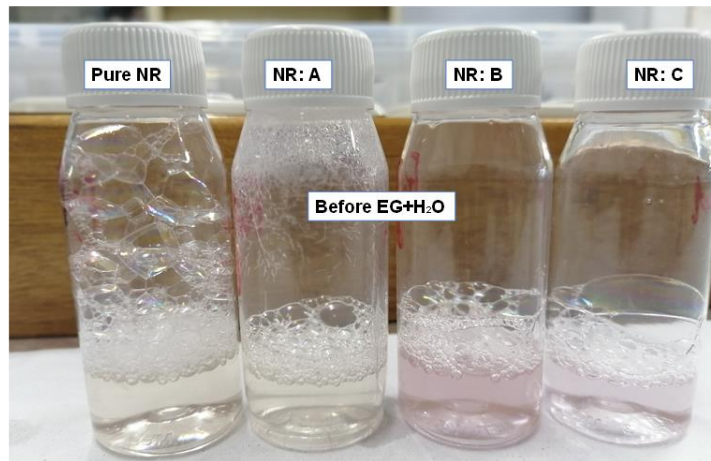
*Figure 4-23: The pure Au-NRs and Au@SnO₂ based nanofluids. Pictured here (Second picture) with only 15% of the appropriate amounts of Ethylene Glycol were added.*

Figure 4-24 (A1, A2 and A3) shows the $\Delta V$ versus $\ln(t)$ plots for the rejected (Noisy) and the accepted (Linear) currents. From these plots, the graphs of m versus $I^3$ were obtained as shown in Figure 4-24 (B1, B2 and B3), whose least-square linear fits are also displayed. The CTAB-stabilised Au-NRs (A1 and B1) sample resulted in a fitted plot with slope 1.70542, which is poorly close to 3, this is because of the difficulty in finding the perfect linear regions. The SnO₂-coated Au-NRs (A2 and B2, and A3 and B3) samples resulted in fitted plots with slopes 2.31822 and 3.32211, respectively, which are also close to the required value of 3. The deviation is attributed to a less-than perfect choice of the required linear regions.
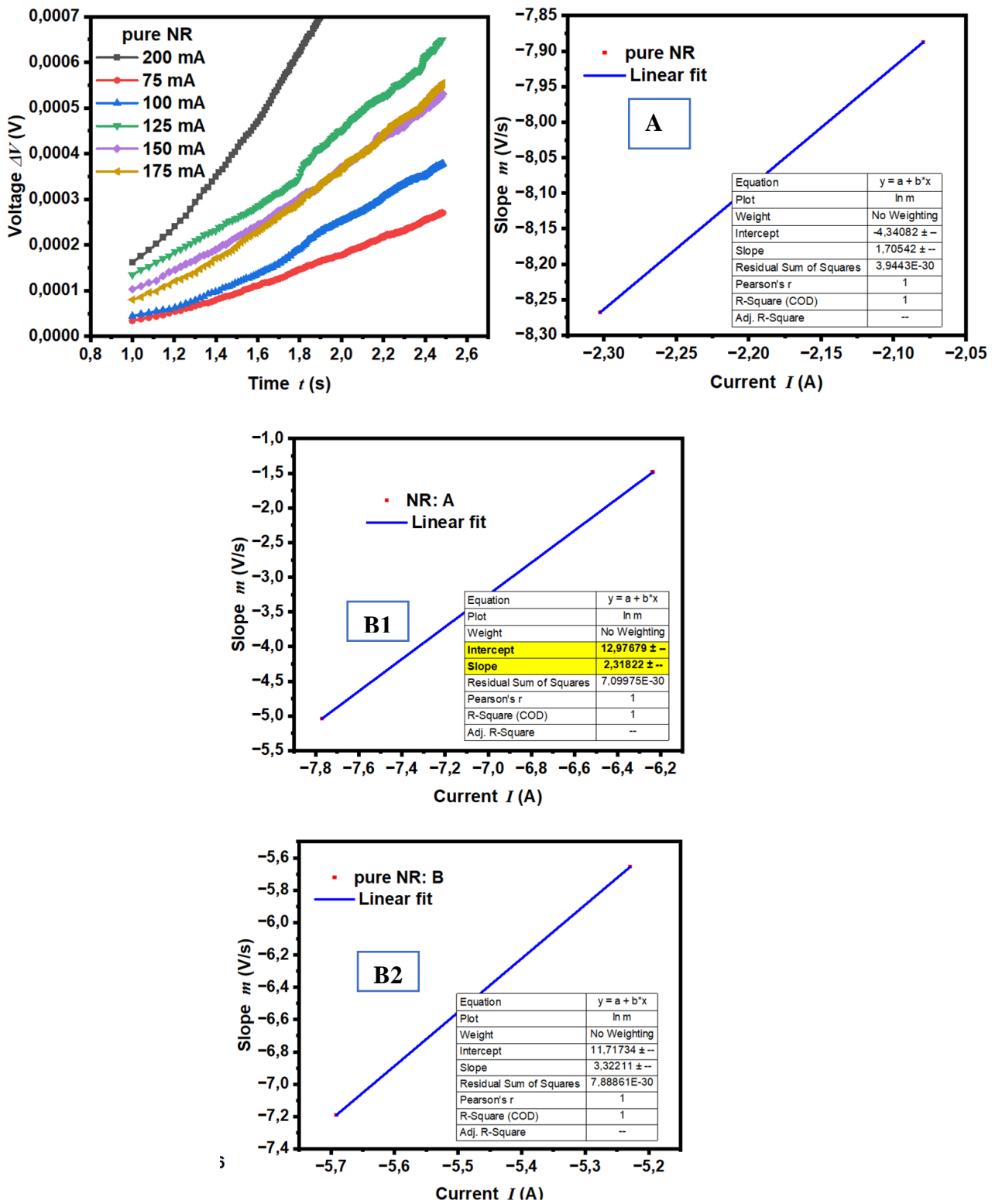
*Figure 4-24: A- Semi-logarithmic plot of the voltage increases as a function of time for different current values showing the best least-squares linear fit over the linear regions of the curves. B- Plot of the slopes ln(m) versus ln(I). The solid line represents the results of the best least-squares linear fit. These are obtained from the nanofluids of (1)- pure Au-NRs, (2)- 1 mM Au@SnO₂, and (3)- 2 mM Au@SnO₂, carried in 80% Ethylene glycol (EG) – water mixture base fluid.*

Then by using the corresponding equations and the graphs of m versus $I^3$ to obtain the value of the coefficient b, we were able to obtain the thermal conductivities shown in Figure 4- 25.The figure reveals that the CTAB-stabilised Au-NRs resulted in thermal properties higher than that of the base fluid (60% EG mixture) with thermal conductivity of 2.043 ± 1.561 $W{\circ}m^{-1}{\circ}K^{-1}$. However, it is worth noting the significant potential error associated the choice of the linear region (which resulted in a slope significantly less than 3), thus caution is advised. The $SnO_2$-coated Au-NRs (NR: A) resulted in the unexpected low thermal conductivity (0.045 ± 0.053 $W{\circ}m^{-1}{\circ}K^{-1}$) as compared to the higher concentrated $SnO_2$-coated, which shows some significant improvement in the thermal properties with thermal conductivity of 0.611 ± 0.509 $W{\circ}m^{-1}{\circ}K^{-1}$. The unexpected low thermal conductivity result of the NR: A sample may be caused by under coating.
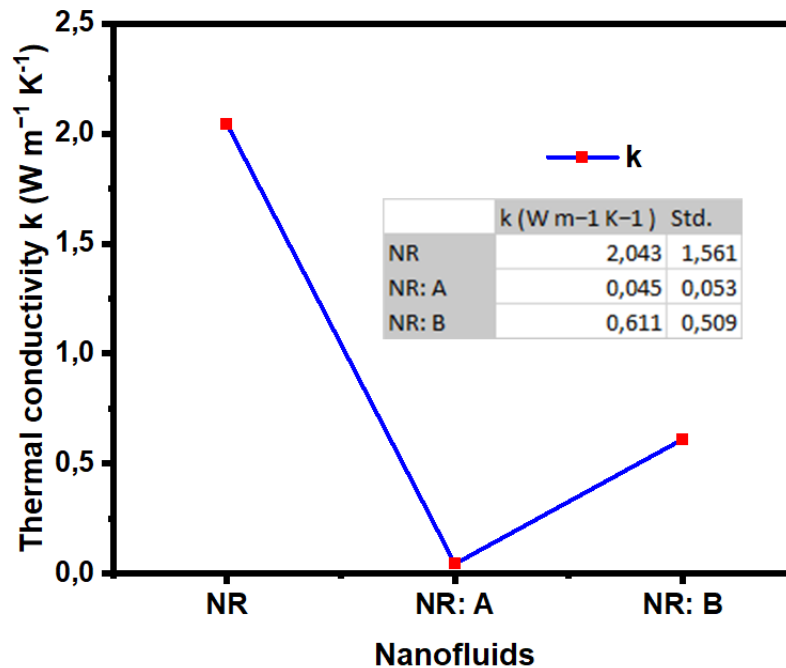


*Figure 4-25: Thermal conductivity variation as a function of SnO₂ coating thickness concentration for the Au-NRs.*

## 4.3 Synthesis, structure, and thermal properties of Au prism nanofluids.

The preparation of CTAB-stabilized and $SnO_2$-coated gold nanoprisms, in contrast to the synthesis of their nanofluids, is well documented in literature [69, 74]. These studies have reported particles with sizes ranging from 50 to 100 nm, with optical surface plasmonic resonance (SPR) absorption in the range 600 nm to 1400 nm, and structural properties typical of

67

FCC crystallinity. For this study, the structures were synthesized using procedures adapted from the indicated literature.

The morphological properties -with respect to particle formation and size distribution were investigated and are reported in sections 4.3.1 and 4.3.2. The optical properties -with respect to UV-VIS wavelength absorbency, of the colloids and their structural properties are reported in sections 4.3.3 and 4.3.4. The thermal properties -the thermal conductivity of various ethylene glycol-based nanofluids are reported in section 4.3.5.

### 4.3.1 Morphological properties: TEM

Transmission electron microscopy (TEM) was used to study the size and morphology of the gold nanoprisms (Au-NPRs). Figure 4-26 shows the TEM micrograph with corresponding particle size distributions. The TEM micrograph reveals the stacked thin films of the crystalline Au nanoprism particles with an average length of ~194 nm. A particle size distribution of ~194 ± 201 nm was obtained in the first month after the optimized synthesis conditions, this led to pure prism products with negligible amounts of by-products.
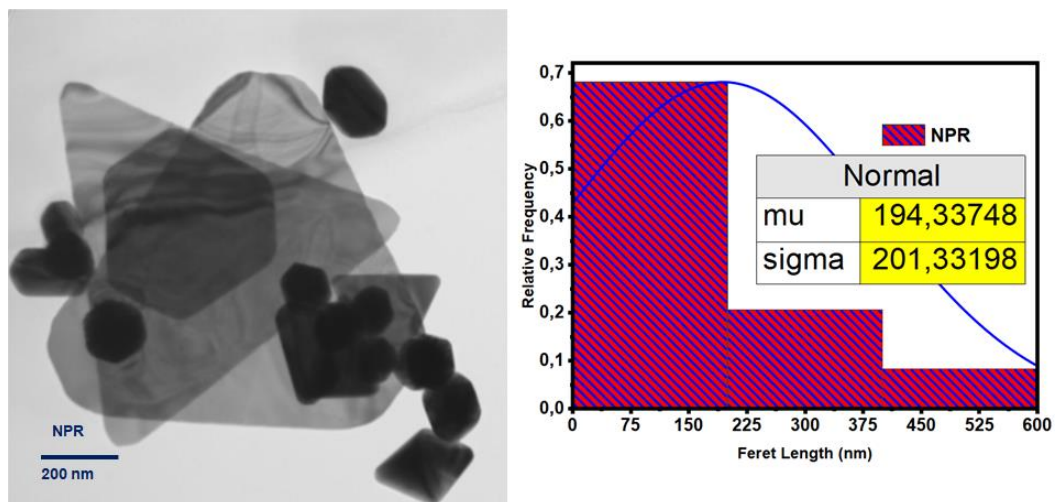


*Figure 4-26: TEM micrograph of the CTAB stabilized- Au nanoprisms (Au-NPRs) and their corresponding particle size distributions.*

Transmission electron microscopy (TEM) was also used to study the size and morphology of the $SnO_2$-coated gold nanoprisms (Au-NPRs@$SnO_2$). Figure 4-27 (A-C) shows the TEM micrographs with corresponding particle length distributions. All the particles in these micrographs are assumed to have the same particle diameter sizes as those were used as the Au-seeds, that is (~12 ± 24 nm diameter and ~194 ± 201 nm length). Thus, the particle size distributions in Figure 4-27 indicate the coating thickness of $SnO_2$ around these Au-NPRs particles. Figure 4-27 (A) shows a TEM micrograph revealing a crystalline Au nanoprism coated with $SnO_2$ nanocrystals with an average coating thickness size of ~68 nm, giving rise to average

68

composite particle length of ~262 nm. Figures 4-27 (B) shows a TEM micrograph revealing slightly dispersed and crystalline Au nanoprisms coated with a $SnO_2$ with average coating thickness sizes of ~137 nm, giving rise to average composite particle length of ~331 nm. The largest $SnO_2$ coating thicknesses are observed in Figures 4-27 (C), which show TEM micrographs revealing a crystalline Au nanoprism coated with a $SnO_2$ with average coating thickness sizes of ~145 nm, giving rise to average composite particle diameters of ~339 nm. These micrographs also reveal presence of gold-free $SnO_2$ nanocrystalline materials, representing less than ~10% of the particle distributions.
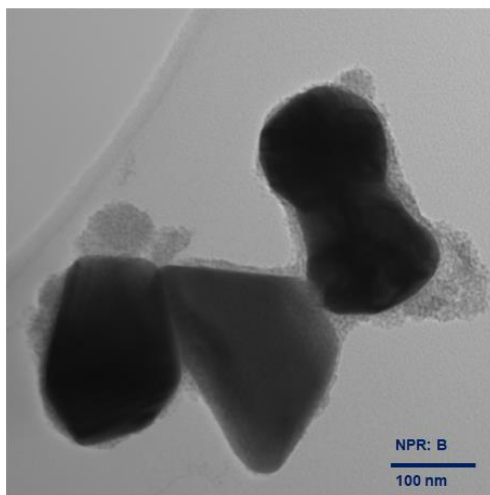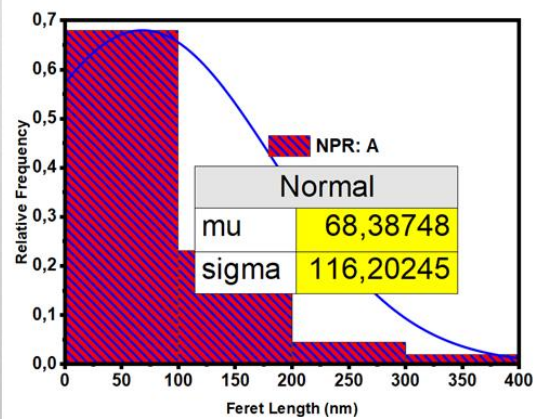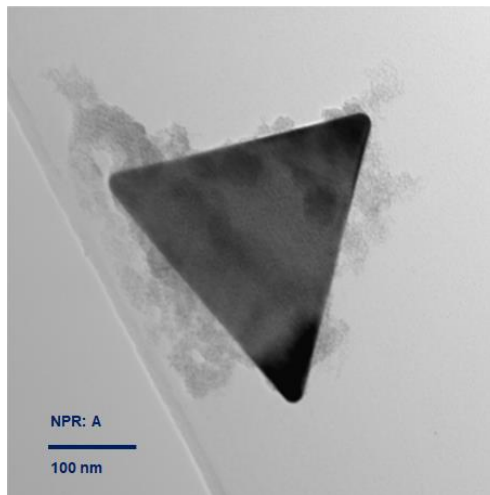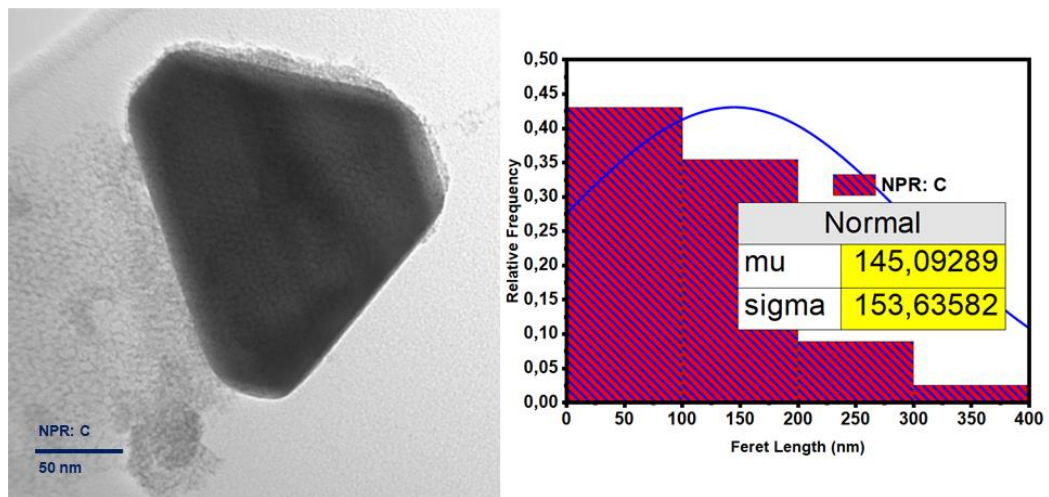
*Figure 4-27: TEM micrographs of the SnO$_2$ stabilized- Au nanoprisms (Au-NPRs) and their corresponding particle size distributions. A- for 1 mM SnO2 concentration, B- for 2 mM SnO$_2$ concentration, and C- for 3 mM SnO$_2$ concentration.*

### 4.3.2 Morphological properties: SEM-EDS

Additional morphological features of the Au-NPR samples and the relationship between the structures and composite elemental distributions were characterized using the Scanning electron microscope (SEM) coupled with Electron Energy Dispersive Spectroscopy (EDS).
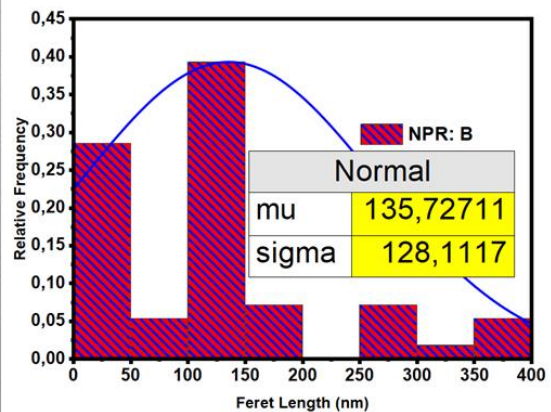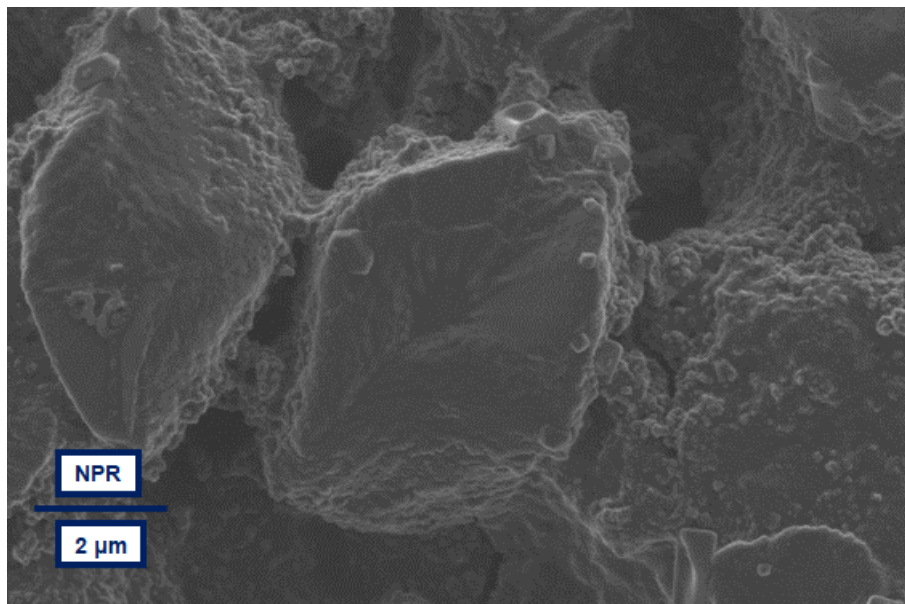


*Figure 4-28: SEM micrograph of the CTAB stabilized- Au nanoprisms (Au-NPRs).*

70

The scanning electron microscopy (SEM) micrographs in Figure 4-28 show the CTAB-stabilized Au-NPR particles formed and their size distributions. The SEM micrographs reveal that the nanoprisms had no agglomeration present.

Figure 4-29 (A and C) show SEM micrographs revealing $SnO_2$-coated gold (Au@$SnO_2$) nanocrystalline materials with varying sizes. The images for NPR: A and NPR: C reveal planar square (cubic) large composite materials. Theses image were further investigated with EDS instrument to reveal the elemental composition of the structures.
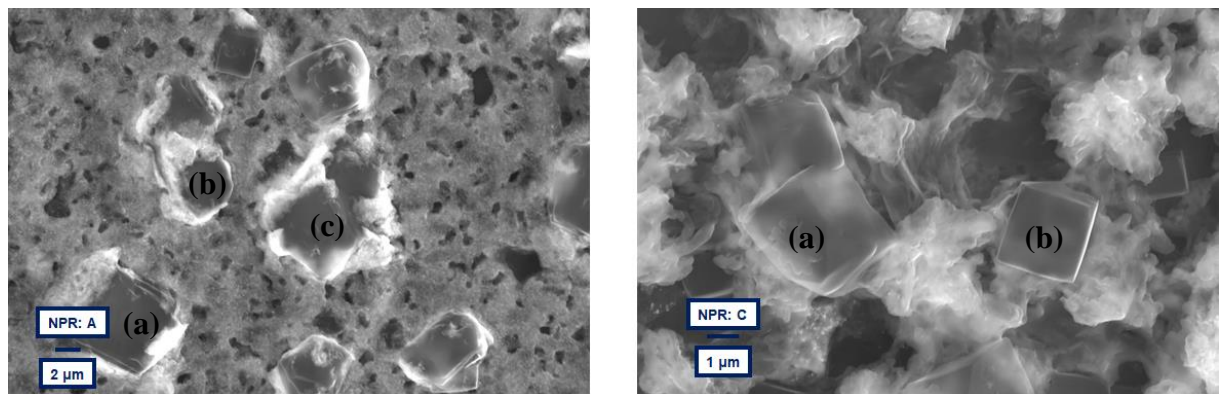


*Figure 4-29: SEM micrographs of the $SnO_2$ stabilized- Au nanoprisms (Au-NPRs). NR: A- for 1 mM $SnO_2$ concentration and NR: C- for 3 mM $SnO_2$ concentration.*

Figure 4-30 consists of the elemental EDS micrographs revealing which elements are presents in the SEM micrographs (NPR: A and NPR: C). From the Figure, we observe the elements of Au, Sn and O. Only the element O appears to be in excess amounts in region (a), (b) and (c) with only in trace amounts of the other elements. This is also consistently observed in Figure 4-31. Which is as expected for coated materials.

71
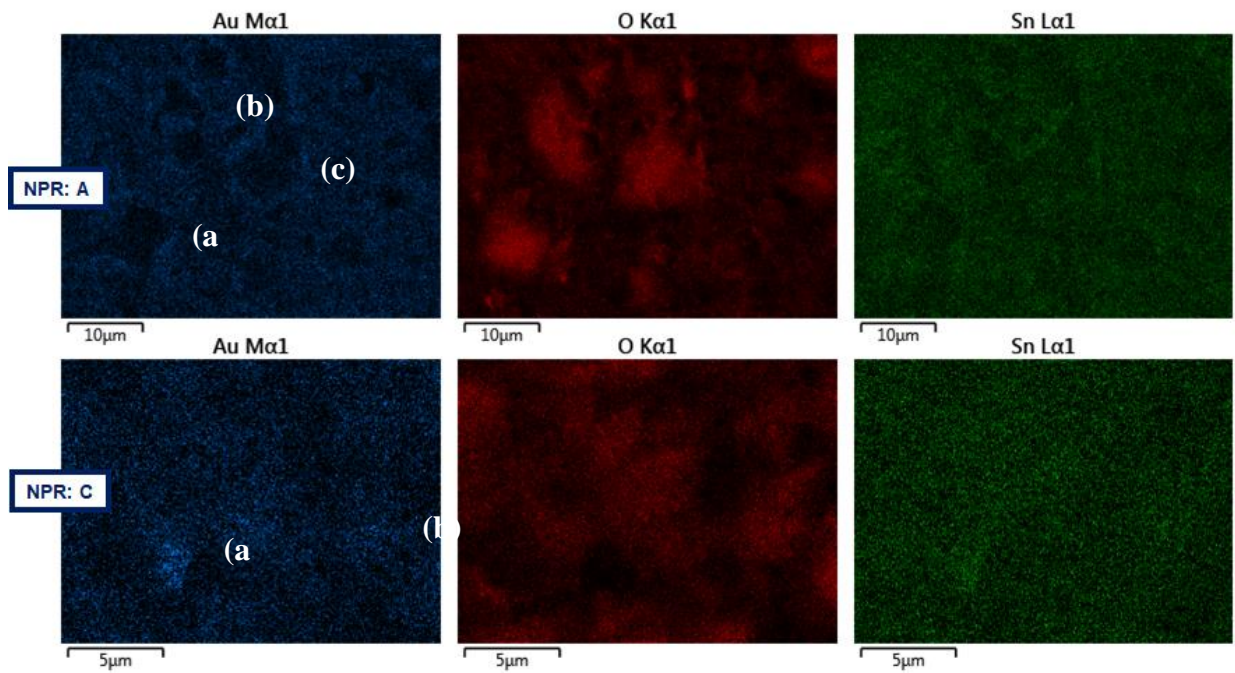
*Figure 4-30: EDS micrographs of samples NR: A- for 1 mM SnO₂ concentration and NR: C- for 3 mM SnO₂ concentration.*
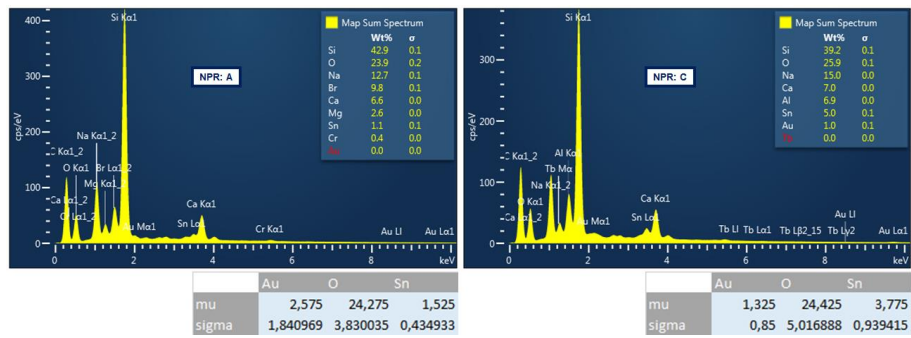


*Figure 4-31: EDS absorption spectra for the samples NPR: A, C for the SnO₂ stabilized- Au nanoprisms (Au-NPRs). Elemental analysis tables showing the percentage amounts of the elements Au, Sn, and O.*

### 4.3.3 Optical properties: UV-Vis

Complicated anisotropic structures such as the Au-NPRs have been reported to exhibit complicated optical properties, as was noted in chapter 2. However, in some cases, localised surface plasmonic resonances (LSPR) can be correlated to the distinct lengths of the particle structures, which give rise to the transverse surface plasmon resonances (SPRT) and the longitudinal plasmon resonance (SPRL), was illustrated by Huang et al [56]. In their study, Huang et al observed SPRT mode as a weak band at ~650 nm and a strong SPRL mode band at ~1200 nm. In their study, both peak positions were demonstrated to be tunable in a large

72

VIS-NIR spectral region by altering either the sizes of the Au-NPRs or the surrounding conditions and arrangement [11, 12].

Figure 4-32 shows the optical absorption properties of the CTAB-stabilized and the $SnO_2$-coated Au nanoprisms (Au-NPRs). Our instrument was only limited to the UV-VIS region, as such only the SPRT band is observed at ~550 nm for the CTAB-stabilised Au-NSs and at ~575 nm for the $Au@SnO_2$ solutions, respectively. These values are slightly consistent with previously reported values [17,28]. Notably redshifts are observed for the coated samples (NPR: A - D). The red shifts of the SPRT bands for the coated particles are, again, attributable to the high refractive index of $SnO_2$ coatings of (2.2) [30]. The intensity of the absorption bands is observed to be dependent on the coating thickness for the $SnO_2$-coated Au-NPR samples, with sample (NPR: E) having the largest intensity.
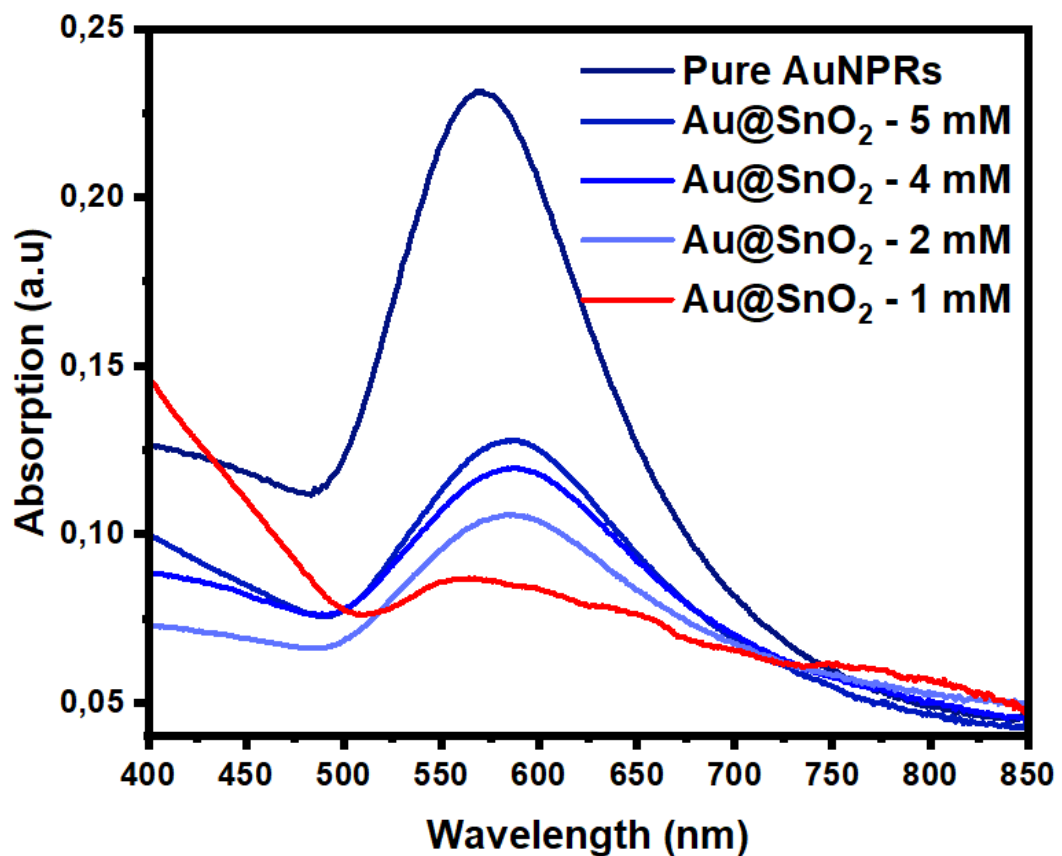


*Figure 4-32: UV-VIS spectra obtained for the CTAB-stabilized and the $SnO_2$-stabilized Au-NPRs. These show absorption peaks in the regions where gold nanoprisms are known to absorb (~570 nm and >1100 nm – the longitudinal peak is out of range for the instrument).*

### 4.3.4 Structural properties: XRD

The XRD profile reported in Figure 4-33 confirms that the gold nanoprisms were crystalline. The diffraction peaks can be indexed to those of pure face-centred cubic (FCC) crystal lattice, corresponding to the (111), (200), (220), and (311) planes respectively, in good agreement with literature [102]. Similar observations were made for the profile for the $SnO_2$-coated Au-NSs, that is, the FCC planes are also observed together with the planes for the $SnO_2$ crystallinity, corresponding to planes (110), (101), (200), (210), (211), (220) and (002). Also, as was observed for the Au-NSs case, Figure 4-33 also shows the reduction in the intensity of the XRD peaks for the CTAB-stabilised Au-NPRs compared to those coated with $SnO_2$. The composite materials Au-NRs@$SnO_2$ had lowered XRD intensity which is observably dependent on the $SnO_2$ coating thickness.
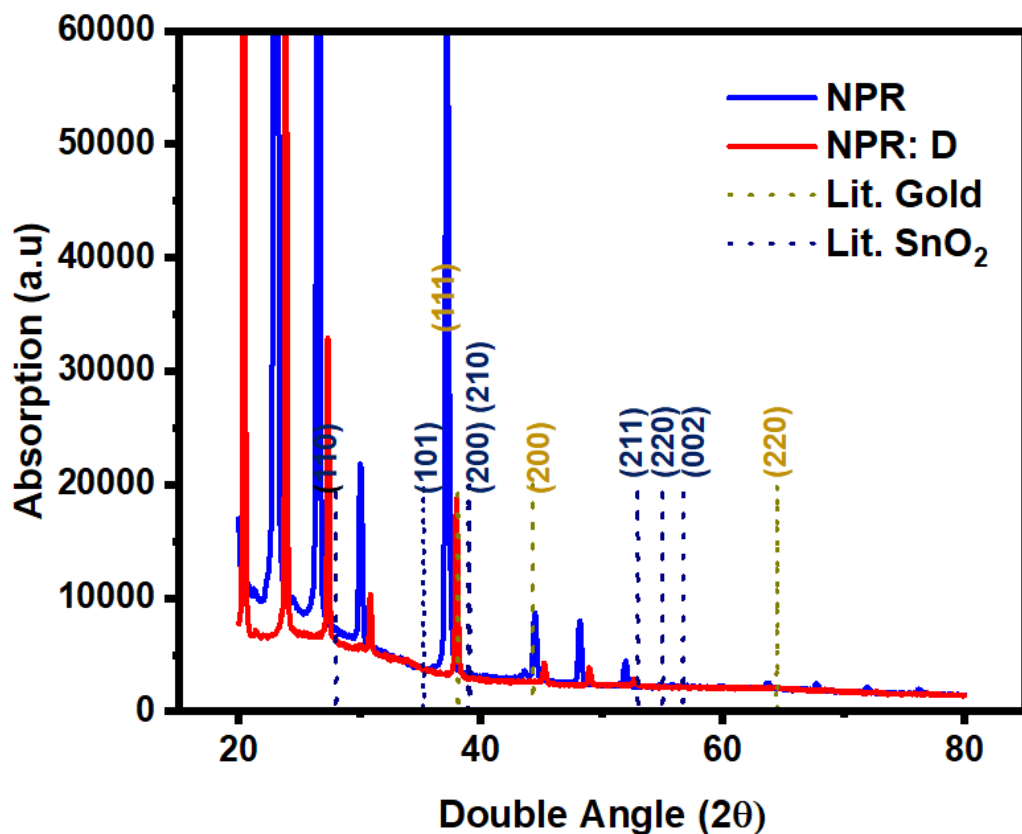


*Figure 4-33: XRD patterns of the pure and SnO₂-protected gold nanoprisms.*

### 4.3.5 Nanofluid Application: Thermal conductivity

The nanofluids composed of the CTAB-stabilised and $SnO_2$-coated gold nanoprisms Au-NPRs, are shown in Figure 4-34. The Figure includes images of the samples before and after pure ethylene glycol was added to make the ~60% EG mixture solutions.

74
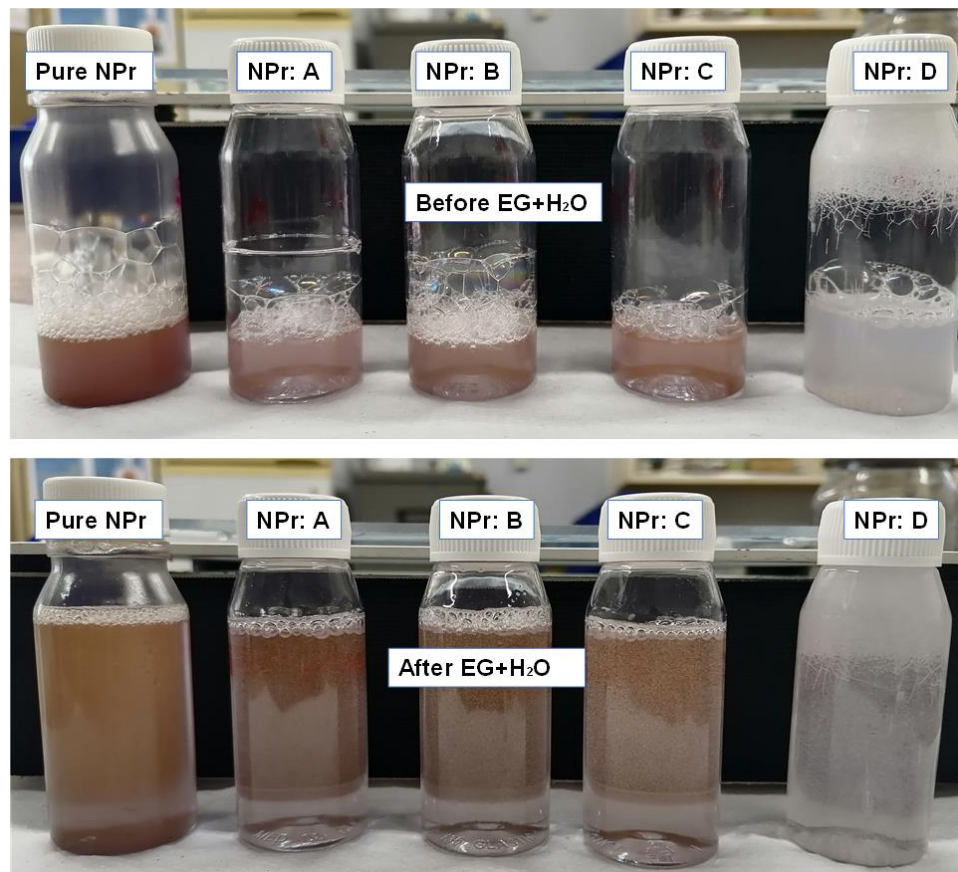
*Figure 4-34: The pure Au-NPRs and Au@SnO2 based nanofluids.*

Figure 4-35 (A1, A2 and A3) shows the $\Delta V$ versus $\ln(t)$ plots for the rejected (Noisy) and the accepted (Linear) currents. From these plots, the graphs of m versus $I^3$ were obtained as shown in Figure 4-35 (B1, B2 and B3), whose least-square linear fits are also displayed. The CTAB-stabilised Au-NPRs (A1 and B1) sample resulted in a fitted plot with slope 2.30136, which is slight close to 3 as required, this is because of the difficulty in finding the perfect linear regions. The SnO2-coated Au-NPRs (A2 and B2, and A3 and B3) samples resulted in fitted plots with slopes 2.57295 and 2.53966 $\pm$ 0.15287, respectively, which are also close to the required value of 3. The deviation is attributed to a less-than perfect choice of the required linear regions.
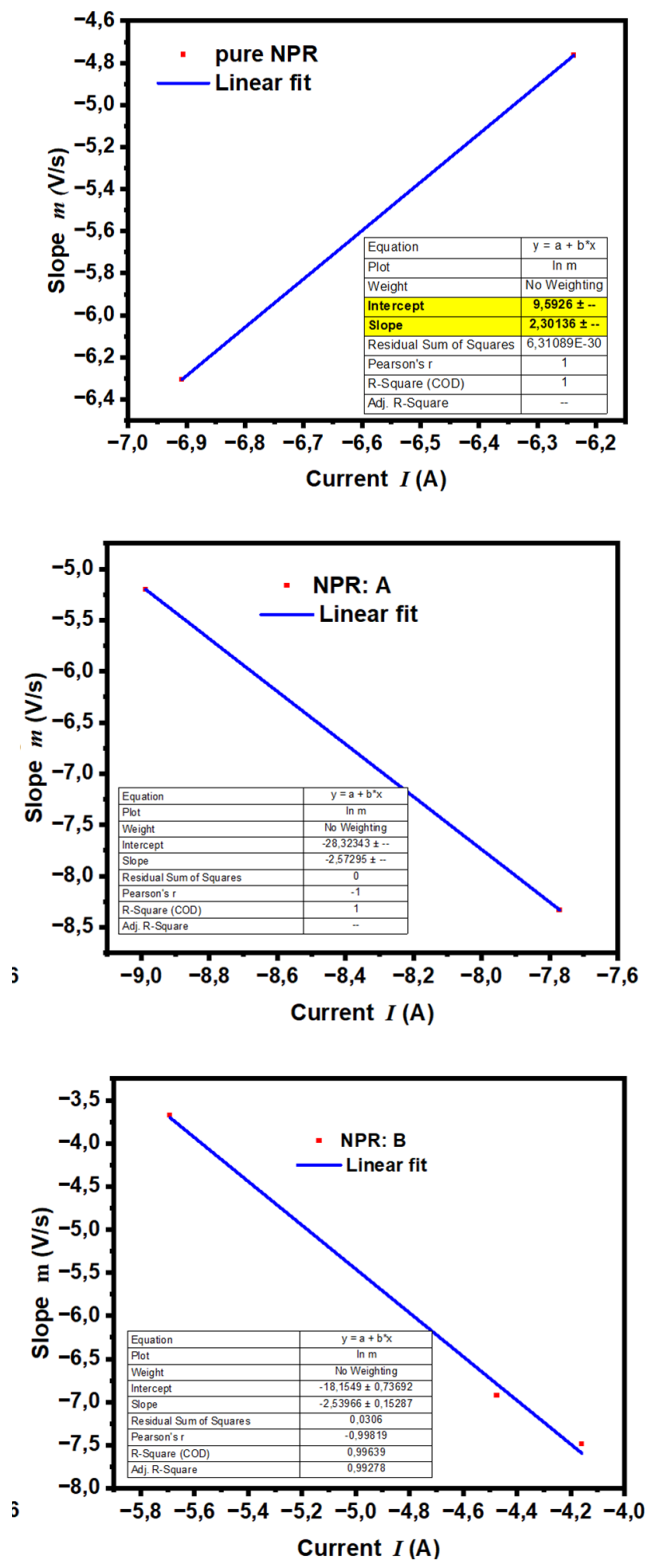
*Figure 4-35: A- Semi-logarithmic plot of the voltage increases as a function of time for different current values showing the best least-squares linear fit over the linear regions of the curves. B- Plot of the slopes ln(m) versus ln(I). The solid line represents the results of the best least-squares linear fit. These are obtained from the nanofluids of (1)- pure Au-NPRs, (2)- 1 mM Au@SnO₂, and (3)- 2 mM Au@SnO₂, carried in 80% Ethylene glycol (EG) – water mixture base fluid.*

76

Then by using the corresponding equations and the graphs of m versus $I^3$ to obtain the value of the coefficient b, we were able to obtain the thermal conductivities shown in Figure 4- 36. Figure 4-36 reveals that the CTAB-stabilised Au-NPRs resulted in thermal properties significantly lowered than that of the base fluid (60% EG mixture) with thermal conductivity of $0.133 \pm 0.098$ W∘m$^{-1}$∘K$^{-1}$. The same observation is made for the SnO$_2$-coated Au-NPR sample (NPR: B), with the low thermal conductivity of $0.110 \pm 0.092$ W∘m$^{-1}$∘K$^{-1}$. The SnO$_2$-coated Au-NRs (NR: A) resulted in the improved thermal conductivity of $(0.462 \pm 0.366$ W∘m$^{-1}$∘K$^{-1})$.



| | k (W m−1 K−1 ) | Std. |
|---|---|---|
| NPR | 0,133 | 0,098 |
| NPR: A | 0,462 | 0,366 |
| NPR: B | 0,110 | 0,092 |
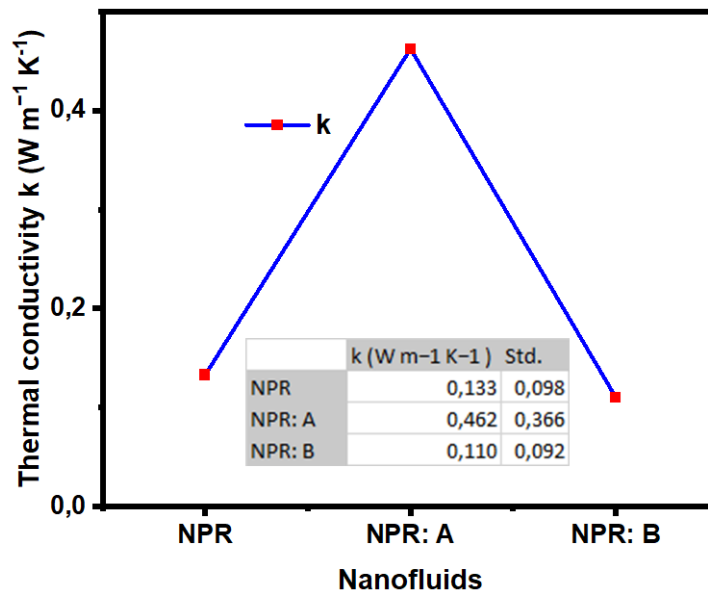
*Figure 4-36: Thermal conductivity variation as a function of SnO$_2$ coating thickness concentration for the Au-NPRs.*

### Summary

Nanofluids containing gold nanomaterials stabilized by CTAB or tin dioxide were successfully prepared using a two-step method. Three different pathways were followed to yield small gold nanospheres, gold nanorods, and gold nanoprisms. The particle sizes ranged from $12 \pm 24$ nm to 339 nm. The nanofluids composed of these particles showed excellent homogeneity with no precipitation visible for the first month after synthesis, implying true colloidal systems.

Replacing CTAB with SnO$_2$ as a surfactant resulted in the enhanced optical and structural properties of the gold nanomaterials. The SnO$_2$ coating improved the structural stability of the particles, and the nanoparticles remained well-dispersed for months after their

initial synthesis. The optical properties of the gold nanoparticles were observed to have a red-shift and an increase in the intensity of the band modes. The increase was further demonstrated to be dependent on the concentration of $SnO_2$.

The ethylene glycol-based nanofluids composed of the CTAB-stabilized and $SnO_2$-coated gold nanoparticles possessed enhanced thermal properties. The surfactant and the distance-holder materials were found to be responsible for this. The thermal conductivity was observed to increase by less than 1% for the CTAB-stabilized Au-NSs and by more than 100% for the $SnO_2$-coated Au-NSs. For the Au-NR particles, the thermal conductivity increased by more than 100% for the CTAB-stabilized particles and by 22% for the highly concentrated SnO2-coated particles. However, the lightly concentrated $SnO_2$-coated Au-NRs showed a 91% decrease in thermal conductivity. The thermal conductivities of the gold nanoprisms were observed to be only slightly increased, which was unexpected, despite having the highest surface area compared to other structures.

Based on the discussion above, the nanofluids containing CTAB-coated Au-NPRs exhibit better thermal conductivity when compared to the $SnO_2$-coated Au-NPRs based nanofluids. However, it is important to consider other factors that might influence the selection of $SnO_2$-coated Au-NPRs nanofluids over their CTAB counterparts. These factors include cost considerations, chemical stability, and environmental impact. The results obtained from the morphological and structural property analysis demonstrate that $SnO_2$-coated materials are superior to CTAB-based materials. Moreover, since $SnO_2$-coated materials remain structurally stable for long durations, their synthesis is less expensive and much more environmentally friendly.

Furthermore, the low thermal conductivity of $SnO_2$-coated Au-NPR nanofluids, despite having Au-NPRs with high surface area, can be explained by considering factors such as phonon scattering, interface and boundary conditions, or the porosity of the Au nanoprism. High surface area alone does not ensure high thermal conductivity. The presence of many interfaces and boundaries in the nanoprism structure can introduce phonon scattering, hindering the efficient transfer of heat. In addition, the TEM micrographs for Au-NPRs show significant porosity in nanoprism structures, and the presence of voids or air gaps can significantly reduce thermal conductivity.

## Chapter 5     Conclusions and Future work

After carefully reviewing the research problem, objectives, and thesis statement provided in the introduction chapter, as well as the research and analysis conducted in the following chapters. Based on this, we have come to the following concluding remarks.

In this study, we were able to prepare gold (Au) nanostructures, including Au nanospheres (Au-NSs), Au nanorods (Au-NRs), and Au nanoprisms (Au-NPrs), using economically attractive, simple, and reproducible methods. These methods were in agreement with the expectations from literature. However, some of the preparation methods we used had uncontrollable features that interfered with our findings. Therefore, alternative preparation methods like plasma-induced non-electrochemical (PINE) synthetic method would be more suitable for future work.

We also investigated the stabilizing effects of $SnO_2$ on these Au nanostructures. We varied the coating thickness layer of $SnO_2$ around the Au nanostructures and found that the structural stability of the Au nanostructures improved with increasing amount of deposited layer. We also showed that the deposited material improved the properties of the coated Au structures, including optical properties, reduced surface activity, and structural and morphological properties. We prepared various nanofluids composed of $SnO_2$-coated Au (Au@$SnO_2$) and CTAB-stabilized Au nanocomposite materials dispersed in ethylene glycol. Due to the improved structural stability of the dispersed Au nanostructures, the resulting nanofluids had improved colloidal stability that lasted for months after their initial synthesis.

We further investigated the effects of $SnO_2$ and CTAB materials on the thermal properties of the nanofluids. We found that in some cases, stabilizing the Au nanostructures with CTAB or $SnO_2$ significantly improved the thermal conductivities of the nanofluids. However, in some cases, the stabilizing agents acted as an insulator around the particles, inhibiting the propagation of phonons and electrons in their transportation of thermal energy, thus giving rise to resistance to the flow of thermal energy.

Moreover, the thermal capacities of the nanofluids were also significant indicators for thermal properties of the fluids. These measurements could indicate if the CTAB-stabilized and $SnO_2$-coated Au nanofluids can be used in applications that are not concerned with thermal energy flow.

The essence of this study is that the stability of gold nanomaterials can be enhanced by incorporating tin dioxide nanocrystalline solids in suitable amounts. The research conducted confirms that this hypothesis is indeed valid. Results demonstrate that the structural stability of gold nanomaterials, such as Au-NSs, Au-NRs, and Au-NPRs, can be significantly improved by coating them with $SnO_2$ nanocrystalline solids, as opposed to CTAB-stabilised structures.

Furthermore, the study revealed that $SnO_2$-stabilised gold nanomaterials possess additional properties due to the combined effects of the two materials. These materials offer enhanced optical, morphological, and structural properties that could be valuable in thermal energy collection, transportation applications, and catalysis.

Concerning applications, the nanofluids created using $SnO_2$-coated Au nanocomposite materials exhibit excellent colloidal stability, which is critical for their thermal energy collection and transportation applications. Additionally, it is believed that these nanofluids have improved thermal conductivities, although further verification is necessary. A parallel study is required to investigate the thermal capacities of the nanofluids as well as their flow behaviour.

# References

[1]     V. Dinca and M. P. Suchea, "Application of metallic nanosctructures in biomedical field," in *Functional nanostructured interfaces for environmental and biomedical applications*, Elsevier: Matthew Deans, 2019, p. 343.

[2]     Jiuhong Yi and Yunlei Xianyu, "Gold Nanomaterials-Implemented Wearable Sensors for Healthcare Applications," *Advanced Functional Materials,* vol. 32, no. 19, 2022.

[3]     M. Ul-Islam, A. Shehzad, S. Khan, W. A. Khattak, M. W. Ullah and J. K. Park, "Antimicrobial and Biocompatible Properties of Nanomaterials," *Journal of Nanoscience and Nanotechnology,* vol. 14, no. 1, pp. 780-791, 2014.

[4]     J. Nam, W.-G. La, S. Hwang, H. Yeong Su, P. Nokyoung, W. Nayoun, J. Sungwook, B. Suk Ho, M. Yoon-Ji, Y.-M. Cho, J. Min, H. Jin, S. Jung-Youn, W. Eun Kyung, K. Sang Geol, C. So-Hye, Y. Jeongsoo and K. Byung-Soo, "pH-Responsive Assembly of Gold Nanoparticles and "Spatiotemporally Concerted" Drug Release for Synergistic Cancer Therapy," *American Chemical Society Nano,* vol. 7, no. 4, pp. 3388-3402, 2013.

[5]     Vempuluru Navakoteswara Rao, "Surfactant controlled metal oxide shell layer deposition for enhanced photocatalytic solar hydrogen generation: CdSe/TiO2 nanocomposite a case study," *Materials Letters,* vol. 298, no. 130025, 2021.

[6]     L. Jing, H. Jishu, X. Tianshu, G. Changrun, B. Xinyuan, Z. Hao, W. Liping, S. Hongchen and Y. Bai, "Coating Urchinlike Gold Nanoparticles with Polypyrrole Thin Shells To Produce Photothermal Agents with High Stability and Photothermal Transduction Efficiency," *ACS Langmuir,* vol. 29, no. 23, pp. 7102-7110, 2013.

[7]     E. Julien, F. Samantha and R. Alberto, "The influence of support materials on the structural and electronic properties of gold nanoparticles – a DFT study," *Physical chemistry chemical physics,* vol. 21, pp. 19011-19025, 2019.

81

[8]    S. Haichao, S. Bing, C. Lijian, X. Zhenning and A. Shiyun, "Colorimetric sensing of dopamine based on the aggregation of gold nanoparticles induced by copper ions," *Analytical Methods,* vol. 4, pp. 3981-3986, 2012.

[9]    D. Vollath, "Nanomaterials and nanocomposites," in *Nanomaterials: An introduction to synthesis, properties and applications.*, 2013, p. 5.

[10]    C. Tsz Him, L. Nannan, B. Xiaopeng, Z. Xiaolu, S. Lei and W. Jianfang, "Gold Nanobipyramids: An Emerging and Versatile Type of Plasmonic Nanoparticles," *Accounts of chemical research,* vol. 52, no. 8, pp. 2136-2146, 2019.

[11]    D. Vollath, "Chapter 6: Nanofluids," in *Nnaomaterials: An introduction to synthesis, properties, and applications*, Wiley-VCH: Verlag GmbH & Co. KGaA, 2013, pp. 123-126.

[12]    B. J. Hornstein and R. G. Finke, "Transition-Metal Nanocluster Catalysts: Scale-uo Synthesis, Characterization, Storage conditions, Stability, and Catalytic Activity before and after storage of Polyoxoanion- and Tetrabutylammonium-Stabilized Ir(0) Nanoclusters," *Chemistry of Materials,* vol. 15, no. 4, pp. 899-909, 2003.

[13]    N. H. Nguyen Thi, Y. Yong, T. N. Nguyen Quang, N. Masayuki, H. P. Le, H. T. Nguyen, V. C. Ho and V. L. Nguyen, "Controlled Synthesis of Au Nanoparticles by Modified Polyol Methods: Determination of Their Size, Shape, and Crystal Structure," *Crystals,* vol. 1297, no. 11, pp. 1-11, 2021.

[14]    B. Nadeem, K. Irshad and F. Wail, "Nanomaterials: a review of synthesis methods, properties, recent progress, and challenges," *Materials Advances,* vol. 1821, no. 2, pp. 1-52, 2021.

[15]    W. H. Michael, D. Amala, S. W. Peter, M. H. Kennedy and W. M. Royce, "Crystal Structure of the Gold Nanoparticle [N(C8H17)4][Au25(SCH2CH2Ph)18]," *American Chemical Society: Communications,* vol. 130, pp. 3754-3755, 2008.

[16]    W. Cheng, W. Huiyuan, H. Tianlong, X. Xuena, Q. Feng and J. Qichuan, "Generalized-stacking-fault energy and twin-boundary energy of hexagonal

close-packed Au: A first-principles calculation," *Scientific reports,* vol. 10213, pp. 1-11, 2015.

[17]      Z. Shengli, L. Lingwen, L. Man-Bo, Y. Chuanhao, Z. Yan, D. Hongwei, L. Jin, D. Haiteng, L. Lingling and W. Zhikun, "The fcc structure isomerization in gold nanoclusters," *Nanoscale,* no. 39, 2017.

[18]      D. C. Agrawal , "Surfaces," in *Introduction to Nanoscience and Nanomaterials*, 2013, pp. 9 - 64.

[19]      D. C. Agrawal, "Chapter 2: Surfaces," in *Introduction to nanoscience and nanomaterials*, 2013, pp. 9-20.

[20]      H. Homa, S. Pradakshina, R. H. Mohd, S. Shiwani, T. Deepanshi and N. Jagriti, "Gold nanomaterials – The golden approach from synthesis to applications," *Materials Science for Energy Technologies,* vol. 5, pp. 375-390, 2022.

[21]      Y. Xuan, Y. Miaoxin, P. Bo, V. Madeline and X. Younan, "Gold Nanomaterials at Work in Biomedicine," *Chemical Reviews,* vol. 115, no. 19, pp. 10410-10489, 2015.

[22]      L. Na, Z. Pengxiang and A. Didier, "Anisotropic Gold Nanoparticles: Synthesis, Properties, Applications, and Toxicity," *Angewandte Chemie International Edition,* vol. 53, no. 7, pp. 1756-1789, 2014.

[23]      S. B, K. H. M, W. M. A and A. A.-S. F, "Nanowires: a new pathway to nanotechnology-based applications," *Journal of Electroceramics,* vol. 37, pp. 34-49, 2016.

[24]      J. Dickson, B. Rengarajan and G. Y. Su, "Multifunctional spiky branched gold-silver nanostars with near-infrared and short-wavelength infrared localized surface plasmon resonances," *Journal of Colloid and Interface Science,* p. 542, 2019.

[25]      D. Vollath, "Chapter 9: Optical properties of Nanoparticles," in *Nanomaterials: An introduction to synthesis, properties, and applications*, Wiley-VCH, 20, pp. 210-267.

[26]    L. Wang, M. Kafshgari and M. Meunier, "Optical Properties and Applications of Plasmonic-Metal Nanoparticles," *Advanced Functional Materials,* vol. 30, pp. 1-28, 2020.

[27]    X. Lu, M. Rycenga, S. Skrabalak, B. Wiley and Y. Xia, "Chemical Synthesis of Novel Plasmonic Nanoparticles," *Annual Review of Physica; Chemistry,* vol. 60, pp. 167-192, 2009.

[28]    R. Gans, "Über die Form ultramikroskopischer Silberteilchen," *Annalen der physik,* p. 270, 1915.

[29]    M. Hu, J. Chen, Z. Y. Li, L. Au, G. V. Hartland, X. Li, M. Marquez and Y. Xia, "Gold nanostructures: engineering their plasmonic properties for biomedical applications," *Chemistry Society Reviews,* vol. 35, pp. 1084-1094, 2006.

[30]    M. A. Garcia, "Surface plasmons in metallic nanoparticles: fundamentals and applications," *Journal of Physics D: Applied Physics,* vol. 44, no. 28, p. 283001, 2011.

[31]    B. Rodrigez-Gonzalez, E. Carbo-Argibay, I. Pastoriza-Santos and J. Perez-Juste, "Overgrowth and crystalline structure of Gold Nanorods," *Microscopy Society of America,* 2012.

[32]    T. Teddy, A. C. Elena, S. B. Jorge and I. Mariana, "Impact of nano-morphology, lattice defects and conductivity on the performance of graphene based electrochemical biosensors," *Journal of Nanobiotechnology,* vol. 17, no. 101, 2019.

[33]    P. G. Jamkhande, N. W. Ghule, A. H. Barner and M. G. Kalaskar, "Metal nanoparticles synthesis: An overview on methods of preparation,," *Elsevier: Journal of Drug Delivery Science and Technology,* vol. 53, p. 101174, 2019.

[34]    C. D. De Souza, B. R. Nogueira and M. E. C. Rostelato, "Review of the methodologies used in the synthesis gold nanoparticles by chemical reduction," *Journal of Alloys and Compounds,* vol. 798, pp. 714-740, 2019.

[35]     Q.-L. Zhang, Z.-M. Yang, B.-J. Ding, X.-Z. Lan and Y.-J. Guo, "Preparation of copper nanoparticles by chemical reduction method using potassium borohydride," *Transactions of Nonferrous Metals Society of China,* vol. 20, no. 1, pp. 240-244, 2010.

[36]     L. Su, S. Hu, L. Zhang and Z. Wang, "A Fast and Efficient Replacement of CTAB with MUA on the surface of Gold Nanorods Assisted by a water-Immiscible Liquid.," *Advanced Science NEWS (SMALL),* pp. 1-9, 2017.

[37]     M. G. Guzman, J. Dille and S. Godet, "Synthesis of silver nanoparticles by chemical," *World Academy of Science, Engineering and Technology,* vol. 19, pp. 1-8, 2008.

[38]     D. Vollath, "Chapter 2: Nanomaterials and Nanocomposites," in *Nanomaterials: An introduction to synthesis, properties, and applications*, Wiley-VCH: Verlag GmbH & Co.KGaA, 2013, p. 7.

[39]     D. C. Agrawal, "Chatper 7: Zero Dimensional nanostructures IV colloids and colloidal crystals," in *Introduction to nanoscience and nanomaterials*, Singapore, World Scientific, 2013, p. 204.

[40]     M. Sastry, "Assembling nanoparticles and biomacromolecules using electrostatic interactions," *The journal of Pure and Applied Chemistry,* vol. 74, no. 9, pp. 1621-1630, 2002.

[41]     D. Vollath, "Bifunctional Nanocomposites with Magnetic and Luminescence properties," *Advanced Materials,* vol. 22, pp. 4410-4415, 2010.

[42]     W. Zhou, Y. Liu, Y. Yang and P. Wu, "Band gap engineering of SnO2 by Epitaxial Stain: Experimental and Theoretical investigations," *The journal of Physical Chemistry,* vol. 12, no. 118, pp. 6448-6453, 2014.

[43]     N. Zhou, L. Polavarapu, Q. Wong and Q.-H. Xu, "Mesoporous SnO2-coated metal Nanoparticles with Enhanced Catalytic Efficiency," *ACS: Applied Materials and Interfaces,* vol. 7, p. 4844−4850, 2015.

[44]     S. Ho Lee, I. Rusakova, D. Hoffman, A. Jacobson and R. Lee, "Monodisperse SnO2-coated Gold Nanoparticles Are Markedly more stable

than analogous SiO2-coated gold nanoparticles.," *ACS: Applied Materials and Interfaces,* vol. 5, pp. 2479-2484, 2013.

[45]     S. U. Choi and J. A. Eastman, "Enhanced heat transfer using nanofluids". United States of America Patent US6221275B1, 2001.

[46]     S. U. Choi and J. A. Eastman, "Enhancing thermal conductivity of fluids with nanoparticles, developments and applications of non-newtonian flows.," *The American Society of Mechanical Engineers,* vol. 66, no. 231, pp. 99-105, 1995.

[47]     M.-S. Lui, M. C.-C. Lin, I.-T. Huang and C.-C. Wang, "Enhancement of thermal conductivity with carbon nanotube for nanofluids," *nternational Communications in Heat and Mass Transfer,* vol. 32, no. 9, pp. 1202-1210, 2005.

[48]     R. McGlynn, S. Chakrabarti, B. Alessi, H. Moghaieb, P. Maguire, H. Singh and D. Mariotti, "Plasma-induced non-equilibrium electrochemistry synthesis of nanoparticles," *Elsevier: Solar Energy,* vol. 203, pp. 37-45, 2020.

[49]     S. H. Lee, I. Rusakova and D. M. Hoffman, "Monodisperse SnO2-Coated Gold Nanoparticles Are Markedly More Stable than Analogous SiO2-Coated Gold Nanoparticles," *ACS: Applied materials and interfaces,* vol. 5, p. 2479−2484, 2013.

[50]     P. Keblinski, S. R. Phillpot, S. U. Choi and J. A. Eastman, "Mechanisms of Heat Flow in Suspensions of Nano-Sized Particles (Nanofluids)," *Journal of Heat and Mass Transfer,* vol. 45, no. 4, pp. 855-863, 2002.

[51]     D. A. Siginer, D. De Kee and R. P. Chhabra, Advances in the flow and rheology of non-newtonian fluids, Elsevier, 1999.

[52]     Y. Xuan and Q. Li, "Heat transfer enhancement of nanofluids," *Journal of Heat and Fluid Flow,* vol. 21, no. 1, pp. 58-64, 2000.

[53]     Y. Xuan and W. Roetzel, "Conceptions for heat transfer correlation of nanofluids," *Jornal of Heat and Mass transfer,* vol. 43, no. 19, pp. 3701-3707, 2000.

[54]     T. Visinee and W. Somchai, "Critical review of heat transfer characteristics of nanofluids," *Renewable and Sustainable Energy Review,* vol. 11, no. 3, pp. 512-523, 2007.

[55]     P. W. Atkins, Physical Chemistry, Oxford: Oxford University Press, 1994, pp. 922-926.

[56]     Y. Huang, R. A. Ferhan, Y. Gao, A. Dandapat and D.-H. Kim, "High-yield synthesis of triangular gold nanoplates with improved shape uniformity, tunable edge length and thickness," *The Royal Society of Chemistry,* vol. 6, no. 6496, pp. 1-3, 2014.

[57]     H. S. Carlslaw and J. C. Jaeger, Conduction of Heat in solids, 2nd ed., Oxford: Oxford University Press, 1959.

[58]     S. Alvarado, E. Marin, A. G. Juarez, A. Calderon and R. Ivanov, "A hot-wire method based thermal conductivity measurement apparatus for teaching purposes," *European journal of Physics,* vol. 33, pp. 897-906, 2012.

[59]     C. J. Orendorff and C. J. Murphy, "Quantitation of Metal Content in the Silver-Assisted Growth of Gold Nanorods," *The journal of Physical Chemistry,* vol. 110, pp. 3990-3994, 2006.

[60]     H. M. Song , B. S. Chon, . S. H. Jeon and P. K. Dutta, "Synthesis of Au@SnO2 coreeshell nanoparticles with controllable shell thickness and their CO sensing properties," *Elsevier: Materials Chemistry and Physics,* vol. 166, pp. 87-94, 2015.

[61]     "Thermal Conductivity of Ethylene Glycol-Water Mixtures," Thermtest, 13 August 2018. [Online]. Available: https://thermtest.com/thermal-conductivity-ethylene-glycol-water-mixtures. [Accessed 25 01 2023].

[62]     T. W. Kim and D. U. Lee, "Microstructural, electrical, and optical properties of SnO2 nanocrystalline thin films grown on InP (100) substrates for applications as gas sensor devices," *Journal of Applied Physics,* vol. 88, p. 3759, 2000.

[63]     A. B. Korczyc, E. Mackiewicz,, K. R. Soliwoda, J. Grobelny and G. Celichowsk, "Facile synthesis of SnO2 shell followed bby microwave treatment for high environmental stability of Ag nanoparticles," *The Royal Society of Chemistry,* vol. 10, pp. 38424-38436, 2020.

[64]     A. Mohammadnia, A. Rezania, B. M. Ziaour, F. Sedaghati and L. Rosendahl, "Hybrid energy harvesting to maximize power generation from solar energy," *Energy Conservation Management,* vol. 112352, p. 205, 2020.

[65]     K. Myeongju and K. Younghun, "Au-coated Fe3O4@SiO2 core-shell particles with photothermal activity," *Elsevier,* vol. 600, no. 124957, pp. 1-7, 2020.

[66]     G. Oldfield, T. Ung and P. Mulvaney, "Au@SnO2 core-shell nanocapacitors," *Advanced AMterials,* vol. 12, no. 20, pp. 1519-1522, 2000.

[67]     M. Sun, G. Ran, Q. Fu and W. Xu, "The effect of Iodide on the synthesis of gold nanoprisms," *Journal of Experimental Nanoscience,* vol. 10, no. 17, pp. 1309-1318, 2015.

[68]     N. Yuan, K. Ciaxia, G. Qi, W. Jingjing, X. Haiying and W. Changshun, "Localised heat generation and stability of a plasmonic material," *Journal of Physics D: Applied Physics,* vol. 49, no. 055302, pp. 1-10, 2015.

[69]     N. Yuan, K. Caixia, G. Qi, W. Jingjing, X. Haiying and W. Changshun, "Heat generation and stability of a plasmonic," *Journal of Physics D: Applied Physics,* vol. 49, no. 055302, pp. 1-10, 2015.

[70]     D. G. Chukhchin, A. V. Malkov, I. V. Tyshkunova, L. V. Mayer and E. V. Novozhilov, "Diffractometric method for determining the degree of crystallinity of materials," *Diffration and Scattering of Ionizing Radiation,* vol. 61, no. 3, pp. 371-375, 2015.

[71]     P. M. Tiwari, K. Vig, V. A. Dennis and S. R. Singh, "Functionalized Gold Nanoparticles and Their Biomedical Applications," *Nanometerials,* vol. 1, no. 1, pp. 31-63, 2011.

[72]     Z. P. Xu, Q. H. Zeng, G. Q. Lu and A. B. Yu, "Inorganic nanoparticles as carriers for efficient cellular delivery," *Elsevier: Chemical Engineering Science,* vol. 61, no. 3, pp. 1027-1040, 2006.

[73]     S. Tedesco, H. Doyle, J. Blasco, G. Redmond and D. Sheehan, "Oxidative stress and toxicity of gold nanoparticles in Mytilus edulis," *Elsevier: Aquatic Toxicology,* vol. 100, no. 2, pp. 178-186, 2010.

[74]     J. H. Youk, "Preparation of gold nanoparticles on poly(methyl methacrylate) nanospheres with surface-grafted poly(allylamine)," *Elsevier: Polymer,* vol. 44, no. 18, pp. 5053-5056, 2003.

[75]     C.-W. Chen, M.-Q. Chen, T. Serizawa and M. Akashi, "In-Situ Formation of Silver Nanoparticles on Poly(N-isopropylacrylamide)-Coated Polystyrene Microspheres," *Advanced Materials,* vol. 10, no. 14, pp. 1122-1126, 1999.

[76]     Q. Kong, X. Chen, J. Yao and D. Xue, "Preparation of poly(N-vinyl-2-pyrrolidone)-stabilized transition metal (Fe, Co, Ni and Cu) hexacyanoferrate nanoparticles," *Nanotechnology,* vol. 16, p. 164, 2004.

[77]     S. Tang and J. Zheng, "Antibacterial Activity of Silver Nanoparticles: Structural Effects," *Advanced Healthcare Materials,* vol. 7, no. 13, 2018.

[78]     H. M. Fahmy, A. M. Mosleh, A. A. Elghany, E. Shams-Eldin, E. S. Serea and A. E. Shalan, "Coated silver nanoparticles: synthesis, cytotoxicity, and optical properties," *Royal Society of Chemistry,* no. 35, 2019.

[79]     D. Vollath, "Chapter 3: Surfaces in Nanomaterials," in *Nanomaterials: An introduction to synthesis, properties, and applications*, Wiley-VCH, 2013, p. 23.

[80]     J. M. Thomas, P. A. Midgley and C. Ducati, "Nanoscale electron tomography and atomic scale high-resolution electron microscopy of nanoparticles and nanoclusters: A short survey," *Progress in Natural Science,* vol. 23, no. 3, pp. 222-234, 2013.

[81]     B. Wunderlich, Macromolecular Physics, New York: Academic Press New York, 1976.

[82]     A. W. Adamson and A. P. Gast, Physical Chemistry of surfaces, New York: Wiley-interscience publication, 1997.

[83]     G. Mie, "Contributions to the optics of turbid media, particularly of colloidal metal solutions," *Annalen der Physik,* vol. 3, pp. 377-445, 1908.

[84]     A. Bansal and S. Verma, "Optical properties of bimetallic (Ag-Cu) core-noble metal shell nanoparticles," *Journal of Optics,* vol. 45, pp. 7-10, 2016.

[85]     E. R. Encina and E. A. Coronado, "Size Optimization of Iron Oxide@Noble Metal Core–Shell Nanohybrids for Photothermal Applications," *Journal of Physical Chemistry,* vol. 120, no. 10, pp. 5630-5639, 2016.

[86]     C. Loo, A. Lin, L. Hirsch, M. H. Lee, J. Barton, N. Halas, J. West and R. Drezek, "Nanoshell-enabled photonics-based imaging and therapy of cancer," *Technology in cancer research & treatment,* vol. 3, no. 1, pp. 33-40, 2004.

[87]     X. Huang, S. Neretina and M. El-Sayed, "Gold Nanorods: From Synthesis and Properties to Biological and Biomedical Applications," *Advanced Materials,* vol. 21, no. 48, pp. 4880-4910, 2009.

[88]     H. Chen, L. Shao and J. Wang, "Gold nanorods and their plasmonic properties," *Chemical Society Reviews,* vol. 42, pp. 2679-2724, 2013.

[89]     P. Zhao, N. Li and D. Astruc, "State of the Art in Gold Nanoparticle Synthesis," *Coordination Chemistry Reviews,* vol. 257, pp. 638-665, 2013.

[90]     J. Kimling, M. Maier, B. Okenve, V. Kotaidis, H. Ballot and A. Plech, "Turkevich Method for Gold Nanoparticle Synthesis Revisited," *The journal of Physical Chemisry,* vol. 110, no. 32, pp. 15700-15707, 2006.

[91]     N. L. Pacioni, C. D. Borzareli, V. Rey and A. V. Veglia, "Chapter Synthetic Routes for the Preparation of Silver Nanoparticles," in *Silver Nanoparticle Applications*, 2015, pp. 13-46.

[92]     N. Rajput, "Methods of Preparation of Nanoparticles- A review," *Journal of Advances in Engineering and Technology,* vol. 7, pp. 1806-1811, 2015.

[93]     B. Swathy, "A Review on Metallic Silver Nanoparticles," *Journal of Pharmacy,* vol. 4, no. 7, pp. 38-44, 2014.

[94]     ThermoFisher Scientific, "Materials Science: Energy Dispersive Spectroscopy," Thermofisher Scientific, [Online]. Available: https://www.thermofisher.com/za/en/home/materials-science/eds-technology.html#em-contact-form. [Accessed 14 September 2022].

[95]     B. L. Dutrow and C. M. Clark, "Instrumentation and Analysis," Integrating research and education, 03 September 2022. [Online]. Available: https://serc.carleton.edu/18400. [Accessed 14 September 2022].

[96]     H. M. Ali, T. R. Shah, H. Babar and A. M. Ali, "Hybrid Nanofluids: Techniques and Challenges of Stability enhancement," *Journal of thermal engineering,* pp. 1-8, 2018.

[97]     Y. Xuan and Q. Li, "Investigation on convective heat transfer and flow features of nanofluids," *Journal of Heat and Mass transfer,* vol. 125, no. 1, pp. 151-155, 2003.

[98]     S. O. Kasap, Principles of Electronic Materials and Devices, New York: McGraw-Hill, 2006, p. 126.

[99]     Y. Wei and X. Huaqing, "A Review on Nanofluids: Preparation, Stability mechanisms, and Applications," *Journal of Nanomaterials,* pp. 1-18, 2012.

[100]     X. Ye, L. Jin, H. Caglayan, J. Chen, G. Xing and C. Zheng, "Improved size-tunable synthesis of monodisperse gold nanorods through the use of aromatic additives," *American chemical society,* vol. 6, no. 3, pp. 2804-2817, 2012.

[101]     Y. Yu, Q. Zhang, Q. Yao, J. Xie and J. Yang, "Guiding Principles in the Galvanic Replacement Reaction of an underpotentially deposited metal layer for site-selective deposistion and shape and size control of satellite nanocrystals," *Chemistry of Materials,* vol. 25, pp. 4746-4756, 2013.